Scattering phase shift for elastic two pion scattering and the rho resonance in lattice QCD

Dissertation

zur Erlangung des Doktorgrades
der Naturwissenschaften (Dr. rer. nat.)
der Fakultät für Physik
der Universität Regensburg

vorgelegt von
Simone Gutzwiller
aus Regensburg

August 2012

Promotionsgesuch eingereicht am: 27.06.2012
Promotionskolloquium am: 08.10.2012
Die Arbeit wurde angeleitet von: PD Dr. Meinulf Göckeler

PRÜFUNGSAUSSCHUSS:

Vorsitzender: Prof. Dr. Ch. Back
1. Gutachter: PD Dr. M. Göckeler
2. Gutachter: Prof. Dr. V. Braun
weitere Prüfer: Prof. Dr. J. Fabian

Abstract

In this thesis we use lattice QCD to compute scattering phase shifts for elastic two-pion scattering in the isospin $I = 1$ channel. Using Lüscher's formalism, we derive the scattering phase shifts for different total momenta of the two-pion system in a non-rest frame. Furthermore we analyse the symmetries of the non-rest frame lattices and construct 2-pion and rho operators transforming in accordance with these symmetries. The data was collected for a $32^3 \times 64$ and a $40^3 \times 64$ lattice with $N_f = 2$ clover improved Wilson fermions at a pion mass around 290 MeV and a lattice spacing of about 0.072 fm.

Contents

1. Introduction **1**
- 1.1. The Standard Model . . . 1
- 1.2. The quark model . . . 2
- 1.3. Unit convention . . . 4

2. Quantum Chromodynamics on the lattice **5**
- 2.1. QCD in the continuum - A review . . . 5
  - 2.1.1. The Euclidean time . . . 5
  - 2.1.2. The fermionic Lagrangian . . . 6
  - 2.1.3. The gauge part of the Lagrangian . . . 9
- 2.2. The lattice discretisation . . . 10
  - 2.2.1. Discretising the free fermion action . . . 11
  - 2.2.2. Introducing gauge fields . . . 12
  - 2.2.3. The lattice gauge action . . . 14
- 2.3. Wilson fermions . . . 16
  - 2.3.1. The Dirac operator . . . 16
  - 2.3.2. Fermion doubling . . . 17
  - 2.3.3. Wilson fermion action . . . 19
  - 2.3.4. Clover improvement . . . 20

3. The path integral on the lattice **21**
- 3.1. The Euclidean correlator . . . 21
- 3.2. Calculating the path integral . . . 23
- 3.3. Numerical evaluation of the path integral . . . 25
  - 3.3.1. Monte Carlo integration . . . 25
  - 3.3.2. Markov chains and Metropolis algorithm . . . 26

4. Mesons on the lattice **29**
- 4.1. Meson interpolators . . . 29
- 4.2. Sources and smearing . . . 32
- 4.3. Extracting energies . . . 34
  - 4.3.1. General considerations . . . 34
  - 4.3.2. The variational method . . . 35
- 4.4. Setting the scale . . . 36

5. Resonance scattering on the lattice **39**
5.1. Derivation of the phase shift formula 40

6. Determination of the scattering phase shift for non-zero total momenta **47**
6.1. Group theory 47
6.2. Scattering phases 48

7. Operators for pion resonance scattering and their transformation behaviour under point groups **53**
7.1. Operators for pion scattering 53
7.2. Transformation of 2-particle operators 54
7.2.1. Transformation under D_{4h} 56
7.2.2. Transformation under D_{2h} 59
7.2.3. Transformation under D_{3d} 60
7.3. The rho meson operator 62
7.3.1. Transformation under D_{4h} 63
7.3.2. Transformation under D_{2h} 64
7.3.3. Transformation under D_{3d} 64

8. Energy levels from resonance scattering **67**
8.1. The effective range model 67
8.2. The 2-pion operators 68
8.2.1. Group D_{4h} 68
8.2.2. Group D_{2h} 69
8.2.3. Group D_{3d} 71
8.3. Energy level plots 71

9. The correlation functions **77**
9.1. The 2-pion correlation function 77
9.2. The remaining correlation functions 83

10. Results **87**
10.1. Results and discussion 87
10.2. Summary and outlook 92

A. Calculation of the generalised zeta function **99**
A.1. General formalism 99
A.2. Derivation for D_{4h}, D_{2h} and D_{3d} 101

B. The jackknife method **107**

C. Energy and phase shift tables **109**

1. Introduction

1.1. The Standard Model

The *Standard Model of particle physics* describes the physics at the level of elementary particles. All observations in nature are the result of the interaction of the elementary particles (leptons and quarks) mediated by four fundamental forces (electromagnetic, weak, strong and gravitational). From the four forces the SM includes just the electromagnetic, weak and strong ones. Figure 1.1.1 gives an overview over the included particles and their quantum numbers.

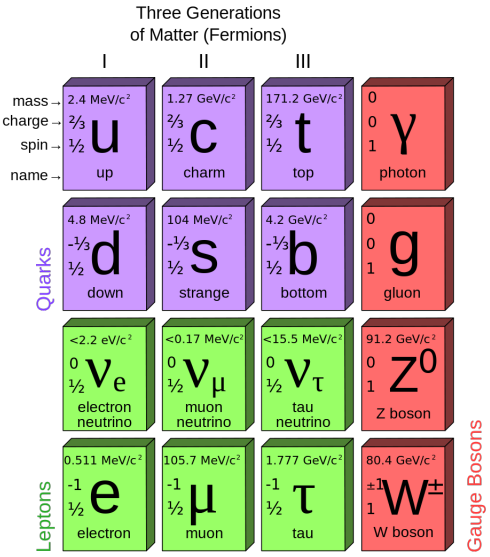

Figure 1.1.1.: The Standard Model of particle physics [1].

From the figure we see that the Standard Model includes three types of particles. The particles marked in green are the so-called *leptons*. The electron-like particles (e, μ, τ) carry electric and weak charge and the neutrinos carry weak charge. The purple coloured *quarks* carry all three types of charges (electric, weak and strong). The quarks are the constituents of the strongly interacting particles called *hadrons* and in contrast to the leptons they cannot exist as free particles. Leptons and quarks are both fermions with

spin $\frac{1}{2}$. The four red coloured *gauge bosons* are responsible for the interaction between the quarks and leptons. The gauge bosons are all spin 1 particles. The photon γ is related to the electromagnetic interaction, the $W^{\pm}, Z$ are the gauge bosons of the weak interaction and the gluons are responsible for the strong force. Quarks and gluons are the particles involved in the theory of the strong interaction, *Quantumchromodynamics* (QCD).

In addition there is the Higgs boson, a massive spin 0 particle which is related to the spontaneous symmetry breaking of the electroweak theory. The Higgs mechanism describes how the gauge bosons of the weak interaction and the fermions acquire their mass. Due to spontaneous symmetry breaking four massless pseudo-Goldstone bosons appear in the theory. Three of them are "absorbed" by the by the gauge bosons of the weak interaction and make them massive. The fourth pseudo-Goldstone boson also acquires a mass. This is the observable Higgs boson.

As their names suggest the interactions are of different strengths. The approximate values of the coupling constants are [25]:

electromagnetic	$\alpha_{em} \approx \frac{1}{137}$
strong	$\alpha_s \approx 1 \quad$ for energies $\lesssim 1$ GeV
weak	$G_F \approx 10^{-5}$ GeV.

The electromagnetic and weak coupling constants are small enough such that perturbation theory can be used to calculate observables. In the case of the strong interaction whose underlying theory is QCD the situation is different. The size of α_s depends on the energy at which the particles interact. For large momentum transfer α_s is small and perturbation theory can be used. In the limit of infinitely large momentum transfer the strong coupling becomes zero and the quarks and gluons behave like free particles (*asymptotic freedom*). This fact can be used in perturbative QCD to calculate hard scattering processes. To describe low energy experiments from first principles we need another approach than perturbative QCD.

The figure also shows a classification of the fermions in three generations. The difference between them are the particle masses. Only the first generation can form stable states and builds up ordinary matter. The others are only produced at high energies like in particle accelerators or in cosmic rays.

For every quark and lepton there also exists a corresponding *antiparticle* with same mass but opposite charge. The antiparticles are marked by a bar, for example $\bar{u}$.

1.2. The quark model

The quark model was developed independently by Gell-Mann and Zweig in 1964 to bring some order into the abundance of known particles at this time. They proposed that these particles were not elementary but consist of quarks and anti-quarks. Three

Quark	I	I_z
u	$1/2$	$1/2$
d	$1/2$	$-1/2$
$\bar{u}$	$1/2$	$-1/2$
$\bar{d}$	$1/2$	$1/2$

Table 1.2.1.: Isospin for up and down quarks.

quarks can form a state called *baryon* (qqq) and a quark together with an anti-quark can build a *meson* ($\bar{q}q$). As already mentioned quarks cannot be observed as free particles (confinement). The reason for this are the self-interactions of the gluons. The potential between heavy quarks is approximately of the form $V(r) = A + \frac{B}{r} + Cr$ [21]. If one wants to separate two quarks the potential grows linearly with r. When the potential energy reaches a critical value a new quark anti-quark pair is produced and one ends up with new hadrons. In 1968 deep inelastic scattering experiments at SLAC finally confirmed that quarks are point-like subparticles of protons.

Figure 1.1.1 shows that the quarks come in different *flavours*: *u*p, *d*own, *c*harm, *s*trange, *t*op and *b*ottom. A special case are the two lightest quarks, u and d, whose masses are much smaller than the masses of hadrons and QCD is approximately invariant under the exchange of them. This can be described by the *isospin*, a quantum number which is related to the u and d flavour symmetry. Table 1.2.1 shows the isospin I for up and down quarks and the third component I_z. All other flavours have $I = 0$. Instead of isospin the s quark has a quantum number called strangeness S, the c quark has charm C and so on. But for our work just the two lightest quarks will be of importance. Mathematically isospin is described by the symmetry group $SU(2)$ which has three generators, the Pauli matrices. All existing hadrons fit in so-called isospin *multiplets*. For the mesons made of u, d and their antiquarks we have

$$2 \otimes \bar{2} = 3 \oplus 1.$$

This is a triplet and a singlet. The triplet is formed e.g. by the three pions π^+, π^- and π^0 with total isospin 1 and $I_z = 1, -1$ and 0 respectively. The pions are pseudoscalar mesons with zero total spin and negative parity. The spins of the two quarks are antiparallel. As expected from particles in the same multiplet the pions have nearly the same mass ($\pi^0 \approx 135$ MeV, $\pi^\pm \approx 140$ MeV.) A singlet is the η-meson with a mass around 547 MeV. But these four mesons are not the only ones made from u and d quarks/anti-quarks that we see in experiments. There are also particles with the same quark content but bigger mass, so-called *resonances*. The resonances have a very short lifetime compared with the lighter states. The resonances which are observed in pion scattering are the rho mesons $\rho^\pm$ and ρ^0 with a mass around 770 MeV. The three rhos are vector mesons, i.e. they have spin 1. Isospin and parity are the same as for the pions.

The rho resonances can be observed in elastic $\pi\pi \to \pi\pi$ scattering with angular momentum $l = 1$ and isospin $I = 1$. But to describe this within QCD is problematic because here perturbative QCD cannot be used. A non-perturbative approach to QCD is *lattice Quantum Chromodynamics*. There one replaces space-time by a box of length L with appropriate boundary conditions. The space-time box itself is also discretised: It consists of lattice points separated by the lattice spacing a. The quarks sit on the lattice sites and the gauge field lives on by the links between the sites. Another important feature is the regularisation effect of the lattice. The finite lattice spacing limits the spatial resolution and produces an ultraviolet cutoff. The lattice size L on the other hand constrains phenomena at long distances and avoids infrared divergences. Furthermore one uses an imaginary Euclidean time τ, which makes the QCD path integral finite. But this is a problem when one wants to analyse resonance scattering. For two-pion scattering we have the following situation: First we have two incoming pions, they interact and build a resonance which decays then again into two pions. Between the two incoming and outgoing pion wave packets one observes a phase shift. This procedure happens in real time and cannot be observed in Euclidean time. The idea to solve this problem was developed in 1990 by Lüscher and Wolff [32]. Their basic idea was to relate the centre-of-mass energy in a finite periodic box with the scattering phase shift by a simple formula. Later this concept was elaborated by Rummukainen and Gottlieb for non-rest-frame systems. First lattice calculations for two pion scattering were performed by Aoki et al. in 2007. In this thesis we apply their approach on a finer lattice with a smaller quark mass using several moving frames.

The thesis is organised as follows: In the second chapter we summarise some basic concepts about lattice QCD, then we talk about the path integral and its numerical evaluation. The fourth chapter will deal with the description of mesons on the lattice and the extraction of energies from correlation functions. Then follows a summary of the derivation of the general form of the phase shift formula based on the papers of Lüscher, Rummukainen and Gottlieb [30, 40]. After this we derive the formula for explicit cases followed by a chapter about the transformation of two pion and rho operators under the relevant symmetry groups. Then we discuss the effective range model and derive the correlation functions which we need for the lattice calculations. In the last chapter we will present and discuss the results.

1.3. Unit convention

Throughout the whole work we will use natural units, i.e. we set

$$\hbar = 1, \quad c = 1.$$

2. Quantum Chromodynamics on the lattice

The first topic of this chapter is a review of the QCD in the continuum. After this we will introduce the lattice and its discretization of space-time. We will see that there are some important differences between the continuum and the lattice.

2.1. QCD in the continuum - A review

2.1.1. The Euclidean time

In continuum quantum field theory, we use the Minkowski space in our calculations. For a lattice gauge theory it is necessary to switch from Minkowski space to the Euclidean space. The reason is the usage of the *path integral formalism*, which we will present in more detail in a later chapter. This formalism is used to numerically calculate n-point functions on the lattice. The explanations in this chapter will generally follow the books of Peskin, Schroeder [38] and Gattringer, Lang [21].

To denote some space-time point in Minkowski space, one uses an object called 4-vector x with components x^μ where $\mu = 0, 1, 2, 3$ and $\mu = 0$ denotes the time direction.

Now we want to calculate the amplitude of a quantum mechanical particle that propagates from x to y in a given time interval T with the *path integral* or *functional integral* formalism

$$\langle y|\mathrm{e}^{-i\hat{H}T}|x\rangle = \int \mathcal{D}x \mathrm{e}^{iS} \tag{2.1.1}$$

where $\hat{H}$ is the Hamilton operator and S the classical action $S = \int dt L$[1]. The expression $\int \mathcal{D}x$ in the functional integral denotes the "sum over all paths from x to y" and the left hand side is a matrix element of the time evolution operator. The functional integral is an infinite dimensional, complex valued and strongly oscillating integral, all bad conditions for a numerical evaluation. This is the point where the Euclidean time (and later the lattice) comes into play. For all 4-vectors we set the time component x^0 equal to the Euclidean time x_4 up to a factor of i

$$x^0 = -ix_4, \quad x_4 > 0. \tag{2.1.2}$$

[1] Equation (2.1.1) can be generalized straightforwardly for field theories, that will be done in Chapter 3.

This means that we replace all time variables t with $-i\tau$, $\tau > 0$, where τ is the euclidean time. With this replacement the path integral becomes well defined. Evaluating the path integral with the substitution (2.1.2), we get the following relation between the action S in Minkowski space and the euclidean action S_E:

$$S = iS_E. \tag{2.1.3}$$

This equation remains also valid in field theories like QCD. Equation (2.1.1) becomes then

$$\langle y|\mathrm{e}^{-H\tau}|x\rangle = \int \mathcal{D}x\mathrm{e}^{-S_E}. \tag{2.1.4}$$

Note that in Euclidean space we do not have to worry about co- and contravariant objects, because the euclidean metric $g^E_{\mu\nu}$ is equal to the identity matrix and therefore the 4-vector-components x_μ and x^μ are identical. For this reason we will use only lower indices. The summation convention then says that over identical indices will be summed.

From this point on all calculations and formulas refer to Euclidean space, so we will drop the subscript E.

2.1.2. The fermionic Lagrangian

A fermion, i.e. a quark, at a given position x in space is described by a Dirac spinor $\psi(x)$. The spinor has a Dirac index α and a color index a. Furthermore the quarks and antiquarks come in six different flavours f namely up, down, charm, strange, top and bottom and we denote the total number of flavours with N_f. Then the spinors have the following form

$$\psi(x)^f_{\alpha a}, \bar{\psi}(x)^f_{\alpha a} \quad \text{with} \quad \alpha = 1,2,3,4 \quad a = 1,2,3 \quad \text{and} \quad f = 1,\ldots,N_f. \tag{2.1.5}$$

For every Dirac index α there are three additional colour indices, so that in the end a fermionic field is described by a "vector" with 12 components. In most of the calculations we will not state the indices explicitly because the notation becomes quickly confusing. Instead a vector notation will be used. In addition we do not write out the sum over the flavours because we are only interested in the strong interaction where the coupling between quarks and gluon fields is the same for all flavours and the only difference belongs to the mass term.

Let us first have a look at the fundamental properties of the QCD Lagrangian. Assume that we have only one flavour of quarks with mass m and let us write down the Dirac-Lagrangian[2]:

$$\mathcal{L}_{Dirac} = \bar{\psi}(x)(\partial_\mu\gamma_\mu + m)\psi(x), \tag{2.1.6}$$

[2]Pay attention to the slight difference of the Dirac-Lagrangian in Minkowski space: $\mathcal{L}_{Dirac} = \bar{\psi}(x)(i\partial_\mu\gamma^\mu - m)\psi$.

where γ_μ with $\mu = 1, 2, 3, 4$ are the Euclidean Dirac-matrices. They obey the anti-commutation relations

$$\{\gamma_\mu, \gamma_\nu\} = 2\delta_{\mu\nu} \cdot \mathbb{1} \tag{2.1.7}$$

and the relationship between Minkowski Dirac-Matrices γ_M and the Euclidean Dirac-matrices γ is given by

$$\gamma_4 = \gamma_M^0 \quad \text{and} \quad \gamma_i = -i\gamma_M^i. \tag{2.1.8}$$

The Lagrangian $\mathcal{L}_{Dirac}$ described in equation (2.1.6) is invariant under the global gauge transformation

$$\psi(x) \quad \rightarrow \quad V\psi(x), \tag{2.1.9}$$

which describes a rotation in colour space. The matrix $V \in SU(3)$ is a unitary 3×3 matrix with $\mathsf{det}(V) = 1$ which is applied to the spinor at every space-time point x. This formalism can easily be generalised to $SU(N)$. Unfortunately the global symmetry transformation is not very helpful, because one has to know $\psi(x)$ for all space-time points. In addition the above equation describes a theory without any interaction, which is not the case we observe in reality. What we wish to have is that $\mathcal{L}_{Dirac}$ is invariant under a symmetry transformation at some space-time point x, a so-called *local gauge transformation*. Then the transformation law should look like

$$\psi(x) \quad \rightarrow \quad V(x)\psi(x). \tag{2.1.10}$$

In order that equation (2.1.6) remains invariant under the above transformation one has to introduce *gauge fields* $A_\mu(x)$. They describe the interaction between the quarks ans lead us to a realistic theory. In equation (2.1.6) we therefore replace the derivative ∂_μ with the *covariant derivative* D_μ:

$$D_\mu = \partial_\mu + igA_\mu(x), \tag{2.1.11}$$

where g denotes the coupling constant. Now we can write down the complete fermionic part of the Euclidean QCD Lagrangian:

$$\begin{aligned} \mathcal{L}_F[\psi, \bar{\psi}, A] &= \sum_{f=1}^{N_f} \bar{\psi}^f_{\alpha a}(x) \Big((\gamma_\mu)_{\alpha\beta}(\delta_{ab}\partial_\mu + igA_\mu(x)_{ab}) + m^f \delta_{\alpha\beta}\delta_{ab} \Big) \psi^f_{\beta b}(x) \\ &= \sum_{f=1}^{N_f} \bar{\psi}^f(x) \Big(\gamma_\mu(\partial_\mu + igA_\mu(x)) + m^f \Big) \psi^f(x). \end{aligned} \tag{2.1.12}$$

Here we used both the explicit and the matrix/vector notation. Note that the four γ_μ's are 4×4 matrices in Dirac space and the gauge fields $A_\mu(x)$, which are called *gluon fields* in QCD, are 3×3 matrices in colour space. Because the coupling g does not depend on the flavour we drop the sum in most calculations and use only $N_f = 1$.

Gauge invariance for fermionic Lagrangian

The fermionic Lagrangian for $N_f = 1$ reads

$$\mathcal{L}_F[\psi, \bar{\psi}, A] = \bar{\psi}(x)\Big(\gamma_\mu(\partial_\mu + igA_\mu(x)) + m\Big)\psi(x). \tag{2.1.13}$$

We already remarked that we want this Lagrangian to be invariant under

$$\begin{aligned} \psi'(x) &= V(x)\psi(x) \\ \bar{\psi}'(x) &= \bar{\psi}(x)V^{-1}(x) \end{aligned} \tag{2.1.14}$$

where $V(x)$ is an element of the group $SU(3)$. We can write it as the exponential of the sum of some basis matrices T_i

$$V = \exp\left(i\sum_{i=1}^{8}\omega_i T_i\right). \tag{2.1.15}$$

The T_i are called the *generators* of $SU(3)$ and the ω_i are real numbers to parametrise the element V. If we change the parameters ω_i continuously, the group element V will also do so. This property makes $SU(3)$, and in general $SU(N)$, a *Lie group*. In the $SU(N)$ case we have $N^2 - 1$ genrators, which are traceless complex hermitian (i.e. $T = (T^*)^T = T^\dagger$) $N \times N$ matrices and they span a vector space, the so-called *Lie algebra* $\mathfrak{su}(N)$, with the following commutation relation

$$[T_i, T_j] = if_{ijk}T_k, \tag{2.1.16}$$

where the f_{ijk} are called *structure constants*. The generators can always be chosen such that the structure constants are completely antisymmetric. In the case of $SU(2)$ and $SU(3)$ the generators are the Pauli matrices and the Gell-Mann matrices, respectively.

More detailed information about Lie groups and Lie algebras can be found in field theory textbooks like [38] or in [22]. Equation (2.1.14) gives us the transformation law for the quark fields but we don't know yet how the gauge fields transform. Nevertheless the local gauge invariance of the Lagrangian requires

$$\mathcal{L}_F[\psi'(x), \bar{\psi}'(x), A'(x)] = \mathcal{L}_F[\psi(x), \bar{\psi}(x), A(x)] \tag{2.1.17}$$

where $A'_\mu(x)$ is the new gauge field. Inserting (2.1.14) in the left hand side of (2.1.17) gives

$$\begin{aligned} \mathcal{L}_F[\psi'(x), \bar{\psi'}(x), A'(x)] &= \bar{\psi}(x)V^{-1}(x)\Big(\gamma_\mu(\partial_\mu + igA'_\mu(x)) + m\Big)V(x)\psi(x) \\ &\overset{!}{=} \bar{\psi}(x)\Big(\gamma_\mu(\partial_\mu + igA_\mu(x)) + m\Big)\psi(x). \end{aligned} \tag{2.1.18}$$

For the mass term we see immediately that in the upper part of (2.1.18) we get $\bar{\psi}m\psi$ and the term cancels. For the rest we look at

$$\begin{aligned}(\partial_\mu + igA_\mu(x))\psi(x) &\stackrel{!}{=} V^{-1}(x)(\partial_\mu + igA'_\mu(x))V(x)\psi(x) \\ &= \partial_\mu\psi(x) + V^{-1}(x)(\partial_\mu V(x))\psi(x) \\ &\quad + igV^{-1}(x)A'_\mu(x)V(x)\psi(x).\end{aligned} \tag{2.1.19}$$

Here we used the product rule for the derivative ∂_μ which gives us an additional term $V^{-1}(x)(\partial_\mu V(x))$. Note that the $V(x) \in SU(3)$ commute with the matrices γ_μ because the $V(x)$ act in colour space and the γ_μ in Dirac space. Using $V^{-1}(x) = V^\dagger(x)$, (2.1.19) gives the equation

$$\partial_\mu + igA_\mu(x) = \partial_\mu + V^\dagger(x)(\partial_\mu V(x)) + igV^\dagger(x)A'_\mu(x))V(x), \tag{2.1.20}$$

which we can solve for A'_μ and finally get the transformation law for the gauge fields

$$A'_\mu = V(x)A_\mu V^\dagger(x) + \frac{i}{g}(\partial_\mu V(x))V^\dagger(x). \tag{2.1.21}$$

2.1.3. The gauge part of the Lagrangian

The gluons are massless particles, therefore their Lagrangian will only contain a kinetic term. The *field strength tensor* $F_{\mu\nu}(x)$ is defined as the commutator of the covariant derivatives:

$$F_{\mu\nu}(x) = -\frac{i}{g}[D_\mu(x), D_\nu(x)] = \partial_\mu A_\nu - \partial_\nu A_\mu + ig[A_\mu, A_\nu]. \tag{2.1.22}$$

The transformation property for the gauge part of the Lagrangian must be the same as for the fermionic Lagrangian

$$S_G[A'(x)] = S_G[A(x)]. \tag{2.1.23}$$

From the first line of (2.1.19) we can read off the transformation property for the covariant derivative

$$D'_\mu(x) = V(x)D_\mu(x)V^\dagger(x). \tag{2.1.24}$$

Inserting $D'_\mu(x)$ in equation (2.1.22) gives the same transformation property for $F_{\mu\nu}(x)$ as for $D_\mu(x)$.

Before we come to the lattice discretisation, let us have another look at the gauge fields $A_\mu(x)$. They are traceless hermitian matrices, i.e. they are elements of the Lie algebra $\mathfrak{su}(3)$ and can therefore be written as a sum over the basis generators

$$A_\mu(x) = \sum_{i=1}^{8} A^i_\mu(x)T_i. \tag{2.1.25}$$

The $A^i_\mu(x)$ are real-valued fields and represent the eight gluons. Putting expression (2.1.25) in (2.1.22) we get

$$\begin{aligned} F_{\mu\nu}(x) &= \sum_{i=1}^{8} \Big\{ \partial_\mu A^i_\nu - \partial_\nu A^i_\mu - igf_{ijk} A^j_\mu A^k_\nu \Big\} T_i \\ &= \sum_{i=1}^{8} F^i_{\mu\nu}(x) T_i \end{aligned} \tag{2.1.26}$$

where we used the Lie algebra commutation relation (2.1.16) in the gauge field commutator. The gauge action then reads

$$\mathcal{L}_G = \frac{1}{4} \sum_{i=1}^{8} F^i_{\mu\nu}(x) F^i_{\mu\nu}(x). \tag{2.1.27}$$

There is an important difference between the gauge field part of the Lagrangian in QED and QCD. In QED, the local gauge group is $U(1)$ and the $V(x)$ are simple phase transformations, which means that the generator is a 1×1 matrix that equals 1. For this reason the gauge fields $A_\mu(x)$ have also to be a 1×1 matrix, i.e., a simple number and therefore commute with each other. In such a case the field commutator in equation (2.1.22) is zero and one gets the field strength tensor familiar from electrodynamics.

In the case of $SU(3)$ or in general in $SU(N)$ with $N \geq 2$, the $V(x)$ are non-commuting matrices and also the matrices representing the Lie algebra do not commute and we speak about a non-abelian gauge theory. The idea of non-abelian gauge theories was first proposed by Yang and Mills, who generalised the invariance under phase rotations to invariance under the continouus symmetry groups $SU(N)$. For non commuting gauge fields the commutator of the right hand side in (2.1.22) does not vanish. This additional term leads to self-interaction terms of the gluons in the Lagrangian and has the effect that we cannot observe free coloured particles in nature, which is called *quark confinement*. The presence of the self-interaction has also consequences for the gauge coupling g: For rising energies the coupling gets smaller and the quarks behave more and more like free particles (*asymptotic freedom*) and one can apply perturbation theory. From experimental measurements one finds that for momentum transfers $Q \gtrsim 1$ GeV the strong coupling constant α_s is about $\alpha_s \approx 0.4$ where $\alpha_s(Q) = g^2/4\pi$ evaluated at $Q^2 = s$ [38]. For smaller energies the coupling g gets strong and we have to find an alternative to the perturbation series expansion. The solution is introducing a lattice discretisation in space-time, which is the topic of the next section.

2.2. The lattice discretisation

We now want to replace the continuum space-time with a lattice. This means that our space-time will be a four-dimensional grid. The fermion fields live only on the nodes

which represent our space-time points x. In contrary we will see that the gauge field lives on the links between two nodes. The next step is clear: One has to replace the expressions for fermion fields, gluon fields, derivatives, integrals and so on with terms from the lattice concept. This approach is called *naive discretisation*. The expression has its right because we will recognise in a later section when we take a closer look at the lattice action, that there are some unphysical poles in the quark propagator caused by the naive discretisation. Because their occurrence is caused by the discretisation they are called lattice artifacts. To remove them one has to introduce an additional correction term.

2.2.1. Discretising the free fermion action

We get the free fermion action $S_F^{free}[\bar{\psi}(x), \psi(x)]$ by integrating the Dirac Lagrangian (2.1.6) over space-time

$$S_F^{free}[\bar{\psi}(x), \psi(x)] = \int d^4x \bar{\psi}(x)(\partial_\mu \gamma_\mu + m)\psi(x). \tag{2.2.1}$$

Now we introduce a lattice Λ where every four vector is given by

$$\begin{aligned} x = (x_1, x_2, x_3, x_4) \quad \text{with} \quad & x_1, x_2, x_3 = 0, 1, \dots N-1, \\ & x_4 = 0, 1, \dots N_T - 1 \end{aligned} \tag{2.2.2}$$

with boundary conditions

$$f(x + N_\mu \hat{\mu}) = \mathrm{e}^{2\pi i \theta_\mu} f(x) \quad \text{where} \quad \mu = 1, 2, 3, 4. \tag{2.2.3}$$

Here $N_\mu = N$ for $\mu = 1, 2, 3$ and $N_\mu = N_T$ for $\mu = 4$. If $\theta_\mu = 0$ we have periodic boundary conditions and antiperiodic for $\theta_\mu = -\frac{1}{2}$. The distance between two neighbouring lattice points x and y is the lattice spacing a. Therefore the relationship between a point in the continuum and on the lattice is given by

$$x_{cont} = a \cdot x_{lat}. \tag{2.2.4}$$

We also define the unit vector $\hat{\mu}$ which points from a lattice site to a neighbouring site in direction $\mu = 1, 2, 3, 4$.

The lattice Λ is the entity of all points x. The fermion fields are then replaced by their lattice version and the integral $\int d^4x$ becomes the sum $a^4 \sum_\Lambda$. What is missing is an appropriate lattice expression for the derivative ∂_μ. For this reason we look at the Taylor expansion of some function $f(x)$ at the lattice points $x + a$ and $x - a$

$$f(x + a) = f(x) + a f'(x) + \frac{a^2}{2} f''(x) + \frac{a^3}{6} f'''(x) + \dots \tag{2.2.5a}$$

$$f(x - a) = f(x) - a f'(x) + \frac{a^2}{2} f''(x) - \frac{a^3}{6} f'''(x) + \dots . \tag{2.2.5b}$$

To obtain an expression for the derivative, we can put $f'(x)$ in (2.2.5a) to the left side, divide by a and get

$$f'(x) = \frac{f(x+a) - f(x)}{a} + O(a). \tag{2.2.6}$$

Another way to get $f'(x)$ is to subtract the second Taylor expansion from the first. Then we have

$$f'(x) = \frac{f(x+a) - f(x-a)}{2a} + O(a^2). \tag{2.2.7}$$

Although both equations give a formula for $f'(x)$ there is an important difference. Equation (2.2.7) has a smaller correction term which is of order a^2. Naturally one wants the errors to be as small as possible, so we will use (2.2.7) as expression for the derivative.

Using $\hat{\mu}$ we can replace

$$\partial_\mu \psi(x) \to \frac{1}{2a}((\psi(x+\hat{\mu}) - \psi(x-\hat{\mu})). \tag{2.2.8}$$

With all the above replacements we get for the free fermion action (2.2.1)

$$S_F^{free}[\bar{\psi}(x), \psi(x)] = a^4 \sum_\Lambda \bar{\psi}(x) \left(\sum_{\mu=1}^{4} \gamma_\mu \frac{\psi(x+\hat{\mu}) - \psi(x-\hat{\mu})}{2a} + m\psi(x) \right). \tag{2.2.9}$$

2.2.2. Introducing gauge fields

In section 2.1.2 we saw that enforcing invariance of the free fermion Lagrangian under local transformations leads to the introduction of gauge fields $A_\mu(x)$, but we cannot directly transfer the continuum expression to the lattice. The condition of invariance under local rotations in $SU(3)$ on the lattice will give us the right term for the gauge field. The transformation behaviour for the fermion field $\psi(x)$ is the same as in the continuum,

$$\begin{aligned} \psi'(x) &= V(x)\psi(x), \\ \bar{\psi}'(x) &= \bar{\psi}(x)V^{-1}(x), \end{aligned} \tag{2.2.10}$$

but note that now the point x refers to a lattice site.

From equation (2.2.9) we see that the mass term causes no problem and remains invariant under the above transformation. But what happens with an expression of the form $\bar{\psi}(x)\psi(x+\hat{\mu})$ which corresponds to the first term in (2.2.9)? If we use our transformation law we simply get

$$\bar{\psi}'(x)\psi'(x+\hat{\mu}) = \bar{\psi}(x)V^\dagger(x)V(x+\hat{\mu})\psi(x+\hat{\mu}). \tag{2.2.11}$$

This is clearly not gauge invariant. For gauge invariance we have to get rid of the colour matrix part $V^\dagger(x)V(x+\hat{\mu})$. We can do this by introducing a field $U_\mu(x)$ that transforms under (2.2.10) like

$$U'_\mu(x) = V(x)U_\mu(x)V^\dagger(x+\hat{\mu}). \tag{2.2.12}$$

If we now look at

$$\bar{\psi}'(x)U'_\mu(x)\psi'(x+\hat{\mu}) \tag{2.2.13}$$

the matrices V cancel and the expression remains invariant under the required gauge transformation.

The $U_\mu(x)$ are the gauge fields we missed in the free equation (2.2.9). The parameter μ gives them a specific orientation. Because the gauge fields live on the links, they are often called also *link variables*. Figure 2.2.1 should give a better understanding what link variables are. The fact that $U_\mu(x)$ points from x to $x+\hat{\mu}$ leads to the idea of link variables pointing in negative direction. In this sense $U_{-\mu}(x)$ then points from x to $x-\hat{\mu}$. The negative link variables are very convenient but they are not independent variables and are related to positive links by the definition

$$U_{-\mu}(x) = U^\dagger_\mu(x-\hat{\mu}). \tag{2.2.14}$$

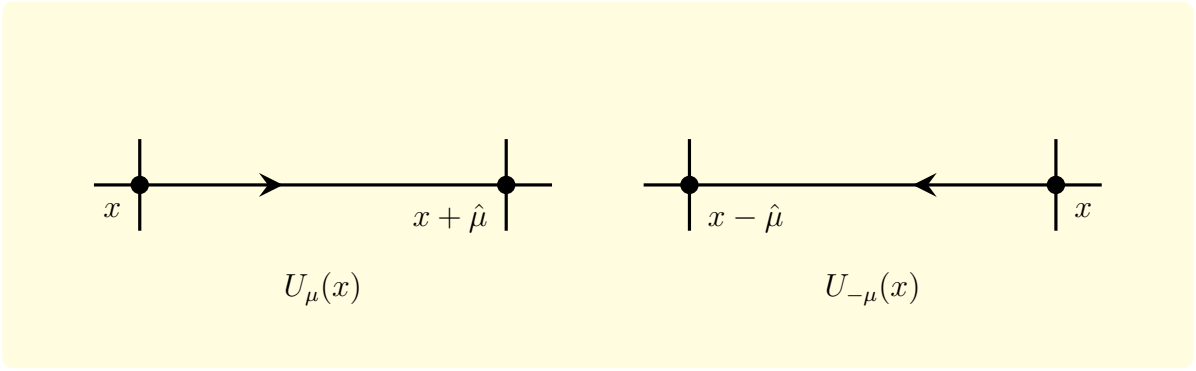

Figure 2.2.1.: Link variables. The black dots represent the lattice sites and the arrows indicate the direction of the gauge field.

Considering (2.2.12) one can construct a gauge invariant fermion action:

$$S_F[\bar{\psi}(x),\psi(x)] = a^4\sum_\Lambda \bar{\psi}(x)\left(\sum_{\mu=1}^{4}\gamma_\mu\frac{U_\mu(x)\psi(x+\hat{\mu})-U_{-\mu}(x)\psi(x-\hat{\mu})}{2a}+m\psi(x)\right). \tag{2.2.15}$$

If the expression (2.2.15) is physically correct it must be possible to connect it with the continuum action (2.1.12). To do so we need a continuum object which transforms in the same way as the link variable $U_\mu(x)$. The so-called *gauge transporter* fulfils this condition. It is a path-ordered exponential of a gauge field $A_\mu(x)$ along a path from y to z:

$$G(y,z) = P\left\{\exp(ig\int_{\mathcal{C}_{yz}} A_\mu(x)\cdot dx_\mu)\right\} \tag{2.2.16}$$

where P means path ordering[3] and $\mathcal{C}_{yz}$ is the path (more about gauge transporters for example in [38]). The transformation property of the gauge transporter is then given by

$$G'(x,y) = V(x)G(x,y)V^\dagger(y). \tag{2.2.17}$$

In this case x and y are points in the continuum. Assuming that our lattice is embedded in the continuum, we can choose $\mathcal{C}_{xy}$ as the path starting at $x_{cont} = ax_{lat}$ and ending at $a(x_{lat} + \hat{\mu})$. In this case the gauge transporter transforms in exactly the same way as the link variable $G'(ax_{lat}, a(x_{lat}+\hat{\mu})) = V(ax_{lat})G(ax_{lat}, a(x_{lat}+\hat{\mu}))V^\dagger(a(x_{lat}+\hat{\mu}))$. For this reason we interpret the link variable as a lattice version of the gauge transporter and write for the first order approximation

$$U_\mu(ax_{lat}) = G(ax_{lat}, a(x_{lat}+\hat{\mu})) + \mathcal{O}(a) = \exp(iagA_\mu(ax_{lat})). \tag{2.2.18}$$

The integral in formula (2.2.16) has been replaced by $aA_\mu(ax_{lat})$. This is true for the first order approximation where we defined the path as the straight line from the point ax_{lat} to $a(x_{lat}+\hat{\mu})$ and the length of the path is a.

We can recover the continuum from the lattice if we require $a \to 0$, i.e. we make the lattice finer and finer what is called the *naive* or *classical continuum limit*. When a is small enough we can expand expression (2.2.18) as

$$U_\mu(ax_{lat}) = \mathbb{1} + \mathrm{i}agA_\mu(ax_{lat}) + \mathcal{O}(a^2) \tag{2.2.19}$$

$$U_{-\mu}(ax_{lat}) = \mathbb{1} - \mathrm{i}agA_\mu(a(x_{lat}-\hat{\mu})) + \mathcal{O}(a^2). \tag{2.2.20}$$

Inserting this in (2.2.15) and setting $\psi(a(x_{lat} \pm \hat{\mu})) = \psi(ax_{lat}) + \mathcal{O}(a)$ and $A_\mu(a(x_{lat} - \hat{\mu})) = A_\mu(ax_{lat}) + \mathcal{O}(a)$ for small a we get the continuum fermion action (2.1.12) by setting $x_{cont} \equiv ax_{lat}$.

The action (2.2.15) is called *naive fermion action* and as the name suggests, it is not the final result. But before we go on working on the fermion action we will first derive the gauge action.

2.2.3. The lattice gauge action

Before it is possible to write down an adequate formula for the gluonic action on the lattice, we first have to find some gauge invariant objects which are constructed from link variables. Let us first have a look at the simplest construction made from links: a path. We assume that this path starts at the point x_0 and the first link points in direction μ_0. The second link then begins at $x_0 + \hat{\mu}_0 \equiv x_1$ pointing in direction μ_1 and so on. Figure 2.2.2 shows a possible path on a two dimensional lattice.

[3] Let $s \in [0,1]$ be the parameter describing the path $\mathcal{C}_{yz}$. We run from $s = 0$ at $x = y$ to $s = 1$ at $x = z$. Define the exponential in (2.2.16) as power series and order the matrices $A_\mu(x(s))$ in each term so that those with higher values of s stand to the right.

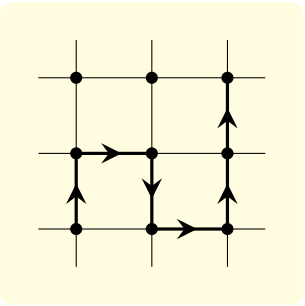

Figure 2.2.2.: Path on a lattice.

Now assume we have a set of k links forming a path $\mathcal{P}$. Then we can write the path as

$$P[U] = U_{\mu_0}(x_0)U_{\mu_1}(x_1)...U_{\mu_{k-1}}(x_{k-1}) \equiv \prod_{(x,\mu)\in\mathcal{P}} U_\mu(x). \tag{2.2.21}$$

The question is how this would behave under a gauge transformation. Let us look at a path which contains only two links and is given by $P[U] = U_{\mu_0}(x_0)U_{\mu_1}(x_1)$. Using transformation law (2.2.12) and $x_1 = x_0 + \hat{\mu}_0$ the expression becomes

$$\begin{aligned} P[U'] &= V(x_0)U_{\mu_0}(x_0)V^\dagger(x_0+\hat{\mu}_0)V(x_1)U_{\mu_1}(x_1)V^\dagger(x_1+\hat{\mu}_1) \\ &= V(x_0)U_{\mu_0}(x_0)U_{x_0+\hat{\mu}_0}(x_0+\hat{\mu}_0)V^\dagger(x_0+\hat{\mu}_0+\hat{\mu}_1). \end{aligned} \tag{2.2.22}$$

We see that the V's between the links cancel and only the two matrices at the end remain. This is true for longer paths as well and therefore a path with k links will transform like

$$P[U'] = V(x_0)U_{\mu_0}(x_0)U_{\mu_1}(x_1)...U_{\mu_{k-1}}(x_{k-1})V^\dagger(x_{k-1}+\hat{\mu}_{k-1}), \tag{2.2.23}$$

where

$$x_{k-1} + \hat{\mu}_{k-1} = x_0 + \hat{\mu}_0 + \hat{\mu}_1 + ... + \hat{\mu}_{k-2} + \hat{\mu}_{k-1}. \tag{2.2.24}$$

We can now turn the path into a closed loop by setting

$$x_0 = x_0 + \hat{\mu}_0 + \hat{\mu}_1 + ... + \hat{\mu}_{k-2} + \hat{\mu}_{k-1}. \tag{2.2.25}$$

Taking the trace of the loop the two remaining V's cancel and the trace of the loop becomes a gauge-invariant object.

To build the gauge action we look at the simplest loop on the lattice, shown in figure 2.2.3.

This construction is called *plaquette*. The plaquette $U_{\mu\nu}(x)$ is the product of four links and we write it as

$$\begin{aligned} U_{\mu\nu}(x) &= U_\mu(x)U_\nu(x+\hat{\mu})U_{-\mu}(x+\hat{\mu}+\hat{\nu})U_{-\nu}(x+\hat{\nu}) \\ &= U_\mu(x)U_\nu(x+\hat{\mu})U_\mu^\dagger(x+\hat{\nu})U_\nu^\dagger(x), \end{aligned} \tag{2.2.26}$$

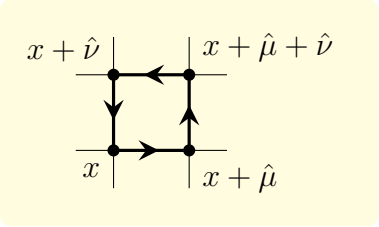

Figure 2.2.3.: The plaquette

where we used (2.2.14) in the second equation. The first lattice gauge action has been formulated by K. G. Wilson [45]. The Wilson gauge action involves a sum over all plaquettes where each plaquette is only counted with one orientation. The Wilson gauge action reads

$$\boxed{S_G[U] = \frac{\beta}{3} \sum_{x \in \Lambda} \sum_{\mu < \nu} \mathfrak{Re}\big[\, \mathrm{tr}[\mathbb{1} - U_{\mu\nu}(x)]\,\big]} \tag{2.2.27}$$

where the indices μ and ν are given by $1 \leq \mu < \nu \leq 4$ and the parameter β (*inverse coupling*) is related to the bare strong coupling g through

$$\beta = \frac{6}{g^2}. \tag{2.2.28}$$

In the naive limit $a \to 0$ we should also in this case recover the continuum gauge action. We do the same as in the fermion action calculation and expand the link variables from formula (2.2.18) for small a. With the help of the Baker-Campbell-Hausdorff formula

$$\exp(A)\exp(B) = \exp\left(A + B + \frac{1}{2}[A, B] + \dots\right) \tag{2.2.29}$$

one can calculate the plaquette up to second order. The resulting expression will contain gauge fields of the form $A_\nu(a(x_{lat} + \hat{\mu}))$. They are replaced by their Taylor expansion

$$A_\nu(a(x_{lat} + \hat{\mu})) = A_\nu(a x_{lat}) + a\partial_\mu A_\nu(a x_{lat}) + \mathcal{O}(a^2). \tag{2.2.30}$$

With all these replacements the continuum gauge action is recovered. A more detailed calculation is given in [21].

2.3. Fermion doubling problem and Wilson's fermion action

2.3.1. The Dirac operator

At the beginning of the last section we already mentioned that there will be some problems discretising the fermion action in the naive way. The problem is caused by

the so-called *fermion doubling*. To understand from where the trouble with the doublers comes, we first want to write the fermion action (2.2.15) as a quadratic form (which will be useful when we calculate the path integrals) and then look at its Fourier transform.

For simplicity we include only one flavour and write the most general action as

$$\boxed{S_F[\psi,\bar{\psi},U] = a^4 \sum_{x,y\in\Lambda} \sum_{a,b,\alpha,\beta} \bar{\psi}(x)_{a\alpha} D(x|y)_{a\alpha,b\beta} \psi(y)_{b\beta}} \tag{2.3.1}$$

where a, b are color and α, β are spin indices. $D(x|y)$ is called the *fermion matrix* or *lattice Dirac operator*. In the case of the naive action the fermion matrix reads

$$D(x|y)_{a\alpha,b\beta} = \sum_{\mu=1}^{4} (\gamma_\mu)_{\alpha\beta} \frac{U_\mu(x)_{ab}\delta_{x+\hat{\mu},y} - U_{-}\mu(x)_{ab}\delta_{x-\hat{\mu},y}}{2a} + m\delta_{\alpha\beta}\delta_{ab}\delta_{x,y}. \tag{2.3.2}$$

In the next section we will see what happens when we calculate the inverse of the Dirac operator.

2.3.2. Fermion doubling

When one wants to calculate the expectation value of an observable with the path integral formalism, then it turns out that we need the inverse of the Dirac operator. This is in general done numerically but in this section we want to show what happens when we calculate the inverse of the naive Dirac operator. Therefore we set all links $U_\mu(x) = \mathbb{1}$ which is called a trivial gauge configuration and the fermions are then non-interacting. The first step will be to calculate the Fourier transform of the Dirac operator, then doing the inversion and finally transform this result back.

First we define the momentum space lattice $\tilde{\Lambda}$ as the set

$$\begin{aligned} p = (p_1, p_2, p_3, p_4) \quad \text{where} \quad & p_\mu = \frac{2\pi}{aN_\mu}(k_\mu + \theta_\mu), \\ & k_\mu = -\frac{N_\mu}{2} + 1, \ldots, \frac{N_\mu}{2} \end{aligned} \tag{2.3.3}$$

and θ_μ is the known phase factor from equation (2.2.3). Using the abbreviation $\delta_{x,y} \equiv \delta_{x_1,y_1}\delta_{x_2,y_2}\delta_{x_3,y_3}\delta_{x_4,y_4}$ for the Kronecker delta we get the relations

$$\begin{aligned} \frac{1}{|\Lambda|} \sum_{p\in\tilde{\Lambda}} \mathrm{e}^{ip\cdot a(x-x')} &= \delta_{x,x'} \\ \frac{1}{|\Lambda|} \sum_{x\in\Lambda} \mathrm{e}^{i(p-p')\cdot ax} &= \delta_{k,k'} \equiv \delta_{p,p'} \end{aligned} \tag{2.3.4}$$

where $|\Lambda| = N_1 N_2 N_3 N_4$ is the volume of the lattice and $p \cdot x = \sum_{\mu=1}^{4} p_\mu x_\mu$ is the scalar product. The Fourier transform on the lattice is then defined as follows:

$$\begin{aligned} \tilde{f}(p) &= \frac{1}{\sqrt{|\Lambda|}} \sum_{x \in \Lambda} f(x) \mathrm{e}^{-ip \cdot ax}, \\ f(x) &= \frac{1}{\sqrt{|\Lambda|}} \sum_{p \in \tilde{\Lambda}} \tilde{f}(p) \mathrm{e}^{ip \cdot ax}. \end{aligned} \tag{2.3.5}$$

With this we write for the Fourier transform of the naive Dirac operator

$$\begin{aligned} \tilde{D}(p|q) &= \frac{1}{|\Lambda|} \sum_{x,y \in \Lambda} \mathrm{e}^{-ip \cdot ax} D(x|y) \mathrm{e}^{iq \cdot ay} \\ &= \delta_{p,q} \tilde{D}(p) \end{aligned} \tag{2.3.6}$$

with

$$\tilde{D}(p) = m\mathbb{1} + \frac{i}{a} \sum_{\mu=1}^{4} \gamma_\mu \sin(a \cdot p_\mu). \tag{2.3.7}$$

Here we considered the Fourier transform as a matrix similarity transformation $B = S^{-1}AS$ in the first line and used the complex conjugate phase factor for y. Then we applied the right phase factor to the Kronecker-delta terms in the action and used expression (2.3.4) for the delta function.

From the above equation we see that the fermion matrix in the Fourier space $\tilde{D}(p|q)$ is diagonal in momentum because of the delta function. For this reason it is enough to calculate the inverse of (2.3.7) and then transform it back to real space. With a formula[4] for the inverse of a linear combination of gamma matrices we get

$$\tilde{D}(p)^{-1} = \frac{m\mathbb{1} - ia^{-1} \sum_\mu \gamma_\mu \sin(a \cdot p_\mu)}{m^2 + a^{-2} \sum_\mu \sin(a \cdot p_\mu)^2}. \tag{2.3.8}$$

Transforming this back to real space one gets

$$\begin{aligned} D^{-1}(x|y) &= \frac{1}{|\Lambda|} \sum_{p,q \in \tilde{\Lambda}} \mathrm{e}^{ip \cdot ax} \tilde{D}^{-1}(p|q) \mathrm{e}^{-iq \cdot ay} \\ &= \frac{1}{|\Lambda|} \sum_{p,q \in \tilde{\Lambda}} \mathrm{e}^{ip \cdot ax} \delta_{p,q} \tilde{D}(p)^{-1} \mathrm{e}^{-iq \cdot ay} \\ &= \frac{1}{|\Lambda|} \sum_{p \in \tilde{\Lambda}} \tilde{D}(p)^{-1} \mathrm{e}^{ip \cdot a(x-y)}. \end{aligned} \tag{2.3.9}$$

[4]The inverse of a combination of gamma matrices with real numbers a and b_μ is

$$(a\mathbb{1} + i \sum_{\mu=1}^{4} \gamma_\mu b_\mu)^{-1} = \frac{a\mathbb{1} - i \sum_{\mu=1}^{4} \gamma_\mu b_\mu}{a^2 + \sum_{\mu=1}^{4} b_\mu^2}.$$

The quantity $D(x|y)^{-1}$ is called the *quark propagator*, which we will meet again in the next section about the path integral.

Now we want to analyse the Fourier quark propagator in more detail. To simplify the process we restrict ourselves to massless fermions with $m = 0$ in equation (2.3.8) and get

$$\tilde{D}_0(p)^{-1} = \frac{-ia^{-1}\sum_\mu \gamma_\mu \sin(a \cdot p_\mu)}{a^{-2}\sum_\mu \sin(a \cdot p_\mu)^2}. \tag{2.3.10}$$

In the continuum limit $a \to 0$ and fixed p the propagator becomes $-i\sum \gamma_\mu p_\mu / p^2$ and has a pole at

$$p = (0, 0, 0, 0). \tag{2.3.11}$$

The lattice situation is different. Because of the sine function in (2.3.10) we have also poles when one or more components of p are equal to $\pm\pi/a$. The definition of the lattice in momentum space, $\tilde{\Lambda}$, defines the components p_μ in the range $p_\mu = -\frac{\pi}{a} + \frac{2\pi}{N_\mu a}, \ldots, \frac{\pi}{a}$ for periodic boundary conditions. Therefore we can exclude the components equal to $-\pi/a$ but nevertheless we have some unphysical poles in the propagator at

$$p = (\tfrac{\pi}{a}, 0, 0, 0), (0, \tfrac{\pi}{a}, 0, 0), \ldots, (\tfrac{\pi}{a}, \tfrac{\pi}{a}, \tfrac{\pi}{a}, \tfrac{\pi}{a}). \tag{2.3.12}$$

These 15 unphysical poles are called *fermion doublers* and the next step will be to remove them from the theory.

2.3.3. Wilson fermion action

The idea is to keep the pole at $(0, 0, 0, 0)$ and to remove the other 15 unwanted poles. This was done the first time by Wilson, who added an additional term to (2.3.7):

$$\tilde{D}(p) = m\mathbb{1} + \frac{i}{a}\sum_{\mu=1}^{4} \gamma_\mu \sin(a \cdot p_\mu) + \mathbb{1}\frac{1}{a}\sum_{\mu=1}^{4}(1 - \cos(a \cdot p_\mu)). \tag{2.3.13}$$

The third summand is the Wilson term in momentum space. It vanishes for the physical pole at $(0, 0, 0, 0)$ and for the other poles it gives an extra contribution $\frac{2}{a}$ for each component $p_\mu = \frac{\pi}{a}$. Therefore we can understand the Wilson term as an extra mass term which gives the doublers the mass $m_{tot} = m + \frac{2l}{a}$ where l is the number of p_μ's with $p_\mu = \frac{\pi}{a}$. We see that in the continuum limit $a \to 0$ the doublers get infinitely heavy and decouple from the theory. For massless fermions the inverse Wilson momentum propagator reads

$$\tilde{D}_0(p)^{-1} = \frac{\mathbb{1}a^{-1}\sum_{\mu=1}^{4}(1 - \cos(a \cdot p_\mu)) - ia^{-1}\sum_\mu \gamma_\mu \sin(a \cdot p_\mu)}{a^{-2}(\sum_{\mu=1}^{4}(1 - \cos(a \cdot p_\mu)))^2 + a^{-2}\sum_{\mu=1}^{4}\sin(a \cdot p_\mu)^2}. \tag{2.3.14}$$

This expression has now the desired properties. We get the Wilson term in real space by transforming $\mathbb{1}\frac{1}{a}\sum_{\mu=1}^{4}(1-\cos(a\cdot p_\mu))$ back and making it gauge invariant:

$$-a\sum_{\mu=1}^{4}\frac{U_\mu(x)_{ab}\delta_{x+\hat{\mu},y}-2\delta_{ab}\delta_{x,y}+U_{-\mu}(x)_{ab}\delta_{x-\hat{\mu},y}}{2a^2}. \tag{2.3.15}$$

Because of the prefactor a the Wilson term vanishes in the classical continuum limit of the lattice action. Combining it with the naive fermion action we get the final result for Wilson's Dirac operator

$$\boxed{D^{(f)}(x|y)_{(a,\alpha)(b,\beta)}=\big(m^{(f)}+\frac{4}{a}\big)\delta_{\alpha\beta}\delta_{ab}\delta_{x,y}-\frac{1}{2a}\sum_{\mu=\pm1}^{\pm4}(\mathbb{1}-\gamma_\mu)_{\alpha\beta}U_\mu(x)_{ab}\delta_{x+\hat{\mu},y},} \tag{2.3.16}$$

where we used the definition

$$\gamma_{-\mu}=-\gamma_\mu \quad \text{for} \quad \mu=1,2,3,4. \tag{2.3.17}$$

Finally the most general expression for the fermion action is

$$\boxed{S_F[\psi,\bar{\psi},U]=\sum_{f=1}^{N_f}a^4\sum_{x,y\in\Lambda}\sum_{a,b,\alpha,\beta}\bar{\psi}^{(f)}(x)_{a\alpha}D^{(f)}(x|y)_{a\alpha,b\beta}\psi^{(f)}(y)_{b\beta}.} \tag{2.3.18}$$

2.3.4. Clover improvement

The correction terms for the fermionic action are of order a but for the gauge action they are of order a^2. It would be desirable to have corrections of order a^2 also for the fermionic action. This can be achieved by the Symanzik improvement programme. The idea is to add certain terms to the fermion action such that the correction terms cancel to the requested order. In the case of the Wilson action the so-called *clover term*, which was written down the first time by Sheikholeslami and Wohlert [42], is added:

$$S_{clover}=c_{sw}a^5\sum_{x\in\Lambda}\sum_{\mu<\nu}\bar{\psi}(x)\frac{1}{2}\sigma_{\mu\nu}\hat{F}_{\mu\nu}(x)\psi(x). \tag{2.3.19}$$

Here c_{sw} is the *Sheikholeslami-Wohlert* or *clover coefficient* and $\hat{F}_{\mu\nu}(x)$ is defined as

$$\hat{F}_{\mu\nu}(x)=-\frac{i}{8a^2}(Q_{\mu\nu}(x)-Q_{\nu\mu}(x)) \tag{2.3.20}$$

with

$$Q_{\mu\nu}(x)=U_{\mu\nu}(x)+U_{\nu-\mu}(x)+U_{-\mu-\nu}(x)+U_{-\nu\mu}(x). \tag{2.3.21}$$

The clover coefficient can be determined non-perturbatively [28], e.g., using the Schrödinger functional.

3. The path integral on the lattice

In this chapter we will first define the Euclidean correlator. Then we will have a closer look at the path integral formalism and the numerical concepts for calculating these path integrals.

From now on the lattice spacing will be set to $a = 1$ for simplicity, unless stated otherwise.

3.1. The Euclidean correlator

We define the Euclidean correlator of $O_1(t_1)$ and $O_2(t_2)$ for times $t_1 = 0$ and $t_2 = t$ by

$$\boxed{\langle O_2(t)O_1(0)\rangle_T = \frac{1}{Z_T}\mathrm{tr}\left[\mathrm{e}^{-(T-t)\hat{H}}\hat{O}_2\mathrm{e}^{-t\hat{H}}\hat{O}_1\right]} \tag{3.1.1}$$

with the partition function

$$Z_T = \mathrm{tr}\left[\mathrm{e}^{-T\hat{H}}\right]. \tag{3.1.2}$$

The quantities O_1 and O_2 in (3.1.1) are usually interpolating fields for one or more particles and $\hat{O}_1$ and $\hat{O}_2$ are the corresponding operators in Hilbert space. Then one can create a state at $t_1 = 0$ and to annihilate it at $t_2 = t$. The Hamilton operator $\hat{H}$ is a self-adjoint operator and governs the time evolution. The Euclidean time parameters t and T are real and positive. The parameter t is the time difference between two events, for example the creation and annihilation of a particle, and T will correspond to the time extent of our lattice, which should be sufficiently large.

To compute expressions (3.1.1) and (3.1.2) we use the representation of the unit operator as a sum over a complete orthonormal basis

$$\mathbb{1} = \sum_n |e_n\rangle\langle e_n| \tag{3.1.3}$$

and the definition of the trace of an operator

$$\mathrm{tr}\big[\hat{O}\big] = \sum_n \langle e_n|\hat{O}|e_n\rangle. \tag{3.1.4}$$

The most natural choice of the basis vectors are the eigenstates $|n\rangle$ of the Hamilton operator

$$\hat{H}|n\rangle = E_n|n\rangle, \tag{3.1.5}$$

where the eigenvalue E_n refers to the energy of the system. The state $|0\rangle$ corresponds to the vacuum and we assume that the energies are obey $E_0 < E_1 \leq E_2 \leq \ldots$. For calculating the partition function Z_T we use the trace formula, write the exponential as a power series and get

$$Z_T = \sum_n \langle n|\mathrm{e}^{-T\hat{H}}|n\rangle = \sum_n \mathrm{e}^{-TE_n}. \tag{3.1.6}$$

For the complete correlation function (3.1.1) we use again (3.1.4) and write it as

$$\langle O_2(t)O_1(0)\rangle_T = \frac{1}{Z_T}\sum_{m,n}\langle m|\mathrm{e}^{-(T-t)\hat{H}}\hat{O}_2|n\rangle\langle n|\mathrm{e}^{-t\hat{H}}\hat{O}_1|m\rangle. \tag{3.1.7}$$

We let now $\hat{H}$ act on $\langle n|$ and $\langle m|$ and get factors of e^{-tE_n} and $\mathrm{e}^{-(T-t)E_m}$, respectively. Thus we can write

$$\langle O_2(t)O_1(0)\rangle_T = \frac{\sum_{m,n}\langle m|\hat{O}_2|n\rangle\langle n|\hat{O}_1|m\rangle\mathrm{e}^{-t\Delta E_n}\mathrm{e}^{-(T-t)\Delta E_m}}{1+\mathrm{e}^{-T\Delta E_1}+\mathrm{e}^{-T\Delta E_2}+\ldots} \tag{3.1.8}$$

with the definition

$$\Delta E_n = E_n - E_0. \tag{3.1.9}$$

This means that the energies we measure for the ground and excited states are strictly speaking the energy differences between the states and the vacuum. To obtain the final result we define $E_0 = 0$, so that $\Delta E_n \equiv E_n$ and let T go to infinity. In this case all exponential terms in the denominator vanish. The term $\mathrm{e}^{-(T-t)\Delta E_m}$ in the numerator is equal to one when $\Delta E_m = 0$ and zero for all other energies if $T \to \infty$. What remains is

$$\boxed{\lim_{T\to\infty}\langle O_2(t)O_1(0)\rangle_T = \sum_n \langle 0|\hat{O}_2|n\rangle\langle n|\hat{O}_1|0\rangle\mathrm{e}^{-tE_n}.} \tag{3.1.10}$$

This is one key equation in lattice QCD when we want to calculate particle energies. It describes the correlator as a sum of matrix elements multiplied by the exponentials of the corresponding energy. For a specific particle p we may choose $\hat{O}_1 = \hat{O}_p^\dagger$ as its creation operator and $\hat{O}_2 = \hat{O}_p$ as the annihilator. Then equation (3.1.10) becomes

$$\lim_{T\to\infty}\langle O_2(t)O_1(0)\rangle_T = |\langle p|\hat{O}_p^\dagger|0\rangle|^2\mathrm{e}^{-tE_p} + |\langle p'|\hat{O}_p^\dagger|0\rangle|^2\mathrm{e}^{-tE_p'} + \ldots \tag{3.1.11}$$

where $|p\rangle, |p'\rangle, \ldots$ describe the ground and excited states. Because the excited states have a higher energy eigenvalue than the ground state, they are exponentially suppressed and we can truncate the sum (3.1.11) after the first one or two terms and use it as a fit function for the correlator, which we can calculate numerically using the path integral technique.

3.2. Calculating the path integral

The Euclidean correlator, defined in equation (3.1.1), can also be written as a path integral:

$$\langle O_2(t)O_1(0)\rangle_T = \frac{1}{Z_T}\int \mathcal{D}[\psi,\bar{\psi},U]\mathrm{e}^{-S_F[\psi,\bar{\psi},U]-S_G[U]}O_2[\psi,\bar{\psi},U,t]O_1[\psi,\bar{\psi},U,t=0]. \tag{3.2.1}$$

To evaluate this kind of integral let us look at the expectation value of an observable O, where O can be an arbitrary function of the field variables, which is given as the path integral over the quark fields $\psi(x)$ and $\bar{\psi}(x)$ and the link variables $U_\mu(x)$

$$\boxed{\langle O\rangle = \frac{1}{Z}\int \mathcal{D}[\psi,\bar{\psi},U]\mathrm{e}^{-S_F[\psi,\bar{\psi},U]-S_G[U]}O[\psi,\bar{\psi},U].} \tag{3.2.2}$$

The *partition function* Z is defined as

$$\boxed{Z = \int \mathcal{D}[\psi,\bar{\psi},U]\mathrm{e}^{-S_F[\psi,\bar{\psi},U]-S_G[U]}.} \tag{3.2.3}$$

The expression $\mathcal{D}[\psi,\bar{\psi},U]$ is a shorthand notation for the measure

$$\mathcal{D}[\psi,\bar{\psi},U] = \prod_{x\in\Lambda}\prod_{\mu=1}^{4}\prod_{i=1}^{N}\mathrm{d}U_\mu(x)\mathrm{d}\bar{\psi}_i(x)\mathrm{d}\psi_i(x), \tag{3.2.4}$$

which is a product over all lattice sites, link directions and the number N of fermion fields. Now we separate (3.2.2) in a fermion and a gauge part. The reason is that we can integrate the fermion part by hand and evaluate the remaining gauge part numerically. We define the fermion expectation value of O as

$$\langle O\rangle_F[U] = \frac{1}{Z_F[U]}\int \mathcal{D}[\psi,\bar{\psi}]\mathrm{e}^{-S_F[\psi,\bar{\psi},U]}O[\psi,\bar{\psi},U] \tag{3.2.5}$$

where $O[\psi,\bar{\psi},U]$ is an arbitrary function of the fermion fields and the link variables and Z_F is the fermionic partition function or *fermion determinant*

$$Z_F[U] = \int \mathcal{D}[\psi,\bar{\psi}]\mathrm{e}^{-S_F[\psi,\bar{\psi},U]}. \tag{3.2.6}$$

The remaining integral over the gauge fields is then

$$\langle O\rangle = \frac{1}{Z_G}\int \mathcal{D}[U]\mathrm{e}^{-S_G[U]}Z_F[U]\langle O\rangle_F[U] \tag{3.2.7}$$

with

$$Z_G = \int \mathcal{D}[U]\mathrm{e}^{-S_G[U]}Z_F[U]. \tag{3.2.8}$$

Fermions have to obey Fermi statistics. This means that ψ and $\bar{\psi}$ in (3.1.1) are so-called *Grassmann numbers* or anticommuting variables. For the calculation of the fermionic path integral we first consider a Grassmann algebra with $2N$ generators $\psi_1, \ldots, \psi_N$ and $\bar{\psi}_1, \ldots, \bar{\psi}_N$ and $M = M_{ij}$ should be a complex $N \times N$ matrix. The Matthews-Salam formula yields a result for an integral similar to the fermionic partition function:

$$\int \mathrm{d}\psi_N \mathrm{d}\bar{\psi}_N \ldots \mathrm{d}\psi_1 \mathrm{d}\bar{\psi}_1 \, \mathrm{e}^{\sum_{i,j=1}^{N} \bar{\psi}_i M_{ij} \psi_j} = \det[M]. \tag{3.2.9}$$

Comparing the fermionic action (2.3.18) with the exponent of the above formula one gets an additional minus sign, but we can put this into the definition of M using $M = -D$ and D is the Dirac operator. With this replacement the fermionic partition function becomes

$$\boxed{Z_F = \det[-D]} \tag{3.2.10}$$

which justifies the name fermion determinant for Z_F.

The second important formula we want to present is *Wick's theorem* where the i_k's and j_k's are multi-indices for colour, spin and space-time:

$$\begin{aligned} \langle \psi_{i_1} \bar{\psi}_{j_1} \ldots \psi_{i_n} \bar{\psi}_{j_n} \rangle = & \\ &= \frac{1}{Z_F} \int \mathrm{d}\psi_1 \mathrm{d}\bar{\psi}_1 \ldots \mathrm{d}\psi_N \mathrm{d}\bar{\psi}_N \; \psi_{i_1} \bar{\psi}_{j_1} \ldots \psi_{i_n} \bar{\psi}_{j_n} \, \mathrm{e}^{\sum_{k,l=1}^{N} \bar{\psi}_k M_{kl} \psi_l} \\ &= (-1)^n \sum_{P(1,2,\ldots,n)} \mathrm{sign}(P) (M^{-1})_{i_1 j_{P_1}} (M^{-1})_{i_2 j_{P_2}} \ldots (M^{-1})_{i_N j_{P_N}}. \end{aligned} \tag{3.2.11}$$

Here the expression $P(1, 2, \ldots, n)$ denotes a permutation of the numbers $1, 2, \ldots, n$ and $\mathrm{sign}(P)$ is the sign of the permutation. Due to this formula we can consider the n-point function as the expectation value of a product of Grassmann numbers. From (3.2.11) we get the expression for the *quark propagator*:

$$\begin{aligned} \langle \psi_{i_1} \bar{\psi}_{j_1} \rangle &= \frac{1}{Z_F} \int \mathrm{d}\psi_1 \mathrm{d}\bar{\psi}_1 \ldots \mathrm{d}\psi_N \mathrm{d}\bar{\psi}_N \; \psi_{i_1} \bar{\psi}_{j_1} \, \mathrm{e}^{\sum_{k,l=1}^{N} \bar{\psi}_k M_{kl} \psi_l} \\ &= (-1) \cdot (M^{-1})_{i_1 j_1} = D^{-1}. \end{aligned} \tag{3.2.12}$$

Looking at equation (2.3.18) and replacing the multi-index by colour, spin and space-time indices the quark propagator reads

$$\boxed{\langle \psi(x)_{a\alpha} \bar{\psi}(y)_{b\beta} \rangle = D^{-1}(x|y)_{a\alpha, b\beta}.} \tag{3.2.13}$$

With all these results we can write down the final formula for the expectation value of an observable $\langle O \rangle$ in equation (3.2.2) after integrating out the fermionic part. Assuming that we have N_f flavours we get

$$\boxed{\langle O \rangle = \frac{1}{Z} \int \mathcal{D}[U] \mathrm{e}^{-S_G[U]} \Big(\prod_{f=1}^{N_f} \det[D_f] \Big) F[D_f^{-1}]} \tag{3.2.14}$$

with

$$\boxed{Z = \int \mathcal{D}[U] \mathrm{e}^{-S_G[U]} \Big(\prod_{f=1}^{N_f} \det[D_f] \Big)} \tag{3.2.15}$$

and F is some function containing the quark propagators.

3.3. Numerical evaluation of the path integral

Expression (3.2.14) can now be evaluated numerically using Monte Carlo integration techniques. The most expensive part of this task is the inclusion of the fermion determinants $\det[D_f]$ containing the sea quarks. In former times supercomputers were much less powerful and the consideration of the determinant was either infeasible or took too much computing time. Therefore the fermion determinant was set to $\det[D_f] = 1$, the so-called *quenched approximation*. In this case the sea quark mass is infinite and there is no production of quark-antiquark pairs from the vacuum. The valence quark mass contained in $F[D_f^{-1}]$ remains finite. In the quenched theory the hadrons cannot decay and the observation of resonances is not directly possible.

With today's supercomputers it is possible to include the effect of the fermion determinant in the path integral which is called *dynamical simulation*. We will shortly explain the technique of Monte Carlo integration following [21, 13].

3.3.1. Monte Carlo integration

Assume that the expectation value $\langle f \rangle$ of some function $f(\vec{x})$ is given by the integral

$$\langle f \rangle = \int_G \mathrm{d}^D x \, f(\vec{x}). \tag{3.3.1}$$

To calculate $\langle f \rangle$ numerically we can randomly generate a set of N_p independent vectors $\vec{x}^0, \vec{x}^1, \ldots, \vec{x}^{N_p-1}$. Assuming that $\int_G \mathrm{d}^D x = 1$ we get the estimate $E(f)$ of the integral (assuming that the data is uncorrelated)

$$E(f) = \frac{1}{N_p} \sum_{i=0}^{N_p-1} f(\vec{x}^i) \tag{3.3.2}$$

with the variance

$$\sigma_f^2 = \frac{1}{N_p - 1} \sum_{i=0}^{N_p-1} \Big(f(\vec{x}^i) - E(f) \Big)^2. \tag{3.3.3}$$

The final result is $E(f) \pm \sigma_f / \sqrt{N_p}$. This is Monte Carlo in its simplest form.

The points $\vec{x}_i$ that we get in simple Monte Carlo are distributed uniformly over the whole integration region. But if the function $f(\vec{x})$ has some significant weight in a

subregion we waste a lot of time for evaluating "uninteresting" points. A solution is using so-called *importance sampling* where we introduce a weight function $w(\vec{x}) > 0$ which should approximate $f(\vec{x})$ in the interesting region. We define the probability distribution

$$p(\vec{x}) = \frac{w(\vec{x})}{\int_G \mathrm{d}^D x w(\vec{x})} \tag{3.3.4}$$

satisfying $\int_G \mathrm{d}^D x\, p(\vec{x}) = 1$. Setting $h(\vec{x}) = f(\vec{x})/p(\vec{x})$ the integral becomes

$$\int_G \mathrm{d}^D x f(\vec{x}) = \int_G \mathrm{d}^D x\, h(\vec{x}) p(\vec{x}) \approx \frac{1}{N_p} \sum_{i=0}^{N_p - 1} h(\vec{x}^i). \tag{3.3.5}$$

The vectors $\vec{x}^i$ are then generated with the probability distribution $p(\vec{x})$. From the form of equation (3.2.14) we see that the path integral is suited for importance sampling. In the quenched approximation the probability density p is then

$$p(U) = \frac{\mathrm{e}^{-S_G[U]}}{\int \mathcal{D}[U] \mathrm{e}^{-S_G[U]}} \tag{3.3.6}$$

where $\mathrm{e}^{-S_G[U]}$ is the weight factor and the expectation value of an observable is

$$\langle O \rangle \approx \frac{1}{N} \sum_{n=1}^{N} O[U_n] \tag{3.3.7}$$

for a set of N gauge configurations $\{U_n\}$. For generating gauge fields and calculating observables one can use a software package like for example Chroma [18]. One first generates and saves the gauge configurations and later they can be read in again by the program for calculating the observables.

3.3.2. Markov chains and Metropolis algorithm

The idea of Markov chains is to produce configurations by a stochastic sequence $U_0 \to U_1 \to \ldots$ starting with some arbitrary configuration U_0. Stepping from one configuration U_i to the subsequent one U_{i+1} is called Markov step and the transition probability is denoted by

$$T(U_{i+1} = U' | U_i = U) = T(U'|U) \tag{3.3.8}$$

which is the probability to get U' when starting with U. Furthermore the probability for reaching U' at a given step has to be the same as the probability for leaving U'. As a consequence the system reaches an equilibrium state after a large enough number of Markov steps.

The Metropolis algorithm can be used to construct such a Markov chain. The goal is to reach the equilibrium distribution $p(U)$ given in (3.3.6). Therefore we choose a new

configuration U' with some given a priori selection probability $T_0(U'|U)$ and we accept U' as next element in the Markov chain with the probability

$$T_{accept}(U'|U) = \min\Big(1, \frac{T_0(U|U')p(U')}{T_0(U'|U)p(U)}\Big). \tag{3.3.9}$$

Often one chooses $T_0(U|U') = T_0(U'|U)$ and the two factors cancel in the above equation. After reaching equilibrium the configurations are generated with the desired probability. It is clear that subsequent configurations in the Markov chain are highly correlated. For the calculation of observables one does the following: In a first step the starting configuration is updated until it reaches equilibrium. Then after doing a "measurement" with the first configuration (or storing it) one does again a number of updates before the next measurement to reduce autocorrelations.

For dynamical fermions one has also to include the determinant $\det[D_f]$ in (3.2.14). Because a direct calculation of the determinant is not possible one treats it as an additional contribution to the gauge action, the so-called *effective fermion action*. We write the determinant as an exponential and get

$$S_F^{eff} = -\mathrm{tr}(\ln(D)) \tag{3.3.10}$$

where $\det[D]$ is assumed as real and positive. With two degenerate flavours u, d for example we can achieve this by writing $\det[D_u]\det[D_d] = \det[D_u D_u^\dagger]$. With $D = D_u D_u^\dagger$ we have the desired property. Then $S_G(U)$ in (3.3.6) is replaced by $S_G(U) + S_F^{eff}(U)$. For updating the configurations one uses the *hybrid Monte Carlo* algorithm which includes a non-local updating process. More about hybrid Monte Carlo can be found in [21, 36, 41, 15].

4. Mesons on the lattice

In this chapter we will show how to describe a meson with given quantum numbers by an appropriate interpolator. The next section then explains how to calculate the quark propagator efficiently using a specific source and how to get a better overlap with the physical state by smearing the source. The last section will deal with the question how to extract the energies from the meson correlator and how the technique can be improved for getting higher energy levels.

4.1. Meson interpolators

Mesons are particles containing a quark and an anti-quark. Our goal is to calculate meson correlation functions and extract the energies. Therefore we bring equation (3.1.10) into the form

$$\begin{aligned}\langle O(t)\bar{O}(0)\rangle &= \sum_n \langle 0|\hat{O}|n\rangle\langle n|\hat{O}^\dagger|0\rangle \mathrm{e}^{-tE_n} \\ &= A\mathrm{e}^{-tE_0}(1+\mathrm{O}(\mathrm{e}^{-t\Delta E}))\end{aligned} \tag{4.1.1}$$

where $\Delta E = E_1 - E_0$ is the energy difference between the first excited and the ground state. The quantities O and $\bar{O}$ are so-called *meson interpolators*. They represent fields with the desired quantum numbers. The operators $\hat{O}^\dagger$ and $\hat{O}$ are the corresponding Hilbert space operators and create/annihilate the meson.

The quantum numbers characterising a certain meson are the total angular momentum $J = L + S$, which is the sum of the orbital angular momentum L and the total spin S, the parity P and the C parity. They are often displayed as J^{PC}. In addition, the flavour content is represented by the isospin (for u and d quarks), strangeness (for s quarks) etc. The charge conjugation transforms particles into antiparticles. The behaviour of fermion and gauge fields under this transformation is given by:

$$\begin{aligned}\psi(x) &\rightarrow C^{-1}\bar{\psi}^T(x) \\ \bar{\psi}(x) &\rightarrow -\psi^T(x)C \\ U_\mu(x) &\rightarrow U_\mu^*(x)\end{aligned} \tag{4.1.2}$$

where T denotes the transpose and * the complex conjugate. The charge conjugation matrix C is defined by the equation

$$C^{-1}\gamma_\mu^T C = -\gamma_\mu. \tag{4.1.3}$$

Applying a parity transformation sends $(\vec{x}, t)$ to $(-\vec{x}, t)$. The fermions and gauge fields then change like

$$\begin{aligned} \psi(\vec{x},t) &\rightarrow \gamma_4\psi(-\vec{x},t) \\ \bar{\psi}(\vec{x},t) &\rightarrow \bar{\psi}(-\vec{x},t)\gamma_4 \\ U_i(\vec{x},t) &\rightarrow U_{-i}(-\vec{x},t) \\ U_4(\vec{x},t) &\rightarrow U_4(-\vec{x},t). \end{aligned} \tag{4.1.4}$$

Note that the behaviour of links in space and time direction is different under a parity transformation. The following formula [2] relates the parity to the angular momentum of a meson:

$$P = (-1)^{L+1}. \tag{4.1.5}$$

A general expression for a meson interpolator $O(\vec{x}, \vec{y}, t)$ reads:

$$O^i(\vec{x},\vec{y},t) = \bar{\psi}^{f_1}_{a\alpha}(\vec{x},t)\Gamma^{\alpha\beta}_{ab}(\vec{x},\vec{y})F^i_{f_1f_2}\psi^{f_2}_{b\beta}(\vec{y},t), \tag{4.1.6}$$

where we used α, β for Dirac indices, a, b for colour, f_1, f_2 for flavour and i denotes a definite isospin state. The matrix Γ can be an arbitrary gauge invariant product of gamma matrices and link fields. This construction allows us to place the quark and anti-quark contained in the meson on different lattice sites, which is a more realistic description of a meson. Another possibility is to start from a pointlike interpolator at one lattice site and then extend it by using a smearing function. We will use the second version in this work and explain later, how point sources and smearing functions are defined.

When using pointlike interpolators, Γ contains only gamma matrices γ_μ and is diagonal in space and colour:

$$\Gamma^{\alpha\beta}_{ab}(\vec{x},\vec{y}) = \delta_{\vec{x},\vec{y}}\delta_{ab}M_{\alpha\beta}, \tag{4.1.7}$$

where M is a product of γ_μ's. Table 4.1.1 (from [21]) gives an overview of the relation between the gamma content of the meson and the J^{PC} quantum number.

state	J^{PC}	Γ	particles
scalar	0^{++}	$\mathbb{1}, \gamma_4$	$f_0, a_0, K_0^*, \ldots$
pseudoscalar	0^{-+}	$\gamma_5, \gamma_4\gamma_5$	$\pi^\pm, \pi^0, \eta, \ldots$
vector	1^{--}	$\gamma_i, \gamma_4\gamma_i$	$\rho^\pm, \rho^0, \omega, K^*, \ldots$
axial-vector	1^{+-}	$\gamma_i\gamma_5$	$a_1, f_1, \ldots$
tensor	1^{++}	$\gamma_i\gamma_j$	$h_1, b_1, \ldots$

Table 4.1.1.: Overview of the gamma matrix content for some meson interpolators.

The *flavour or isospin matrix* $F^i_{f_1 f_2}$ contained in (4.1.6) determines the quark content of the meson and thus which particle we have. In the case of the pions which we are interested in, the flavour matrices are given by the three Pauli matrices

$$\sigma^1 = \begin{pmatrix} 0 & 1 \\ 1 & 0 \end{pmatrix} \quad \sigma^2 = \begin{pmatrix} 0 & -i \\ i & 0 \end{pmatrix} \quad \sigma^3 = \begin{pmatrix} 1 & 0 \\ 0 & -1 \end{pmatrix}. \tag{4.1.8}$$

Defining the quark field as

$$\psi_{a\alpha} = \begin{pmatrix} u \\ d \end{pmatrix}_{a\alpha} \tag{4.1.9}$$

we get three pions $\pi^i, i = 1, 2, 3$,

$$\pi^i = \bar{\psi}\gamma_5 F^i \psi, \tag{4.1.10}$$

where we set $F^i = \sigma^i$ and omitted the Dirac and colour indices for simplicity. Combining them correctly gives us the well-known pions π^+, π^- and π^0:

$$\frac{1}{2}(\pi^1 + i \cdot \pi^2) \equiv \pi^- \tag{4.1.11a}$$

$$\frac{1}{2}(\pi^1 - i \cdot \pi^2) \equiv \pi^+ \tag{4.1.11b}$$

$$\frac{1}{\sqrt{2}} \cdot \pi^3 \equiv \pi^0. \tag{4.1.11c}$$

The rho mesons can be constructed in the same way, the only difference is a γ_i instead of γ_5 in the interpolator (4.1.10).

Meson	Isospin	J^{PC}	quark content
π^+	$I = 1, I_z = 1$	0^-	$\bar{d}\gamma_5 u$
π^-	$I = 1, I_z = -1$	0^-	$\bar{u}\gamma_5 d$
π^0	$I = 1, I_z = 0$	0^{-+}	$\frac{1}{\sqrt{2}}(\bar{u}\gamma_5 u - \bar{d}\gamma_5 d)$
ρ^+	$I = 1, I_z = 1$	1^-	$\bar{d}\gamma_i u$
ρ^-	$I = 1, I_z = -1$	1^-	$\bar{u}\gamma_i d$
ρ^0	$I = 1, I_z = 0$	1^{--}	$\frac{1}{\sqrt{2}}(\bar{u}\gamma_i u - \bar{d}\gamma_i d)$

Table 4.1.2.: The pi and rho mesons.

At this point we want to give the meson 2-point function as a simple example. We define the correlation function of two meson interpolators m', m''

$$\begin{aligned} &\langle m'(\vec{x}_1, t) m''(\vec{x}_2, 0)\rangle \\ &\quad = \langle \bar{\psi}_{\alpha_1 f_1'}(\vec{x}_1, t) \Gamma'_{\alpha_1\beta_1} F'_{f_1' g_1'} \psi_{\beta_1 g_1'}(\vec{x}_1, t) \bar{\psi}_{\alpha_2 f_2''}(\vec{x}_2, 0) \Gamma''_{\alpha_2\beta_2} F''_{f_2'' g_2''} \psi_{\beta_2 g_2''}(\vec{x}_2, 0)\rangle \end{aligned} \tag{4.1.12}$$

with Dirac indices α, β and flavour indices f, g. We did not explicitly write out the sums over all indices. We have assumed that Γ', Γ'' only contain gamma matrices and therefore omitted the colour indices. To simplify the calculation of (4.1.12) we introduce multi-indices A, B for spin, flavour and position. We define $\psi, \bar{\psi}$ and the quark propagator G as

$$\begin{aligned} \psi(A) = \psi_{\alpha f}(\vec{x}, t_a), \quad \bar{\psi}(B) = \bar{\psi}_{\beta g}(\vec{y}, t_b), \\ \Gamma_{AB} = \Gamma_{\alpha\beta}, \quad F_{AB} = F_{fg}, \\ \psi(\underbrace{B)\bar{\psi}(}A) = G(B, A) = \delta_{fg} G_{\beta\alpha}(\vec{y}, t_b | \vec{x}, t_a). \end{aligned} \tag{4.1.13}$$

The Kronecker delta comes from the fact that only contractions of quarks with the same flavour are non-zero. For the 2-point function we get

$$\Gamma'_{A_1B_1}\Gamma''_{A_2B_2}F'_{A_1B_1}F''_{A_2B_2}\langle\bar{\psi}(A_1)\psi(B_1)\bar{\psi}(A_2)\psi(B_2)\rangle \tag{4.1.14}$$

$$\begin{aligned} = \Gamma'_{A_1B_1}\Gamma''_{A_2B_2}F'_{A_1B_1}F''_{A_2B_2}\langle &\psi(\underbrace{B_1)\bar{\psi}(}A_1)\psi(\underbrace{B_2)\bar{\psi}(}A_2) \\ &-\psi(\underbrace{B_1)\bar{\psi}(}A_2)\psi(\underbrace{B_2)\bar{\psi}(}A_1)\rangle_g \end{aligned} \tag{4.1.15}$$

$$\begin{aligned} = \langle &-\mathrm{tr}(F'F'')\mathrm{tr}_{DC}(G(\vec{x}_1, t|\vec{x}_2, 0)\Gamma''G(\vec{x}_2, 0|\vec{x}_1, t)\Gamma') \\ &+\mathrm{tr}(F')\mathrm{tr}(F'') \cdot \mathrm{tr}_{DC}(G(\vec{x}_1, t|\vec{x}_1, t)\Gamma') \cdot \mathrm{tr}_{DC}(G(\vec{x}_2, 0|\vec{x}_2, 0)\Gamma'')\rangle_g. \end{aligned} \tag{4.1.16}$$

Here $\langle\cdots\rangle_g$ denotes the integration over the gauge fields and tr_{DC} is the trace over Dirac and colour indices. The second term in the last expression is the so-called quark-line *disconnected part*.

4.2. Sources and smearing

In the previous chapter we saw that calculating the quark propagator is equivalent to inverting the Dirac operator D. The lattice Dirac operator is a huge matrix of size $(N_c \times N_s \times V)^2$ where $V = N \times N \times N \times N_T$ is the volume of the lattice. The resulting quark propagator describes a quark travelling from one lattice site x to another site y on one configuration. Thereby x and y run over the whole lattice which means that the quark propagates from every site to every site. This propagator is called an *all-to-all propagator*. Inverting the full D takes too much time and computer memory. A practicable solution is the calculation of a *point-to-all propagator*. This means that now the quark travels from one fixed point x_0 to any other point x on the lattice. We get the point-to-all propagator by multiplying the full propagator with a so-called *point source* S,

$$D^{-1}(x|x_0)_{a\alpha,a_0\alpha_0} = \sum_{y,b,\beta} D^{-1}(x|y)_{a\alpha,b\beta} S(y|x_0)_{b\beta,a_0\alpha_0}, \tag{4.2.1}$$

and the point source sitting at the lattice site x_0, a_0, α_0 is defined as

$$S(y|x_0)_{b\beta,a_0\alpha_0} = \delta_{ba_0}\delta_{\beta\alpha_0}\delta_{y,x_0}. \tag{4.2.2}$$

The point source picks out just one column of the all-to-all propagator which is the resulting point-to-all propagator. Because of the three colour and four spin components there are 12 possible combinations to create a point source for fixed x_0. The point-to-all propagator is usually calculated for all 12 sources. Note that $D^{-1}(x|x_0)$ in (4.2.1) is to be identified with $G(x|x_0)$. Using matrix/vector notation and omitting Dirac and colour indices we get

$$G(x|x_0) = \sum_y D^{-1}(x|y)S(y|x_0). \tag{4.2.3}$$

Multiplying this with the Dirac operator $D(z|x)$ from the left gives

$$\sum_x D(y|x)G(x|x_0) = S(y|x_0). \tag{4.2.4}$$

This is a system of linear equations of the well-known form $Ax = b$ which can be solved iteratively using methods like CG (conjugate gradient) or an improved version of it. More details can be found in [21] or in the papers [9, 44].

For the calculation of a correlation function we will also need the propagator in the inverse direction $G(x_0|x)$. Evaluating this numerically would be as expensive as the full propagator but fortunately one can use the γ_5-hermiticity relation

$$\boxed{\gamma_5 G(x_0|x)\gamma_5 = G^\dagger(x|x_0).} \tag{4.2.5}$$

Using a point source means that the two quarks in the meson would sit on the same lattice site. This situation is not really satisfying and for improving the overlap of the meson interpolator with the physical state one needs a more realistic spatial wavefunction. This can be achieved by employing *extended* or *smeared sources* where the quarks will sit on different spatial points but on the same timeslice. A common way to realise it is using some gauge-covariant smearing function $M(x|x')$ on a point source $S(x'|x_0)$:

$$S^{smear}(x|x_0) = \sum_{x'} M(x|x')S(x'|x_0). \tag{4.2.6}$$

An example of a gauge-covariant smearing is Jacobi smearing which is defined as

$$M = \sum_{n=0}^{N} \kappa^n H^n \tag{4.2.7}$$

and

$$H(y,x) = \sum_{j=1}^{3} \Big(U_j(\vec{y},t)\delta_{\vec{y}+\hat{\jmath},\vec{x}} + U_j^\dagger(\vec{y}-\hat{\jmath},t)\delta_{\vec{y}-\hat{\jmath},\vec{x}} \Big) \tag{4.2.8}$$

where the timeslice t in H is fixed. The two free parameters κ and n, the hopping parameter and the number of smearing steps, are used to tune the shape of the source and to get the best possible overlap with the physical state.

The extended source now depends also on gauge links $U_j(x)$ which separate the quarks in spatial direction. The source-smeared propagator G^s is then $G^s(y|x_0) = \sum_{x'} D^{-1}(y|x')S^{smear}(x'|x_0)$ and we solve

$$\sum_y D(x'|y)G^s(y|x_0) = S^{smear}(x'|x_0). \tag{4.2.9}$$

In addition we can apply the smearing at the sink and define the source-sink-smeared propagator G^{ss} as

$$\begin{aligned} G^{ss}(x|x_0) &= \sum_{y,x'} S^{smear}(x|y)D^{-1}(y|x')S^{smear}(x'|x_0) \\ &= \sum_y S^{smear}(x|y)G^s(y|x_0). \end{aligned} \tag{4.2.10}$$

After solving equation (4.2.9) we can insert the result G^s in the second line of (4.2.10) to get the source-sink-smeared propagator G^{ss}.

There are also other methods to get extended sources like constructing a source with a specific shape, for example a so-called wall source which is constant in a timeslice. The advantage is that one has more freedom in constructing a suitable meson operator but these sources often do not preserve gauge invariance. The consequence is that the gauge has to be fixed and one has to take care that the gauge fixing does not affect the final result.

There is also a technique called link smearing which is used to improve the signal to noise ratio for correlation functions. The original links (thin links) are replaced by a local average of neighbouring links (fat links) which are contained in a short path connecting the ends of the thin links. This helps to compensate short ranged fluctuations of the gauge field which distort the correlators. The literature [6, 27, 37] treats different types of link smearings like APE, HYP or stout smearing.

4.3. Extracting energies

4.3.1. General considerations

Our goal in this section is to extract the energies (or mass which is nothing more than the ground state energy) from the 2-point correlation function. The general form of the *meson correlation function* or *meson correlator* is

$$C(t) = \langle O(t)\bar{O}(0)\rangle - \langle O(t)\rangle\langle\bar{O}(t)\rangle. \tag{4.3.1}$$

The first term on the right hand side, called connected part, is the 2-point function which we showed already in (3.1.10). In the second one, the disconnected part, $\langle O\rangle$ corresponds to the vacuum expectation value. For non-vanishing vacuum expectation

values the disconnected part is just a constant but one has to subtract it from the connected part or include it in the fit function. In most cases $\langle O \rangle$ is zero anyway so that just the 2-point function has to be calculated. For the meson correlators that we calculate in this work the disconnected part vanishes as well and therefore we will consider just the first term of (4.3.1) in the energy calculation.

From equation (3.1.10) we get the connection between the meson correlation function and the particle energies:

$$C(t) = \langle O(t)\bar{O}(0)\rangle = A_0 \mathrm{e}^{-E_0 t} + A_1 \mathrm{e}^{-E_1 t} + \dots . \tag{4.3.2}$$

The $A_0, A_1, \dots$ are the amplitudes and $E_0, E_1, \dots$ are the energies. Because the lattice is of finite extent one gets not only the meson that propagates forward in time, but also the anti-meson going backward. The meson and anti-meson have the same mass and equation (4.3.2) is changed to the form

$$C(t) = A_0(\mathrm{e}^{-E_0 t} \pm \mathrm{e}^{-E_0(L_T - t)}) + A_1(\mathrm{e}^{-E_1 t} \pm \mathrm{e}^{-E_1(L_T - t)}) + \dots \tag{4.3.3}$$

where the plus or minus sign depends on the choice of the source and sink operators in the 2-point function and L_T is the extent of the time direction. We see that higher states are exponentially suppressed for large t where we suppose to have just the ground state contribution. However for small values of t we expect a mixing of the ground state with the first excited state or even higher ones. To extract the mass one can perform a two- or four-parameter fit for large values of t. With a four-parameter fit we can take into account the first excited state for smaller t. The direct fitting is useful for determining the mass, but for higher energies one has to look for more sophisticated methods.

To get an idea of a good fitting range for the mass extraction a common way is to check the *effective mass*. It is defined as

$$m_{eff}(t + \tfrac{1}{2}) = \ln\Big[\frac{C(t)}{C(t+1)}\Big]. \tag{4.3.4}$$

The effective mass curve shows a plateau for large enough t when the correlator is dominated by the ground state energy $E_0 \equiv m$. The range with constant effective mass and sufficiently small errors can then be used to perform the mass fits. One can find more details about fitting techniques in lattice QCD, e.g., in [16] and for correlated data sets in [34].

4.3.2. The variational method

The variational method was first proposed by K.G. Wilson [46] to extract particle energies in lattice QCD and later elaborated by C. Michael and M. Lüscher and U. Wolff [33, 32]. The basic idea is to calculate not only a single correlation function but a whole

matrix of correlators (see e.g. [32, 10, 11, 12])

$$\begin{aligned} C_{ij}(t) &= \langle O_i(t)\bar{O}_j(0)\rangle - \langle O_i(t)\rangle\langle\bar{O}_j(0)\rangle \\ &= \sum_{n=1}^{\infty}\langle 0|O_i|n\rangle\langle n|O_j^\dagger|0\rangle \mathrm{e}^{-tE_n}, \end{aligned} \tag{4.3.5}$$

where the $O_i, i = 1, \ldots, N$ are linearly independent interpolators for the desired states. In the second line we used again (3.1.10). In the paper by Lüscher and Wolff [32] it was shown that diagonalising the correlation matrix (4.3.5), that means solving $C(t)\vec{v}^{(k)} = \lambda^{(k)}(t)\vec{v}^{(k)}$, gives eigenvalues which are proportional to the exponential of the energy:

$$\lambda^{(k)}(t) = c_k \mathrm{e}^{-tE_k}[1 + \mathrm{O}(\mathrm{e}^{-t\Delta E_k})] \quad \text{for all} \quad k = 1, \ldots, N \tag{4.3.6}$$

where ΔE_k is the difference between the energy E_k and the energy lying closest to it and c_k is some constant. We see that the smallest energy will give the largest eigenvalue. Diagonalising the correlation matrix suppresses the additional contributions from excited states. Therefore the energies can be determined by using a two-parameter fit of $\lambda^{(k)}(t)$ [12].

Equation (4.3.6) holds as well when one solves the *generalised eigenvalue problem* (GEVP):

$$C(t)\vec{v}^{(k)} = \lambda^{(k)}(t, t_0)C(t_0)\vec{v}^{(k)} \tag{4.3.7}$$

$$\lambda^{(k)}(t, t_0) = \mathrm{e}^{-(t-t_0)E_k}[1 + \mathrm{O}(\mathrm{e}^{-t\Delta E_k})] \quad \text{for all} \quad k = 1, \ldots, N \tag{4.3.8}$$

with t_0 fixed at some not too large time. Identifying $\mathrm{e}^{t_0 E_k}$ with c_k gives back equation (4.3.6). The GEVP has the advantage that the correction term in (4.3.6) is negligible already for moderately large times t [32, 21]. Note that in this case ΔE_k is the difference between the energy E_k and the energy of the $N+1$-th level, E_{N+1} if $t \leq 2t_0$ [10].

The success of the variational method depends crucially on the choice of the operator basis $\{O_i\}$. They have to be independent from each other and should have a good overlap with the desired states.

4.4. Setting the scale

To estimate the lattice spacing a in physical units for a given coupling β, one can make use of the static quark potential $V(r)$. From $V(r)$ one defines the *Sommer parameter* r_0 [43] by

$$r^2 \frac{\mathrm{d}V}{\mathrm{d}r}\Big|_{r=r_0} = 1.65. \tag{4.4.1}$$

It has a physical value of $r_0 \approx 0.5$ fm. In the simulations one determines its value in lattice units r_0/a so that a in physical units is then given by $a = \frac{r_0}{r_0/a}$.

After determining the lattice spacing we can also calculate the energies in physical units. The energies that we get from fitting the correlators with an exponential function are of the form

$$E_{lat} = a \cdot E_{phys} \tag{4.4.2}$$

where E_{lat} is dimensionless. Therefore E_{phys} must have dimension of fm^{-1}. To convert this to a more common unit, e.g. MeV, we use the fact that we set $\hbar = c = 1$ and get according to [21]

$$1\,\mathrm{fm}^{-1} = 197.327\,\mathrm{MeV}. \tag{4.4.3}$$

5. Resonance scattering on the lattice

How can one describe phenomena from low-energy hadron-hadron scattering, like for example the rho resonance, in QCD? The rho can be observed as a resonance in the elastic $\pi\pi \to \pi\pi$ scattering with angular momentum $l = 1$ and Isospin $I = 1$. Assume that we have a 2-pion state at the beginning which transforms into a rho state and then decays again into two pions. Between the incoming and outgoing 2-pion wavepacket there will be a difference in the phase, the scattering phase shift, which is related to the mass and the width of the resonance. Scattering is a time dependent procedure but on the lattice we are working in imaginary time and it is not possible to observe the resonance directly.

A first paper concerning this problem was written by Lüscher and Wolff [32] in 1990. They related the 2-particle energy in a finite, 1-dimensional box with periodic boundary conditions to the scattering phase shift in infinite volume for a simple quantum mechanical model and also discussed considerations leading to the relativistic case. In the same year Lüscher generalised the 1-dimensional theory to 3 space dimensions [30]. To determine the resonance parameters Lüscher proposed in a later paper [31] to determine the phase shift curve by calculating energies at fixed coupling and quark mass via lattice simulations and extract the resonance parameters from these phase shifts.

The scattering phase method was worked out in [30] for the simplest case with two identical spin-0 particles in the centre-of-mass frame and later generalised by Rummukainen and Gottlieb [40] for a system with total momentum $\vec{P} \neq \vec{0}$. This has the advantage that more points on the resonance curve can be determined without the need of higher energy levels. They tested it with a simple ϕ^4 model containing a light massive field ϕ and a heavier field ρ interacting via a 3-point coupling. Scattering in the centre-of-mass frame was also tested by Göckeler et al. [23]. They used the 4-dimensional ϕ^4 theory with spontaneous symmetry breaking. It contains four different scalar fields $\phi^i, i = 1, 2, 3, 4$ and three Goldstone bosons from symmetry breaking representing the three pions.

A first dynamical calculation in QCD with $N_f = 2$ was done in 2007 by Aoki et al. [7] on a $12^2 \times 24$ lattice with $m_\pi/m_\rho = 0.41$. Further dynamical calculations were performed later in 2010 by Feng, Jansen, Renner [19] and Frison et al. [20] and in 2011 by Aoki et al. [8] and Lang et al. [29].

5.1. Derivation of the phase shift formula

In this section we want to give at first the relations between energy and momentum of two identical spin-0 particles in a periodic box of length L and later derive the formula for the phase shift following the papers [30, 40].

The lattice is a 3-dimensional box of length L with periodic boundary conditions (i.e. a torus). The time direction is assumed to be infinite. Assume now that there are two free spin-0 particles with mass m_π (pions) and momenta $\vec{k}_1$ and $\vec{k}_2$ in the box. Define the total momentum as

$$\vec{P} = \vec{k}_1 + \vec{k}_2. \tag{5.1.1}$$

The total energy in the laboratory frame (= rest frame of the box) is then

$$W_L = W_1 + W_2 = \sqrt{\vec{k}_1^2 + m_\pi^2} + \sqrt{\vec{k}_2^2 + m_\pi^2}. \tag{5.1.2}$$

We define the centre-of-mass frame momentum as

$$\vec{k}_{CM} = \vec{k}_1^{CM} = -\vec{k}_2^{CM}. \tag{5.1.3}$$

The energy in the centre-of-mass frame is

$$\boxed{W_{CM} = 2\sqrt{\vec{k}_{CM}^2 + m_\pi^2}} \tag{5.1.4}$$

and the two energies are then related by

$$\boxed{W_L = \sqrt{\vec{P}^2 + W_{CM}^2}.} \tag{5.1.5}$$

In the case of non-interacting particles the total momentum and also the momenta in the laboratory frame are quantised by the box:

$$\vec{P} = \frac{2\pi}{L}\vec{d} \tag{5.1.6}$$

$$\vec{k}_1 = (\vec{d} + \vec{n})\frac{2\pi}{L} \tag{5.1.7}$$

$$\vec{k}_2 = -\vec{n}\frac{2\pi}{L} \tag{5.1.8}$$

with $\vec{n}$ and $\vec{d}$ in $\mathbb{Z}^3$.

When we turn on the interaction between the two pions then the quantisation conditions (5.1.7), (5.1.8) for the pions are no longer valid. Instead one will get a relation between the scattering phase shift and the centre-of-mass momentum $\vec{k}_{CM}$ which we will derive now.

We consider the two particles as a relativistic quantum mechanical system and assume that there is no interaction at the moment. They can be described in Minkowski space by a 2-particle wavefunction $\psi(x_1, x_2)$ satisfying Bose symmetry. To shift the whole system to another inertial frame we use a Lorentz transformation $\Lambda^\mu{}_\nu$:

$$\psi(x_1, x_2) \to \psi(x_1', x_2') = \psi(\Lambda x_1, \Lambda x_2) \tag{5.1.9}$$

with

$$(x')^\mu = \Lambda^\mu{}_\nu x^\nu \tag{5.1.10a}$$
$$x'^{\,0} = \gamma(x^0 + \vec{v} \cdot \vec{x}) \tag{5.1.10b}$$
$$\vec{x}' = \gamma(\vec{x} + \vec{v} \cdot x^0). \tag{5.1.10c}$$

The metric is $g_{\mu\nu} = \mathrm{diag}(1, -1, -1, -1)$, $\vec{v}$ is the relative velocity between the two inertial systems and the Lorentz factor γ is given by

$$\gamma = \frac{1}{\sqrt{1 - \vec{v}^2}}. \tag{5.1.11}$$

When there is no interaction the wavefunction $\psi(x_1, x_2)$ has to satisfy the Klein-Gordon equations in the laboratory frame

$$(\hat{p}_i^\mu \hat{p}_{i\,\mu} - m_\pi^2)\psi(x_1, x_2) = 0, \quad i = 1, 2, \tag{5.1.12}$$

where $\hat{p}_{i\,\mu} = -i\frac{\partial}{\partial x_i^\mu}$ is the momentum operator. Making a change of variables

$$\begin{aligned} X &= \tfrac{1}{2}(x_1 + x_2) \\ x &= x_1 - x_2 \end{aligned} \tag{5.1.13}$$

and defining the new momentum operators

$$\begin{aligned} \hat{P} &= \hat{p}_1 + \hat{p}_2 \\ \hat{p} &= \tfrac{1}{2}(\hat{p}_1 - \hat{p}_2) \end{aligned} \tag{5.1.14}$$

transforms the equations in (5.1.12) into

$$[4(\hat{p}_\mu \hat{p}^\mu - m_\pi^2) + \hat{P}_\mu \hat{P}^\mu]\psi(x, X) = 0 \tag{5.1.15}$$
$$\hat{p}_\mu \hat{P}^\mu \psi(x, X) = 0. \tag{5.1.16}$$

Because the total momentum has to be conserved we can make a separation ansatz for $\psi(x, X)$

$$\psi(x, X) = \mathrm{e}^{-iP_\mu X^\mu}\phi(x). \tag{5.1.17}$$

In the centre-of-mass frame the total momentum is $P = (W_{CM}, \vec{0})$. Using this with equation (5.1.16) we see that the function $\phi_{CM}(x_{CM})$ does not depend on x^0_{CM}. Therefore we can write (5.1.17) in the centre-of-mass frame as

$$\psi_{CM}(t_{CM}, \vec{x}_{CM}) \equiv \psi_{CM}(X^0_{CM}, \vec{x}_{CM}) = \mathrm{e}^{-iW_{CM}t_{CM}}\phi_{CM}(\vec{x}_{CM}). \tag{5.1.18}$$

With the Lorentz transformation defined in (5.1.10) and $\vec{v} = \vec{P}/W_{CM}$ we can relate the laboratory frame with the centre-of-mass frame by $x_{CM} = \Lambda x_L$ and $X_{CM} = \Lambda X_L$. Comparing the laboratory frame version of equation (5.1.17) with the centre-of-mass equation (5.1.18) and using momentum conservation $P_\mu X^\mu = W_{CM} x^0_{CM}$ we get the relation:

$$\phi_L(x^0, \vec{x}) = \phi_{CM}(\gamma(\vec{x} + \vec{v} \cdot x^0)). \tag{5.1.19}$$

In the laboratory frame we assume that the two particles have identical time coordinates such that the variable x^0 vanishes. The above equation is then further simplified into

$$\boxed{\phi_L(\vec{x}) = \phi_{CM}(\gamma\vec{x})}. \tag{5.1.20}$$

From equation (5.1.18) and the Klein-Gordon equation (5.1.15) we can conclude that ϕ_{CM} satisfies the Helmholtz equation

$$\boxed{(\nabla^2 + k^2_{CM})\phi_{CM}(x_{CM}) = 0} \tag{5.1.21}$$

in the centre-of-mass frame where

$$k^2_{CM} \equiv |\vec{k}_{CM}|^2 = \frac{W^2_{CM}}{4} - m^2_\pi. \tag{5.1.22}$$

In the next step we take a look at the interacting theory. We assume that the interaction between the pions is of finite range R. This means that for $|\vec{x}_{CM}| > R$ the Klein-Gordon equations must be satisfied. Because the potential is spherically symmetric in the centre-of-mass frame we can switch to spherical coordinates and expand ϕ_{CM} in spherical harmonics:

$$\phi_{CM}(\vec{x}) = \sum_{l=0}^{\infty} \sum_{m=-l}^{m=l} Y_{lm}(\theta, \phi)\phi_{lm}(r). \tag{5.1.23}$$

In the region $r > R$ the function ϕ_{CM} satisfies the Helmholtz equation (5.1.21). One can transform the Helmholtz equation into spherical coordinates and use a separation ansatz. The radial equation reads

$$\left[\frac{\mathrm{d}^2}{\mathrm{d}r^2} + \frac{2}{r}\frac{\mathrm{d}}{\mathrm{d}r} - \frac{l(l+1)}{r^2} - k^2_{CM}\right]\phi_{lm}(r) = 0 \tag{5.1.24}$$

and its solution is given by a linear combination of spherical Bessel functions

$$\phi_{lm}(r) = c_{lm}\big[a_l(k_{CM})j_l(k_{CM}r) + b_l(k_{CM})n_l(k_{CM}r)\big] \tag{5.1.25}$$

with coefficients $c_{lm}, a_l(k_{CM})$ and $b_l(k_{CM})$. For $r < R$ the functions ϕ_{lm} are unknown but following [30] one can assume that we have a unique regular solution for every l, m in this region and we can determine the coefficients in (5.1.25) by joining both solutions at $r = R$.

The pion is a spinless, pseudoscalar meson which corresponds to the characteristics of the hypothetical particle we introduced before, i.e. the spin-0 boson. A single pion state in the centre-of-mass frame is characterised by its momentum $\vec{k}_i^{CM}, i = 1, 2$, and an isospin index $a = 1, 2, 3$ (or the z-component of the isospin $I_z = -1, 0, 1$). A 2-pion state can have total isospin $I = 0, 1, 2$. The 2-pion scattering amplitude can be written as [23]

$$T = \sum_{I=0}^{2} Q^I T_I \tag{5.1.26}$$

where Q^I are the *isospin projectors*

$$Q^0_{a'b',ab} = \tfrac{1}{3}\delta_{a'b'}\delta_{ab} \tag{5.1.27}$$

$$Q^1_{a'b',ab} = \tfrac{1}{2}(\delta_{a'a}\delta_{b'b} - \delta_{a'b}\delta_{b'a}) \tag{5.1.28}$$

$$Q^2_{a'b',ab} = \tfrac{1}{2}(\delta_{a'a}\delta_{b'b} + \delta_{a'b}\delta_{b'a}) - \tfrac{1}{3}\delta_{a'b'}\delta_{ab} \tag{5.1.29}$$

with isospin indices a, a', b, b'. The scattering amplitude T_I in the isopin I channel is a function of the absolute value of the pion momentum k_{CM} and the scattering angle θ and we can write it in the partial wave decomposition

$$T_I(k_{CM}, \theta) = \frac{16\pi W_{CM}}{k_{CM}} \sum_{l=0}^{\infty} (2l+1) P_l(\cos\theta) t_{Il}(k_{CM}). \tag{5.1.30}$$

The pions have to obey Bose symmetry and therefore t_{Il} must vanish when $I + l$ is odd. In the elastic range $2m_\pi < W_{CM} < 4m_\pi$ the amplitude can be expressed in terms of the scattering phase δ_{Il} as

$$t_{Il}(k_{CM}) = \frac{1}{2ik_{CM}}\Big(\mathrm{e}^{2i\delta_{Il}(k_{CM})} - 1\Big). \tag{5.1.31}$$

The scattering phase can be related to the coefficients a_l and b_l in (5.1.25) via

$$\mathrm{e}^{2i\delta_{Il}(k_{CM})} = \frac{a_l(k_{CM}) + ib_l(k_{CM})}{a_l(k_{CM}) - ib_l(k_{CM})}. \tag{5.1.32}$$

Now we want to analyse the behaviour of the 2-pion wave function in a periodic box of length L. Due to the periodic boundary conditions the 2-particle wave function in the laboratory frame has to fulfil

$$\psi_L(\vec{x}_1, \vec{x}_2) = \psi_L(\vec{x}_1 + \vec{n}L, \vec{x}_2 + \vec{m}L) \tag{5.1.33}$$

with $\vec{n}, \vec{m} \in \mathbb{Z}^3$. To determine the shape of ψ_L we use the separation ansatz (5.1.17) and $x_1^0 = x_2^0 = 0$ for the time coordinates which gives us

$$\psi_L(\vec{x}_1, \vec{x}_2) = \mathrm{e}^{\frac{1}{2}i\vec{P}(\vec{x}_1+\vec{x}_2)}\phi_L(\vec{x}_1 - \vec{x}_2). \tag{5.1.34}$$

Plugging this into the boundary conditions gives the following constraint on the total momentum:

$$\boxed{\vec{P} = \frac{2\pi}{L} \cdot \vec{d}, \quad \vec{d} \in \mathbb{Z}^3.} \tag{5.1.35}$$

Assuming that $\vec{n} \neq \vec{m}$ and using the relation (5.1.20) together with (5.1.35) and the periodicity of the box we obtain

$$\boxed{\phi_{CM}(\vec{x}_{CM}) = (-1)^{\vec{d}\cdot\vec{n}}\phi_{CM}(\vec{x}_{CM} + \hat{\gamma}\vec{n}L) \quad \forall \quad \vec{n} \in \mathbb{Z}^3} \tag{5.1.36}$$

for fixed $\vec{d}$. The definition of the operator $\hat{\gamma}$ is given in Appendix A. In [40] these functions are called *$\vec{d}$-periodic functions*. For $\vec{d} \neq \vec{0}$ the cubic box in the laboratory frame is deformed into a parallelepiped in the centre-of-mass frame due to Lorentz contraction in the direction of the total momentum. This also means that the cubic symmetry is reduced to smaller symmetry groups, for example to the tetragonal group when $\vec{d} = (0, 0, 1)$.

The goal is now to find the general form of $\vec{d}$-periodic solutions of the Helmholtz equation and expand these in spherical harmonics and Bessel functions to determine the coefficients $a_l(k_{CM})$ and $b_l(k_{CM})$ in (5.1.25). Because all these calculations are done in the centre-of-mass frame we will omit the subscript CM in the $\vec{x}$-variable. We assume that $L > 2R$ where R is the range of the interaction. For $R < r < L/2$ we can then expand the solutions in spherical harmonics and Bessel functions. According to [40, 30] the Green function

$$G^{\vec{d}}(\vec{x}, k_{CM}) = \frac{1}{\gamma L^3} \sum_{\vec{k}\in\Gamma} \frac{\mathrm{e}^{i\vec{k}\vec{x}}}{\vec{k}^2 - k_{CM}^2} \tag{5.1.37}$$

is a singular $\vec{d}$-periodic solution of the Helmholtz equation (5.1.21) with the momentum lattice given by

$$\Gamma = \{\vec{k} \in \mathbb{R}^3 | \vec{k} = \frac{2\pi\hat{\gamma}^{-1}}{L}(\vec{n} + \tfrac{1}{2}\vec{d}), \vec{n} \in \mathbb{Z}^3\}. \tag{5.1.38}$$

This means that $G^{\vec{d}}$ is a smooth function which is defined for all $\vec{x} \neq \hat{\gamma}\vec{n}L$ with $\vec{n} \in \mathbb{Z}^3$, provided that k_{CM} does not take a singular value, $k_{CM} \neq \frac{2\pi}{L}|\hat{\gamma}^{-1}(\vec{n} + \frac{1}{2}\vec{d})|$. Then the following equation is satisfied:

$$(\nabla^2 + k_{CM}^2)G^{\vec{d}}(\vec{x}, k_{CM}) = -\sum_{\vec{n}\in\mathbb{Z}^3} (-1)^{\vec{d}\cdot\vec{n}}\delta(\vec{x} + \hat{\gamma}\vec{n}L). \tag{5.1.39}$$

We can generate further solutions if we differentiate $G^{\vec{d}}(\vec{x}, k_{CM})$ with respect to $\vec{x}$. We define the functions

$$G^{\vec{d}}_{lm}(\vec{x}, k_{CM}) = \mathcal{Y}_{lm}(\nabla) G^{\vec{d}}(\vec{x}, k_{CM}) \tag{5.1.40}$$

where $\mathcal{Y}_{lm}(\vec{x}) = x^l Y_{lm}(\theta, \phi)$ are harmonic polynomials. Normally the expansion in spherical harmonics includes infinitely many angular momenta l. Introducing an angular momentum cutoff Λ one can show [30] that for $l \leq \Lambda$ the $G^{\vec{d}}_{lm}$ form a complete set of singular $\vec{d}$-periodic solutions of the Helmholtz equation, i.e. every singular $\vec{d}$-periodic solution of degree Λ is a linear combination of the $G^{\vec{d}}_{lm}$. In the region $0 < x < L/2$ we can expand the $G^{\vec{d}}_{lm}$ in spherical harmonics:

$$G^{\vec{d}}_{lm}(\vec{x}, k_{CM}) = \frac{(-1)^l k_{CM}^{l+1}}{4\pi} \Bigg\{ n_l(k_{CM} x) Y_{lm}(\theta, \phi) + \sum_{l'=0}^{\infty} \sum_{m'=-l'}^{l'} M^{\vec{d}}_{lm,l'm'}(k_{CM}) j_{l'}(k_{CM} x) Y_{l'm'}(\theta, \phi) \Bigg\}. \tag{5.1.41}$$

The coefficients $M^{\vec{d}}_{lm,l'm'}$ are defined as

$$M^{\vec{d}}_{lm,l'm'}(k_{CM}) = \frac{(-1)^l}{\gamma \pi^{3/2}} \sum_{j=|l-l'|}^{l+l'} \sum_{s=-j}^{j} \frac{i^j}{q^{j+1}} \big(Z^{\vec{d}}_{js}(1; q^2)\big)^* C_{lm,js,l'm'} \tag{5.1.42}$$

with

$$q = \frac{L}{2\pi} k_{CM}. \tag{5.1.43}$$

(Note that in [40] the complex conjugation $(\dots)^*$ is missing.) The tensors $C_{lm,js,l'm'}$ contain Wigner $3j$-symbols

$$C_{lm,js,l'm'} = (-1)^{m'} i^{l-j+l'} \sqrt{(2l+1)(2j+1)(2l'+1)} \times \begin{pmatrix} l & j & l' \\ m & s & -m' \end{pmatrix} \begin{pmatrix} l & j & l' \\ 0 & 0 & 0 \end{pmatrix}. \tag{5.1.44}$$

The function $Z^{\vec{d}}_{js}$ in (5.1.42) is a *generalised zeta function* defined as

$$Z^{\vec{d}}_{lm}(s; q^2) = \sum_{\vec{r} \in P_{\vec{d}}} \frac{r^l Y_{lm}(\theta, \phi)}{(\vec{r}^2 - q^2)^s}, \tag{5.1.45}$$

where the summation is done over the set

$$P_{\vec{d}} = \{\vec{r} \in \mathbb{R}^3 |\ \vec{r} = \hat{\gamma}^{-1}(\vec{n} + \tfrac{1}{2}\vec{d})\} \quad \vec{n}, \vec{d} \in \mathbb{Z}^3. \tag{5.1.46}$$

The sum in (5.1.45) converges if $\mathfrak{Re}(2s) > l+3$ and the zeta function can be analytically continued to the complex plane. The evaluation of the zeta function for $s = 1$ will be discussed in Appendix A.

Now we can bring together the solutions from (5.1.41), (5.1.23) and (5.1.25). The most general $\vec{d}$-periodic solution of degree Λ is a superposition of (5.1.40) for $l \leq \Lambda$ and we get the equation

$$\sum_{l=0}^{\Lambda} \sum_{m=-l}^{l} v_{lm} G^{\vec{d}}_{lm}(\vec{x}, k_{CM}) = \sum_{l=0}^{\Lambda} \sum_{m=-l}^{l} c_{lm} \big[a_l(k_{CM}) j_l(k_{CM} x) + b_l(k_{CM}) n_l(k_{CM} x)\big] Y_{lm}(\theta, \phi). \quad (5.1.47)$$

Using equation (5.1.41) the coefficient v_{lm} can be eliminated and we remain with

$$c_{lm} a_l(k_{CM}) = \sum_{l'=0}^{\Lambda} \sum_{m'=-l'}^{l'} c_{l'm'} b_{l'}(k_{CM}) M^{\vec{d}}_{l'm',lm}(k_{CM}). \quad (5.1.48)$$

We can introduce the new coefficients

$$A_{lm,l'm'} = a_l(k_{CM}) \delta_{ll'} \delta_{mm'} \quad \text{and} \quad B_{lm,l'm'} = b_l(k_{CM}) \delta_{ll'} \delta_{mm'}. \quad (5.1.49)$$

Then A and B are diagonal matrices and we change equation (5.1.48) into a matrix equation

$$C(A - BM) = 0. \quad (5.1.50)$$

This system of linear equations has a non-trivial solution if $\det[A - BM] = 0$. Also the equation (5.1.32) for the phase shift can be converted into

$$\mathrm{e}^{2i\delta} = \frac{A + iB}{A - iB}. \quad (5.1.51)$$

Applying the decomposition $A - BM = \frac{i}{2}[(A + iB)(M - i) - (A - iB)(M + i)]$ and factoring out $A - iB$ we use the above equation and the fact that $\det(A - BM) = 0$ to get the final result for the phase shift

$$\boxed{\det\left[\mathrm{e}^{2i\delta} - \frac{M + i}{M - i}\right] = 0.} \quad (5.1.52)$$

The shape of M depends on the momentum direction $\vec{d}$, which also determines the shape of the box (the lattice) and the underlying point symmetry group in the centre-of-mass frame. The group theoretical aspects will be discussed in the next chapter.

6. Determination of the scattering phase shift for non-zero total momenta

The task of this section is the calculation of the scattering phases for three different momentum directions. The first section is a short recapitulation of some important terms and propositions of finite group theory which we will need for further calculations. In the second section the derivation of the scattering phase formulas follows.

6.1. Group theory

The symmetry groups which we will consider in this section are finite subgroups of $O(3)$ (rotations and rotation-inversions) and are called point groups. We want to calculate the phase shift formulas for the directions $(0,0,1)$, $(1,1,0)$ and $(1,1,1)$ of the total momentum. In the last chapter we already mentioned that a non-zero total momentum leads to a deformation of the cube in the centre-of-mass frame. This new shape has less symmetries than the original one underlying the cubic group. Table 6.1.1 gives an overview of the total momentum directions used in this work and the related point groups.

In this subsection we want to recapitulate briefly some important tools from group theory that we will need for our analysis. Assume that the considered group G is finite and the number of elements is N. Furthermore there is a representation $D : G \to GL(V)$ of G, where V is some vector space and D is reducible. If D is a finite dimensional (unitary) representation of G, we can decompose D into a direct sum of (unitary) irreducible representations

$$D = \sum_{j=1}^{k} \oplus a_j D_j \tag{6.1.1}$$

where the irreducible representations D_j are pairwise non-equivalent. The a_j's are unique and called multiplicity of D_j. If $g \in G$ is an element of G and D is a matrix representation, $D(g)$ is a block diagonal matrix.

The character χ of a representation D is the trace of the representation matrix

$$\chi(g) = \mathrm{tr}(D(g)), \quad g \in G. \tag{6.1.2}$$

Direction	point group	# of elements	Name
$(0,0,0)$	O_h	48	cubic
$(0,0,1)$	D_{4h}	16	tetragonal
$(1,1,0)$	D_{2h}	8	orthorhombic
$(1,1,1)$	D_{3d}	12	trigonal

Table 6.1.1.: Overview of the used point groups.

Equivalent representations have the same character and representations with the same character are equivalent. Special cases are one-dimensional representations where $\chi(g) = D(g)$ and the character of the identity element e, which is the dimension of the representation. Furthermore if the irreducible representations D_j are of dimension n_j with $j = 1, \ldots, k$ the following holds:

$$\sum_{j=1}^{k} n_j^2 = N. \tag{6.1.3}$$

Finally we give the formula for computing the multiplicities:

$$a_j = \frac{1}{N} \sum_{g \in G} (\chi^{(j)}(g))^* \cdot \chi(g) \quad j = 1, \ldots, k \tag{6.1.4}$$

where $\chi^{(j)}$ is the character of the j-th irreducible representation.

6.2. Scattering phases

Now we want to present the derivation of the explicit scattering phase formulas for the different total momenta. The direction $\vec{d} = (0,0,1)$ will serve as a detailed example for the calculation. The remaining directions can be analysed in the same way and we restrict ourselves to the main results.

Let us assume that R is an element of one of the considered point groups. According to [30], the transformation of the harmonic polynomials under R is given by

$$\mathcal{Y}_{lm}(R \cdot \vec{r}) = \sum_{m'=-l}^{l} D^{(l)}_{mm'}(R) \mathcal{Y}_{lm'}(\vec{r}) \tag{6.2.1}$$

where $D^{(l)}_{mm'}(R)$ is a unitary matrix representation of R. From this formula and the definition of the zeta function (5.1.45) we can immediately derive the transformation properties of the zeta function under an element of the cubic group:

$$Z^{\vec{d}}_{lm}(s; q^2) = \sum_{m'=-l}^{l} D^{(l)}_{mm'}(R) Z^{\vec{d}}_{lm'}(s; q^2). \tag{6.2.2}$$

The spin of the rho is equal to 1 so we set the maximal angular momentum to $\Lambda = 1$. At this point we restrict our calculations to the tetragonal group D_{4h}. It is the symmetry group of the cubic box warped by the Lorentz factor γ in $(0, 0, 1)$ direction. Setting $l = 1$ gives us a 3-dimensional matrix representation $D^{(1)}$ which decomposes into irreducible representations. A good overview of the point groups with character tables gives for example [3]. We see that D_{4h} possesses 10 irreducible representations called $A_1^{\pm}, A_2^{\pm}, B_1^{\pm}, B_2^{\pm}$ and $E^{\pm}$ with dimensions $1, 1, 1, 1$ and 2, respectively. Using character tables and equation (6.1.4) we can decompose $D^{(0)}$ and $D^{(1)}$ into

$$\begin{aligned} D^{(0)} &= A_1^+ \\ D^{(1)} &= A_2^- \oplus E^-. \end{aligned} \tag{6.2.3}$$

This means that the case $l = 0$ is characterised by the trivial representation A_1^+. When $l = 1$ the representation space is 3-dimensional but we can decompose it into a 1- and 2-dimensional irreducible subspace, which correspond to the longitudinal and transverse polarisations, respectively. Here polarisation refers to the polarisation of the intermediate rho state: The spin of the rho can be either parallel to its momentum (longitudinal polarisation) or orthogonal to it (transverse polarisation). With the angular momentum cut $\Lambda = 1$ the matrix M in (5.1.52) reads

$$M_{lm,l'm'} = \begin{pmatrix} M_{00,00} & M_{00,1-1} & M_{00,10} & M_{00,11} \\ M_{1-1,00} & M_{1-1,1-1} & M_{1-1,10} & M_{1-1,11} \\ M_{10,00} & M_{10,1-1} & M_{10,10} & M_{10,11} \\ M_{11,00} & M_{11,1-1} & M_{11,10} & M_{11,11} \end{pmatrix}. \tag{6.2.4}$$

The matrix elements contain the tensors (5.1.44) but just a small number of the j, s combinations gives nonzero values (see table 6.2.1). This is the starting point for all scattering phase shift calculations. The next step is to consider the symmetry transformations of the warped box (elements of D_{4h}). Using the group elements in equation (6.2.2) leads to the transformation properties of the zeta function under the tetragonal group. The consequences are further restrictions on the matrix elements. For D_{4h} we get

$$\begin{aligned} &Z_{js}^{\vec{d}}(1; q^2) = 0 \quad \text{if } j \text{ is odd} \\ &Z_{js}^{\vec{d}}(1; q^2) = Z_{j-s}^{\vec{d}}(1; q^2) \\ &Z_{js}^{\vec{d}}(1; q^2) = 0 \quad \text{if } s \neq 0, \pm 4, \pm 8, \ldots. \end{aligned} \tag{6.2.5}$$

Including this makes $M_{lm,l'm'}$ diagonal. Writing our key equation (5.1.52) as $\det(A) = 0$ gives

$$\det(A_{00}) \det(A_{11}) \det(A_{22}) \det(A_{33}) = 0 \tag{6.2.6}$$

l	m	l'	m'	(j,s) combinations
0	0	0	0	$(0,0)$
0	0	1	-1	$(1,-1)$
0	0	1	0	$(1,0)$
0	0	1	1	$(1,1)$
1	-1	0	0	$(1,1)$
1	-1	1	-1	$(0,0)$, $(2,0)$
1	-1	1	0	$(2,1)$
1	-1	1	1	$(2,2)$
1	0	0	0	$(1,0)$
1	0	1	-1	$(2,-1)$
1	0	1	0	$(0,0)$, $(2,0)$
1	0	1	1	$(2,1)$
1	1	0	0	$(1,-1)$
1	1	1	-1	$(2,-2)$
1	1	1	0	$(2,-1)$
1	1	1	1	$(0,0)$, $(2,0)$

Table 6.2.1.: Index combinations giving nonzero values of $C_{lm,js,l'm'}$ (see (5.1.44)).

with

$$\begin{aligned} A_{00} &= \mathrm{e}^{2i\delta_0}(M_{00,00} - i) - (M_{00,00} + i) \\ A_{11} &= \mathrm{e}^{2i\delta_1}(M_{1-1,1-1} - i) - (M_{1-1,1-1} + i) \\ A_{22} &= \mathrm{e}^{2i\delta_1}(M_{10,10} - i) - (M_{10,10} + i) \\ A_{33} &= \mathrm{e}^{2i\delta_1}(M_{11,11} - i) - (M_{11,11} + i) \end{aligned} \tag{6.2.7}$$

To solve (6.2.6) we set every determinant equal to zero and then $\det(A_{00}) = 0$ for example gives

$$\mathrm{e}^{2i\delta_0} = \frac{M_{00,00} + i}{M_{00,00} - i}. \tag{6.2.8}$$

Multiplying numerator and denominator with $M_{00,00} + i$ we finally get

$$\tan\delta_0 = \frac{1}{M_{00,00}}, \tag{6.2.9}$$

where the matrix element is

$$M_{00,00} = \gamma^{-1}\frac{1}{q\pi^{3/2}}(Z_{00}^{\vec{d}}(1;q^2))^* \tag{6.2.10}$$

and we have defined q as in (5.1.43)

$$q = \frac{|\vec{k}_{CM}|L}{2\pi}. \tag{6.2.11}$$

This is the result for angular momentum $l = 0$ analogous to the result in [30]. The solutions for $l = 1$ are obtained in the same way. Using the symmetries (6.2.5) and the Wigner $3j$-symbols we find that $M_{1-1,1-1} = M_{11,11}$ and conclude that the phase determined from $A_{11} = A_{33} = 0$ corresponds to the transverse polarisation. The results for $l = 1$ are

$$\frac{1}{\tan\delta_1} = \frac{\gamma^{-1}}{q\pi^{3/2}}\Big((Z^{\vec{d}}_{00}(1;q^2))^* + \frac{2}{\sqrt{5}q^2}(Z^{\vec{d}}_{20}(1;q^2))^*\Big) \quad \text{longitudinal} \tag{6.2.12}$$

$$\frac{1}{\tan\delta_1} = \frac{\gamma^{-1}}{q\pi^{3/2}}\Big((Z^{\vec{d}}_{00}(1;q^2))^* - \frac{1}{\sqrt{5}q^2}(Z^{\vec{d}}_{20}(1;q^2))^*\Big) \quad \text{transverse} \tag{6.2.13}$$

which agree with the results obtained in [40].

The calculations of the scattering phases for D_{2h} and D_{3d} follow the above example with the difference that the calculation of the determinant in (5.1.52) gets more involved. We note that the $l = 0$ case is always included in the matrix $M_{lm.l'm'}$ which gives us the previous result (6.2.9). Therefore we just concentrate on the case $l = 1$ and give the main results. The orthorhombic group D_{2h} possesses 8 irreducible representations $A^{\pm}, B_1^{\pm}, B_2^{\pm}$ and $B_3^{\pm}$ which all have dimension one. Then $D^{(1)}$ decomposes into

$$D^{(1)} = B_1^- \oplus B_2^- \oplus B_3^- \tag{6.2.14}$$

with one longitudinal (B_1^-) and two transverse representations which we called transverse 1 (B_2^-) and transverse 2 (B_3^-). The conditions on the zeta function are

$$\begin{aligned} Z^{\vec{d}}_{js}(1;q^2) &= 0 \quad \text{if } j \text{ or } s \text{ is odd} \\ Z^{\vec{d}}_{j-s}(1;q^2) &= \frac{1}{i^s} Z^{\vec{d}}_{js}(1;q^2). \end{aligned} \tag{6.2.15}$$

The $l = 1$ submatrix of (6.2.4) has the form

$$M_{1m,l'm'} = \begin{pmatrix} M_{11,11} & 0 & M_{1-1,11} \\ 0 & M_{10,10} & 0 \\ -M_{1-1,11} & 0 & M_{11,11} \end{pmatrix}. \tag{6.2.16}$$

where we already made use of the symmetries and the final scattering phase shifts are

$$\frac{1}{\tan\delta_1} = \frac{\gamma^{-1}}{q\pi^{3/2}}\Big((Z^{\vec{d}}_{00}(1;q^2))^* - \frac{1}{\sqrt{5}q^2}(Z^{\vec{d}}_{20}(1;q^2))^* + \frac{i}{q^2}\sqrt{\frac{6}{5}}(Z^{\vec{d}}_{22}(1;q^2))^*\Big) \quad \text{longitudinal} \tag{6.2.17}$$

$$\frac{1}{\tan\delta_1} = \frac{\gamma^{-1}}{q\pi^{3/2}}\Big((Z^{\vec{d}}_{00}(1;q^2))^* + \frac{2}{\sqrt{5}q^2}(Z^{\vec{d}}_{20}(1;q^2))^*\Big) \quad \text{transverse 2} \tag{6.2.18}$$

$$\frac{1}{\tan\delta_1} = \frac{\gamma^{-1}}{q\pi^{3/2}}\Big((Z_{00}^{\vec{d}}(1;q^2))^* - \frac{1}{\sqrt{5}q^2}(Z_{20}^{\vec{d}}(1;q^2))^* - \frac{i}{q^2}\sqrt{\frac{6}{5}}(Z_{22}^{\vec{d}}(1;q^2))^*\Big) \quad \text{transverse 1} \tag{6.2.19}$$

The last group we take into account is the trigonal one, D_{3d}. The 6 irreducible representations $A_1^{\pm}, A_2^{\pm}$ and $E^{\pm}$ have dimension 1, 1 and 2. The 3-dimensional space decomposes into a 1- and a 2-dimensional subspace

$$D^{(1)} = A_2^- \oplus E^-. \tag{6.2.20}$$

Note that A_2^- corresponds to the longitudinal and E^- to the transverse state. Inserting group elements in (6.2.2) we find

$$\begin{aligned} Z_{js}^{\vec{d}}(1;q^2) &= 0 \quad \text{if } j \text{ is odd} \\ Z_{j-s}^{\vec{d}}(1;q^2) &= \frac{1}{(-i)^s} Z_{js}^{\vec{d}}(1;q^2) \end{aligned} \tag{6.2.21}$$

and for the submatrix

$$M_{1m,l'm'} = \begin{pmatrix} M_{11,11} & -M_{10,11} & M_{1-1,11} \\ -iM_{10,11} & M_{10,10} & M_{10,11} \\ -M_{1-1,11} & iM_{10,11} & M_{11,11} \end{pmatrix}. \tag{6.2.22}$$

The final phase shifts δ_1 for the longitudinal and transverse case are

$$\frac{1}{\tan\delta_1} = \frac{\gamma^{-1}}{q\pi^{3/2}}\Big((Z_{00}^{\vec{d}}(1;q^2))^* + \frac{2i}{q^2}\sqrt{\frac{6}{5}}(Z_{22}^{\vec{d}}(1;q^2))^*\Big) \quad \text{longitudinal} \tag{6.2.23}$$

$$\frac{1}{\tan\delta_1} = \frac{\gamma^{-1}}{q\pi^{3/2}}\Big((Z_{00}^{\vec{d}}(1;q^2))^* - \frac{i}{q^2}\sqrt{\frac{6}{5}}(Z_{22}^{\vec{d}}(1;q^2))^*\Big) \quad \text{transverse.} \tag{6.2.24}$$

In the next chapter we want to construct the appropriate operators for pion resonance scattering and analyse their transformation behaviour under the three point groups D_{4h}, D_{2h} and D_{3d}.

7. Operators for pion resonance scattering and their transformation behaviour under point groups

In this chapter we first define the operators for the 2-pion state and the rho with definite momentum. Then we describe a general formalism how we can find 2-pion operator combinations which transform according to an irreducible representation of a given point group followed by concrete calculations for the groups D_{4h}, D_{2h} and D_{3d}. Subsequently the same will be done for the rho operator. For a more general treatment see, e.g., [24].

7.1. Operators for pion scattering

In the section about meson interpolators we mentioned that we will use the variational method for extracting the energy levels. Therefore we have to find suitable operators. We construct the rho interpolator as

$$\rho^a(\vec{x},t) = \bar{\psi}(\vec{x},t)\gamma_i F^a \psi(\vec{x},t) \tag{7.1.1}$$

with isospin index $a = 1,2,3$ and $F^a = \sigma^a$ are the Pauli matrices. The pion operator π is constructed analogously to the rho

$$\pi^a(\vec{x},t) = \bar{\psi}(\vec{x},t)\gamma_5 F^a \psi(\vec{x},t), \tag{7.1.2}$$

and 2-pion operators can be constructed from

$$\pi^a(\vec{x},t)\pi^b(\vec{y},t). \tag{7.1.3}$$

Operators with definite momentum are given by

$$\rho^a(\vec{p},t) = \sum_{\vec{x}} \mathrm{e}^{i\vec{p}\vec{x}}\rho^a(\vec{x},t), \tag{7.1.4}$$

$$\begin{aligned}\pi\pi^{ab}(\vec{p}_1,\vec{p}_2,t) &= \pi^a(\vec{p}_1,t)\pi^b(\vec{p}_2,t) \\ &= \sum_{\vec{x},\vec{y}} \mathrm{e}^{i\vec{p}_1\vec{x}}\mathrm{e}^{i\vec{p}_2\vec{y}}\pi^a(\vec{x},t)\pi^b(\vec{y},t),\end{aligned} \tag{7.1.5}$$

where the pion at position $\vec{x}$ has momentum $\vec{p}_1$ and the other pion has momentum $\vec{p}_2$ and all momentum components are integer multiples of $\frac{2\pi}{L}$. In addition we define

$$\overline{\rho}^a(\vec{p},t) = -\sum_{\vec{x}} \mathrm{e}^{-i\vec{p}\vec{x}}\rho^a(\vec{x},t) \tag{7.1.6}$$

$$\overline{\pi\pi}^{ab}(\vec{p}_1,\vec{p}_2,t) = \sum_{\vec{x},\vec{y}} \mathrm{e}^{-i\vec{p}_1\vec{x}}\mathrm{e}^{-i\vec{p}_2\vec{y}}\pi^a(\vec{x},t)\pi^b(\vec{y},t). \tag{7.1.7}$$

The minus sign in (7.1.6) takes care of the behaviour of the corresponding Hilbert space operator under hermitian conjugation.

7.2. Transformation properties of 2-particle operators under point groups

Now we want to analyse the transformation behaviour of $\pi\pi^{ab}(\vec{p}_1,\vec{p}_2,t)$ and $\rho^a(\vec{p},t)$ under certain subgroups of D_{4h}, D_{2h} and D_{3d}. For the action of a group element R on an operator O we write

$$O \xrightarrow{R} O' \tag{7.2.1}$$

such that $\hat{O}' = \hat{U}^\dagger(R)\hat{O}\hat{U}(R)$ for the corresponding operators $\hat{O}, \hat{O}'$ and a unitary representation $\hat{U}$ in the Hilbert space. Using

$$\bar{\psi}(\vec{x},t)\gamma_5\psi(\vec{x},t) \xrightarrow{R} \det(R)\bar{\psi}(R^{-1}\vec{x},t)\gamma_5\psi(R^{-1}\vec{x},t) \tag{7.2.2}$$

and $\det^2(R) = 1$ we get

$$\begin{aligned} O(\vec{p}_1,\vec{p}_2,t) &\xrightarrow{R} \sum_{\vec{x},\vec{y}} \mathrm{e}^{i\vec{p}_1\vec{x}}\mathrm{e}^{i\vec{p}_2\vec{y}}\bar{\psi}(R^{-1}\vec{x},t)\gamma_5 F^a\psi(R^{-1}\vec{x},t)\bar{\psi}(R^{-1}\vec{y},t)\gamma_5 F^b\psi(R^{-1}\vec{y},t) \\ &= \sum_{\vec{x},\vec{y}} \mathrm{e}^{i(R^{-1}\vec{p}_1)\vec{x}}\mathrm{e}^{i(R^{-1}\vec{p}_2)\vec{y}}\bar{\psi}(\vec{x},t)\gamma_5 F^a\psi(\vec{x},t)\bar{\psi}(\vec{y},t)\gamma_5 F^b\psi(\vec{y},t) \\ &= O(R^{-1}\vec{p}_1, R^{-1}\vec{p}_2,t) \end{aligned} \tag{7.2.3}$$

where $O(\vec{p}_1,\vec{p}_2,t)$ is an abbreviation for the 2-pion operator $\pi\pi^{ab}(\vec{p}_1,\vec{p}_2,t)$. For the later treatment it is convenient to define the total momentum $\vec{q} = \vec{p}_1 + \vec{p}_2$ and to set

$$\vec{p}_1 = \vec{p} + \vec{q}, \qquad \vec{p}_2 = -\vec{p} \tag{7.2.4}$$

where $\vec{p}$ is arbitrary. Moreover we write $O[\vec{q},\vec{p}] \equiv O(\vec{p}_1,\vec{p}_2,t)$.

Now let G be some finite subgroup of $O(3)$ with N elements $R_1, R_2, \ldots, R_N$ where $R_i \cdot \vec{q} = \vec{q}$ holds for all $i = 1,\ldots,N$. If we apply all R_i to $\vec{p}$ we get a set P of N vectors $\vec{p}_i$ some of which can be identical. From these we choose the subset $\mathcal{P} = \{\vec{p}_1,\vec{p}_2,\ldots,\vec{p}_{N'}\} \subset$

P of the N' pairwise different momenta. Because $R_i^{-1} \in G$ also $R_i^{-1} \cdot \vec{p} \in \mathcal{P}$ if $\vec{p} \in \mathcal{P}$. From (7.2.3) we immediately see that

$$O[\vec{q}, \vec{p}] \xrightarrow{R} O[\vec{q}, R^{-1}\vec{p}] \tag{7.2.5}$$

holds where $R \in \{R_1, \dots R_N\}$. With the momenta $\vec{p}_i \in \mathcal{P}$ we can build a whole set of operators $O[\vec{q}, \vec{p}_i]$ and we can write down an equation in matrix/vector notation for their transformation behaviour under R:

$$\begin{pmatrix} O[\vec{q}, \vec{p}_1] \\ O[\vec{q}, \vec{p}_2] \\ \vdots \\ O[\vec{q}, \vec{p}_{N'}] \end{pmatrix} \xrightarrow{R} \begin{pmatrix} M_{11}(R) & \dots & M_{1N'}(R) \\ \vdots & & \vdots \\ M_{N'1}(R) & \dots & M_{N'N'}(R) \end{pmatrix} \begin{pmatrix} O[\vec{q}, \vec{p}_1] \\ O[\vec{q}, \vec{p}_2] \\ \vdots \\ O[\vec{q}, \vec{p}_{N'}] \end{pmatrix} \tag{7.2.6}$$

or in shorthand notation

$$O[\vec{q}, \vec{p}_i] \xrightarrow{R} \sum_{j=1}^{N'} M_{ij}(R) O[\vec{q}, \vec{p}_j] \quad \text{for all } i \in \{1, \dots, N'\}. \tag{7.2.7}$$

The matrix $M_{ij}(R)$ is an N'-dimensional representation of the group element R. For a linear combination of operators

$$\sum_{i=1}^{N'} a_i O[\vec{q}, \vec{p}_i] \tag{7.2.8}$$

we get

$$\sum_{i=1}^{N'} a_i O[\vec{q}, \vec{p}_i] \xrightarrow{R} \sum_{i,j=1}^{N'} a_i M_{ij}(R) O[\vec{q}, \vec{p}_j]. \tag{7.2.9}$$

The goal is now to find linear combinations of the operators $O[\vec{q}, \vec{p}_i]$ such that they transform according to one of the irreducible representations of the point group G. Instead of applying the projection operators constructed in abstract group theory (see for example [35]) we use a somewhat "pedestrian" approach. So let L be some M-dimensional ($M \leq N' \leq N$) irreducible representation of G with matrices $L(R)$. If an appropriate combination of $O[\vec{q}, \vec{p}_i]$ should transform according to the irreducible representation L the following equation must be fulfilled:

$$\sum_{i,j=1}^{N'} a_i^m M_{ij}(R) O[\vec{q}, \vec{p}_j] = \sum_{k=1}^{M} L_{mk}(R) \sum_{i=1}^{N'} a_i^k O[\vec{q}, \vec{p}_i] \quad \text{for all } m \in \{1, \dots, M\}. \tag{7.2.10}$$

For a given irreducible representation (7.2.10) yields a set of linear equations for every group element R. From these we can then determine the coefficients a_i^m. Let us now consider the different point groups that are of interest to us.

7.2.1. Transformation under D_{4h}

We already analysed D_{4h} in section 6. Here we restrict ourselves to the subgroup C_{4v} (isomorphic to the dihedral group D_4), which leaves the total momentum $\vec{q} \propto (0,0,1)$ invariant, i.e., $R \cdot \vec{q} = \vec{q}\ \forall\ R \in C_{4v}$. This group has 8 elements in 5 conjugacy classes. The 3-dimensional matrix representations of these elements are

$$\begin{aligned} R_1 &= \begin{pmatrix} 1 & 0 & 0 \\ 0 & 1 & 0 \\ 0 & 0 & 1 \end{pmatrix} & R_2 &= \begin{pmatrix} 1 & 0 & 0 \\ 0 & -1 & 0 \\ 0 & 0 & 1 \end{pmatrix} & R_3 &= \begin{pmatrix} -1 & 0 & 0 \\ 0 & 1 & 0 \\ 0 & 0 & 1 \end{pmatrix} \\ R_4 &= \begin{pmatrix} -1 & 0 & 0 \\ 0 & -1 & 0 \\ 0 & 0 & 1 \end{pmatrix} & R_5 &= \begin{pmatrix} 0 & 1 & 0 \\ -1 & 0 & 0 \\ 0 & 0 & 1 \end{pmatrix} & R_6 &= \begin{pmatrix} 0 & -1 & 0 \\ 1 & 0 & 0 \\ 0 & 0 & 1 \end{pmatrix} \\ R_7 &= \begin{pmatrix} 0 & 1 & 0 \\ 1 & 0 & 0 \\ 0 & 0 & 1 \end{pmatrix} & R_8 &= \begin{pmatrix} 0 & -1 & 0 \\ -1 & 0 & 0 \\ 0 & 0 & 1 \end{pmatrix}. \end{aligned} \tag{7.2.11}$$

The conjugacy classes are $\{R_1\}, \{R_4\}, \{R_5, R_6\}, \{R_2, R_3\}$ and $\{R_7, R_8\}$. If we choose $\vec{p} = (0,0,p)$ then $\mathcal{P} = \{\vec{p}\}$ and $R\vec{p} = \vec{p}$ holds for all $R \in G$. Therefore the representation is 1-dimensional and we have

$$O[\vec{q},\vec{p}] \xrightarrow{R} O[\vec{q},\vec{p}]. \tag{7.2.12}$$

In this case we have the trivial representation.

Now we set $\vec{p} = (p,0,0)$. Applying all R in (7.2.11) to $\vec{p}$ we get the set

$$\mathcal{P} = \left\{ \vec{p}_1 = \begin{pmatrix} p \\ 0 \\ 0 \end{pmatrix}, \vec{p}_2 = \begin{pmatrix} 0 \\ p \\ 0 \end{pmatrix}, \vec{p}_3 = \begin{pmatrix} -p \\ 0 \\ 0 \end{pmatrix}, \vec{p}_4 = \begin{pmatrix} 0 \\ -p \\ 0 \end{pmatrix} \right\} \tag{7.2.13}$$

which gives us a 4-dimensional representation. For every R we construct the correspond-

	$\{R_1\}$	$\{R_4\}$	$\{R_5, R_6\}$	$\{R_2, R_3\}$	$\{R_8, R_7\}$
A_1	1	1	1	1	1
A_2	1	1	1	-1	-1
B_1	1	1	-1	1	-1
B_2	1	1	-1	-1	1
E	2	-2	0	0	0

Table 7.2.1.: Character table of C_{4v}.

ing transformation matrix $M(R)$:

$$M(R_1) = \begin{pmatrix} 1 & 0 & 0 & 0 \\ 0 & 1 & 0 & 0 \\ 0 & 0 & 1 & 0 \\ 0 & 0 & 0 & 1 \end{pmatrix} \qquad M(R_2) = \begin{pmatrix} 1 & 0 & 0 & 0 \\ 0 & 0 & 0 & 1 \\ 0 & 0 & 1 & 0 \\ 0 & 1 & 0 & 0 \end{pmatrix}$$

$$M(R_3) = \begin{pmatrix} 0 & 0 & 1 & 0 \\ 0 & 1 & 0 & 0 \\ 1 & 0 & 0 & 0 \\ 0 & 0 & 0 & 1 \end{pmatrix} \qquad M(R_4) = \begin{pmatrix} 0 & 0 & 1 & 0 \\ 0 & 0 & 0 & 1 \\ 1 & 0 & 0 & 0 \\ 0 & 1 & 0 & 0 \end{pmatrix}$$

$$M(R_5) = \begin{pmatrix} 0 & 1 & 0 & 0 \\ 0 & 0 & 1 & 0 \\ 0 & 0 & 0 & 1 \\ 1 & 0 & 0 & 0 \end{pmatrix} \qquad M(R_6) = \begin{pmatrix} 0 & 0 & 0 & 1 \\ 1 & 0 & 0 & 0 \\ 0 & 1 & 0 & 0 \\ 0 & 0 & 1 & 0 \end{pmatrix}$$

$$M(R_7) = \begin{pmatrix} 0 & 1 & 0 & 0 \\ 1 & 0 & 0 & 0 \\ 0 & 0 & 0 & 1 \\ 0 & 0 & 1 & 0 \end{pmatrix} \qquad M(R_8) = \begin{pmatrix} 0 & 0 & 0 & 1 \\ 0 & 0 & 1 & 0 \\ 0 & 1 & 0 & 0 \\ 1 & 0 & 0 & 0 \end{pmatrix}. \tag{7.2.14}$$

With the help of character tables [3, 35] we can decompose this representation into the irreducible representations

$$A_1 \oplus B_1 \oplus E \tag{7.2.15}$$

where A_1 and B_1 are 1-dimensional and E is 2-dimensional (see table 7.2.1). To find a combination $\sum a_i O[\vec{q}, \vec{p}_i]$ that transforms according to the trivial representation A_1 is not hard. Using (7.2.10) we get $a_1 = a_2 = a_3 = a_4$ for the coefficients and defining $a_1 = 1$ gives

$$O[\vec{q}, \vec{p}_1] + O[\vec{q}, \vec{p}_2] + O[\vec{q}, \vec{p}_3] + O[\vec{q}, \vec{p}_4] \tag{7.2.16}$$

for A_1.

Doing the same for B_1, equation (7.2.10) gives us a set of relations for the coefficients a_i, for example $a_1 = a_3 = -a_2 = -a_4$ under R_5. Choosing $a_1 = 1$ it follows that

$$O[\vec{q}, \vec{p}_1] - O[\vec{q}, \vec{p}_2] + O[\vec{q}, \vec{p}_3] - O[\vec{q}, \vec{p}_4] \tag{7.2.17}$$

transforms according to the irreducible representation B_1.

For the 2-dimensional representation E we give here an explicit form of its elements:

$$\begin{aligned} L(R_1) &= \begin{pmatrix} 1 & 0 \\ 0 & 1 \end{pmatrix} & L(R_2) &= \begin{pmatrix} 1 & 0 \\ 0 & -1 \end{pmatrix} & L(R_3) &= \begin{pmatrix} -1 & 0 \\ 0 & 1 \end{pmatrix} \\ L(R_4) &= \begin{pmatrix} -1 & 0 \\ 0 & -1 \end{pmatrix} & L(R_5) &= \begin{pmatrix} 0 & 1 \\ -1 & 0 \end{pmatrix} & L(R_6) &= \begin{pmatrix} 0 & -1 \\ 1 & 0 \end{pmatrix} \\ L(R_7) &= \begin{pmatrix} 0 & 1 \\ 1 & 0 \end{pmatrix} & L(R_8) &= \begin{pmatrix} 0 & -1 \\ -1 & 0 \end{pmatrix}. \end{aligned} \tag{7.2.18}$$

The equation that has to be solved reads

$$\sum_{i,j=1}^{4} \begin{pmatrix} a_i M_{ij}(R) O[\vec{q},\vec{p}_j] \\ b_i M_{ij}(R) O[\vec{q},\vec{p}_j] \end{pmatrix} = \sum_{i=1}^{4} L(R) \begin{pmatrix} a_i O[\vec{q},\vec{p}_i] \\ b_i O[\vec{q},\vec{p}_i] \end{pmatrix}. \tag{7.2.19}$$

Setting $R = R_2$ and $R = R_5$ we obtain the two coefficient vectors $\vec{a} = (1, 0, -1, 0)$ and $\vec{b} = (0, 1, 0, -1)$ (choosing $a_1 = 1$) and the operator doublet transforming according to E is

$$\begin{pmatrix} O[\vec{q},\vec{p}_1] - O[\vec{q},\vec{p}_3] \\ O[\vec{q},\vec{p}_2] - O[\vec{q},\vec{p}_4] \end{pmatrix}. \tag{7.2.20}$$

The next momentum $\vec{p}$ that we analyse is $\vec{p} = (p, p, 0)$ which generates the momentum set

$$\mathcal{P} = \left\{ \vec{p}_1 = \begin{pmatrix} p \\ p \\ 0 \end{pmatrix}, \vec{p}_2 = \begin{pmatrix} -p \\ -p \\ 0 \end{pmatrix}, \vec{p}_3 = \begin{pmatrix} p \\ -p \\ 0 \end{pmatrix}, \vec{p}_4 = \begin{pmatrix} -p \\ p \\ 0 \end{pmatrix} \right\} \tag{7.2.21}$$

under (7.2.11). The 4-dimensional representation matrices are then

$$\begin{aligned} M(R_1) &= \begin{pmatrix} 1 & 0 & 0 & 0 \\ 0 & 1 & 0 & 0 \\ 0 & 0 & 1 & 0 \\ 0 & 0 & 0 & 1 \end{pmatrix} & M(R_2) &= \begin{pmatrix} 0 & 0 & 1 & 0 \\ 0 & 0 & 0 & 1 \\ 1 & 0 & 0 & 0 \\ 0 & 1 & 0 & 0 \end{pmatrix} \\ M(R_3) &= \begin{pmatrix} 0 & 0 & 0 & 1 \\ 0 & 0 & 1 & 0 \\ 0 & 1 & 0 & 0 \\ 1 & 0 & 0 & 0 \end{pmatrix} & M(R_4) &= \begin{pmatrix} 0 & 1 & 0 & 0 \\ 1 & 0 & 0 & 0 \\ 0 & 0 & 0 & 1 \\ 0 & 0 & 1 & 0 \end{pmatrix} \\ M(R_5) &= \begin{pmatrix} 0 & 0 & 0 & 1 \\ 0 & 0 & 1 & 0 \\ 1 & 0 & 0 & 0 \\ 0 & 1 & 0 & 0 \end{pmatrix} & M(R_6) &= \begin{pmatrix} 0 & 0 & 1 & 0 \\ 0 & 0 & 0 & 1 \\ 0 & 1 & 0 & 0 \\ 1 & 0 & 0 & 0 \end{pmatrix} \\ M(R_7) &= \begin{pmatrix} 1 & 0 & 0 & 0 \\ 0 & 1 & 0 & 0 \\ 0 & 0 & 0 & 1 \\ 0 & 0 & 1 & 0 \end{pmatrix} & M(R_8) &= \begin{pmatrix} 0 & 1 & 0 & 0 \\ 1 & 0 & 0 & 0 \\ 0 & 0 & 1 & 0 \\ 0 & 0 & 0 & 1 \end{pmatrix}. \end{aligned} \tag{7.2.22}$$

	$\{R_1\}$	$\{R_2\}$	$\{R_3\}$	$\{R_4\}$
A_1	1	1	1	1
A_2	1	-1	-1	1
B_2	1	1	-1	-1
B_1	1	-1	1	-1

Table 7.2.2.: Character table of C_{2v}.

This representation decomposes into the three irreducible representations

$$A_1 \oplus B_2 \oplus E. \tag{7.2.23}$$

The trivial representation A_1 is again easy to find and analogous to the previous case

$$O[\vec{q},\vec{p}_1] + O[\vec{q},\vec{p}_2] + O[\vec{q},\vec{p}_3] + O[\vec{q},\vec{p}_4]. \tag{7.2.24}$$

For B_2 we get the operator combination

$$O[\vec{q},\vec{p}_1] + O[\vec{q},\vec{p}_2] - O[\vec{q},\vec{p}_3] - O[\vec{q},\vec{p}_4] \tag{7.2.25}$$

and for the 2-dimensional representation E the result is

$$\begin{pmatrix} O[\vec{q},\vec{p}_1] - O[\vec{q},\vec{p}_2] + O[\vec{q},\vec{p}_3] - O[\vec{q},\vec{p}_4] \\ O[\vec{q},\vec{p}_1] - O[\vec{q},\vec{p}_2] - O[\vec{q},\vec{p}_3] + O[\vec{q},\vec{p}_4] \end{pmatrix}. \tag{7.2.26}$$

7.2.2. Transformation under D_{2h}

We consider the subgroup C_{2v} of D_{2h} which leaves invariant the total momentum $\vec{q} \propto (1,1,0)$, like in the previous section. This group consists of the four elements

$$R_1 = \begin{pmatrix} 1 & 0 & 0 \\ 0 & 1 & 0 \\ 0 & 0 & 1 \end{pmatrix} \qquad R_2 = \begin{pmatrix} 1 & 0 & 0 \\ 0 & 1 & 0 \\ 0 & 0 & -1 \end{pmatrix}$$
$$R_3 = \begin{pmatrix} 0 & 1 & 0 \\ 1 & 0 & 0 \\ 0 & 0 & 1 \end{pmatrix} \qquad R_4 = \begin{pmatrix} 0 & 1 & 0 \\ 1 & 0 & 0 \\ 0 & 0 & -1 \end{pmatrix}. \tag{7.2.27}$$

Because the group is Abelian all irreducible representations are 1-dimensional. In total there are four irreducible representations whose characters are given in table 7.2.2.

Our first choice of $\vec{p}$ is $\vec{p} = (p,p,0)$. Then $R_i \cdot \vec{p} = \vec{p}$ holds for all $i = 1,\ldots,4$. Therefore $\mathcal{P} = \{\vec{p}\}$ and the operator $O[\vec{q},\vec{p}]$ transforms according to the trivial representation. Next we choose $\vec{p} = (0,0,p)$ and get the momentum set

$$\mathcal{P} = \left\{ \vec{p}_1 = \begin{pmatrix} 0 \\ 0 \\ p \end{pmatrix}, \vec{p}_2 = \begin{pmatrix} 0 \\ 0 \\ -p \end{pmatrix} \right\} \tag{7.2.28}$$

The matrices for this 2-dimensional representation are

$$\begin{aligned} M(R_1) &= \begin{pmatrix} 1 & 0 \\ 0 & 1 \end{pmatrix} & M(R_2) &= \begin{pmatrix} 0 & 1 \\ 1 & 0 \end{pmatrix} \\ M(R_3) &= M(R_1) & M(R_4) &= M(R_2) \end{aligned} \tag{7.2.29}$$

and the representation space decomposes into

$$A_1 \oplus B_1. \tag{7.2.30}$$

The operator combination transforming according to A_1, the trivial representation, is easy to construct and reads

$$O[\vec{q}, \vec{p}_1] + O[\vec{q}, \vec{p}_2]. \tag{7.2.31}$$

The operator transforming according to B_1 is

$$O[\vec{q}, \vec{p}_1] - O[\vec{q}, \vec{p}_2]. \tag{7.2.32}$$

Choosing $\vec{p} = (p, 0, 0)$ gives us the set

$$\mathcal{P} = \left\{ \vec{p}_1 = \begin{pmatrix} p \\ 0 \\ 0 \end{pmatrix}, \vec{p}_2 = \begin{pmatrix} 0 \\ p \\ 0 \end{pmatrix} \right\} \tag{7.2.33}$$

and the matrices of this representation are

$$\begin{aligned} M(R_1) &= \begin{pmatrix} 1 & 0 \\ 0 & 1 \end{pmatrix} & M(R_3) &= \begin{pmatrix} 0 & 1 \\ 1 & 0 \end{pmatrix} \\ M(R_2) &= M(R_1) & M(R_4) &= M(R_3). \end{aligned} \tag{7.2.34}$$

Again, the 2-dimensional representation decomposes into two 1-dimensional irreducible spaces

$$A_1 \oplus B_2. \tag{7.2.35}$$

The operator for the trivial representation is clear. It looks like (7.2.31) and the operator transforming according to B_2 has the same form as (7.2.32). The difference here is that we just use different momenta $\vec{p}_1, \vec{p}_2$.

7.2.3. Transformation under D_{3d}

The last case we pay attention to is the total momentum $\vec{q} \propto (1, 1, 1)$. The subgroup of D_{3d} which leaves $\vec{q}$ invariant is C_{3v} possessing three conjugacy classes. This group

	$\{R_1\}$	$\{R_2, R_3, R_4\}$	$\{R_5, R_6\}$
A_1	1	1	1
A_2	1	-1	1
E	2	0	-1

Table 7.2.3.: Character table of C_{3v}.

interchanges the three components of the vector $\vec{p}$ and is therefore isomorphic to the permutation group S_3. The six group elements are

$$R_1 = \begin{pmatrix} 1 & 0 & 0 \\ 0 & 1 & 0 \\ 0 & 0 & 1 \end{pmatrix} \qquad R_2 = \begin{pmatrix} 0 & 1 & 0 \\ 1 & 0 & 0 \\ 0 & 0 & 1 \end{pmatrix} \qquad R_3 = \begin{pmatrix} 0 & 0 & 1 \\ 0 & 1 & 0 \\ 1 & 0 & 0 \end{pmatrix}$$
$$R_4 = \begin{pmatrix} 1 & 0 & 0 \\ 0 & 0 & 1 \\ 0 & 1 & 0 \end{pmatrix} \qquad R_5 = \begin{pmatrix} 0 & 0 & 1 \\ 1 & 0 & 0 \\ 0 & 1 & 0 \end{pmatrix} \qquad R_6 = \begin{pmatrix} 0 & 1 & 0 \\ 0 & 0 & 1 \\ 1 & 0 & 0 \end{pmatrix}. \tag{7.2.36}$$

Table 7.2.3 summarises the irreducible characters and the conjugacy classes. Here again, we have the trivial case when we use $\vec{p} = (p, p, p)$ and $O[\vec{q}, \vec{p}] \xrightarrow{R} O[\vec{q}, \vec{p}]$ for all R in C_{3v}.

A more interesting case is $\vec{p} = (0, 0, p)$ which leads to a 3-dimensional representation with momenta

$$\mathcal{P} = \left\{ \vec{p}_1 = \begin{pmatrix} 0 \\ 0 \\ p \end{pmatrix}, \vec{p}_2 = \begin{pmatrix} 0 \\ p \\ 0 \end{pmatrix}, \vec{p}_3 = \begin{pmatrix} p \\ 0 \\ 0 \end{pmatrix} \right\}. \tag{7.2.37}$$

The matrices generated by this momentum set are

$$\begin{aligned} M(R_1) &= R_1 & M(R_2) &= R_4 & M(R_3) &= R_3 \\ M(R_4) &= R_2 & M(R_5) &= R_6 & M(R_6) &= R_5 \end{aligned} \tag{7.2.38}$$

and the space decomposes into the trivial representation A_1 and the 2-dimensional representation E:

$$A_1 \oplus E. \tag{7.2.39}$$

An operator transforming according to A_1 is

$$O[\vec{q}, \vec{p}_1] + O[\vec{q}, \vec{p}_2] + O[\vec{q}, \vec{p}_3]. \tag{7.2.40}$$

The unitary representation matrices for E are

$$L(R_1) = \begin{pmatrix} 1 & 0 \\ 0 & 1 \end{pmatrix} \qquad L(R_2) = \begin{pmatrix} -\frac{1}{2} & \frac{\sqrt{3}}{2} \\ \frac{\sqrt{3}}{2} & \frac{1}{2} \end{pmatrix} \qquad L(R_3) = \begin{pmatrix} -\frac{1}{2} & -\frac{\sqrt{3}}{2} \\ -\frac{\sqrt{3}}{2} & \frac{1}{2} \end{pmatrix}$$
$$L(R_4) = \begin{pmatrix} 1 & 0 \\ 0 & -1 \end{pmatrix} \qquad L(R_5) = \begin{pmatrix} -\frac{1}{2} & -\frac{\sqrt{3}}{2} \\ \frac{\sqrt{3}}{2} & -\frac{1}{2} \end{pmatrix} \qquad L(R_6) = \begin{pmatrix} -\frac{1}{2} & \frac{\sqrt{3}}{2} \\ -\frac{\sqrt{3}}{2} & -\frac{1}{2} \end{pmatrix}. \tag{7.2.41}$$

With the help of R_3 and R_5 we get the coefficient vectors $\vec{a} = (1, 1, -2)$ and $\vec{b} = (\sqrt{3}, -\sqrt{3}, 0)$ and the operator is

$$\begin{pmatrix} O[\vec{q}, \vec{p}_1] + O[\vec{q}, \vec{p}_2] - 2O[\vec{q}, \vec{p}_3] \\ \sqrt{3}O[\vec{q}, \vec{p}_1] - \sqrt{3}O[\vec{q}, \vec{p}_2] \end{pmatrix}. \tag{7.2.42}$$

Another possibility to choose $\vec{p}$ is $\vec{p} = (p, p, 0)$. This leads to the set

$$\mathcal{P} = \left\{ \vec{p}_1 = \begin{pmatrix} p \\ p \\ 0 \end{pmatrix}, \vec{p}_2 = \begin{pmatrix} 0 \\ p \\ p \end{pmatrix}, \vec{p}_3 = \begin{pmatrix} p \\ 0 \\ p \end{pmatrix} \right\} \tag{7.2.43}$$

with representation matrices

$$\begin{aligned} M(R_1) &= R_1 & M(R_2) &= R_4 & M(R_3) &= R_2 \\ M(R_4) &= R_3 & M(R_5) &= R_5 & M(R_6) &= R_6. \end{aligned} \tag{7.2.44}$$

The decomposition of this 3-dimensional space is the same as (7.2.39) and the A_1 operator looks like (7.2.40). But the operator combination transforming according to E is different and reads

$$\begin{pmatrix} O[\vec{q}, \vec{p}_1] - 2O[\vec{q}, \vec{p}_2] + O[\vec{q}, \vec{p}_3] \\ \sqrt{3}O[\vec{q}, \vec{p}_1] - \sqrt{3}O[\vec{q}, \vec{p}_3] \end{pmatrix}. \tag{7.2.45}$$

7.3. Transformation of the rho meson operator under point groups

The situation for the rho is the same as the 2-pion case: We want to find a combination of rho operators which transforms according to the irreducible representation of some point group. For total momentum $\vec{q}$ we define the rho meson operator as

$$O_i(\vec{q}) = \sum_{\vec{x}} \mathrm{e}^{i\vec{q}\vec{x}} \bar{\psi}(\vec{x}) \gamma_i F^a \psi(\vec{x}) \tag{7.3.1}$$

where we omitted the time t in $\psi, \bar{\psi}$ for simplicity. For $R \in O(3)$ the following holds:

$$\bar{\psi}(\vec{x}) \gamma_i \psi(\vec{x}) \xrightarrow{R} \sum_{j=1}^{3} R_{ij} \bar{\psi}(R^{-1}\vec{x}) \gamma_j \psi(R^{-1}\vec{x}). \tag{7.3.2}$$

The same is true for the rho with Dirac structure $\gamma_i\gamma_4$, therefore we will restrict the calculations to γ_i. In the previous section we constructed different operators by choosing different values for the momentum $\vec{p}$. In the actual case the particle momentum is

fixed but we can combine rho mesons with different Dirac structure γ_i. An arbitrary combination would then be

$$O_{\vec{a}\cdot\vec{\gamma}}(\vec{q}) \equiv \sum_{i=1}^{3} a_i O_i(\vec{q}) = \sum_{i=1}^{3} a_i \sum_{\vec{x}} \mathrm{e}^{i\vec{q}\vec{x}} \bar{\psi}(\vec{x}) \gamma_i F^a \psi(\vec{x}). \tag{7.3.3}$$

From equation (7.3.2) together with (7.3.3) we deduce

$$\sum_{i=1}^{3} a_i \sum_{\vec{x}} \mathrm{e}^{i\vec{q}\vec{x}} \bar{\psi}(\vec{x}) \gamma_i F^a \psi(\vec{x}) \xrightarrow{R} \sum_{i,j=1}^{3} a_i R_{ij} \sum_{\vec{x}} \mathrm{e}^{i(R^{-1}\vec{q})\vec{x}} \bar{\psi}(\vec{x}) \gamma_j F^a \psi(\vec{x}) \tag{7.3.4}$$

and in a shorthand notation using (7.3.1) this equation reads

$$\sum_{i=1}^{3} a_i O_i(\vec{q}) \xrightarrow{R} \sum_{i,j=1}^{3} a_i R_{ij} O_j(R^{-1}\vec{q}). \tag{7.3.5}$$

Now assume that an M-dimensional irreducible representation L of one point group G is given. According to (7.3.3) we construct a set of M operators $O_{\vec{a}^1\cdot\vec{\gamma}}(\vec{q})$, $O_{\vec{a}^2\cdot\vec{\gamma}}(\vec{q}), \ldots,$ $O_{\vec{a}^M\cdot\vec{\gamma}}(\vec{q})$. Using (7.3.5) we get the relation

$$\sum_{i,j=1}^{3} \begin{pmatrix} a_i^1 R_{ij} O_j(R^{-1}\vec{q}) \\ \vdots \\ a_i^M R_{ij} O_j(R^{-1}\vec{q}) \end{pmatrix} = \sum_{i=1}^{3} \begin{pmatrix} L_{11}(R) & \ldots & L_{1M}(R) \\ \vdots & & \vdots \\ L_{M1}(R) & \ldots & L_{MM}(R) \end{pmatrix} \begin{pmatrix} a_i^1 O_i(R^{-1}\vec{q}) \\ \vdots \\ a_i^M O_i(R^{-1}\vec{q}) \end{pmatrix}. \tag{7.3.6}$$

A shorthand notation is

$$\sum_{i,j=1}^{3} a_i^m R_{ij} O_j(R^{-1}\vec{q}) = \sum_{k=1}^{M} L_{mk}(R) \sum_{i=1}^{3} a_i^k O_i(R^{-1}\vec{q}) \tag{7.3.7}$$

This means that the set $O_{\vec{a}^1\cdot\vec{\gamma}}(\vec{q}), \ldots, O_{\vec{a}^M\cdot\vec{\gamma}}(\vec{q})$ transforms according to the irreducible representation L. As in the case of 2-particle operators we use the R and $L(R)$ with (7.3.6) to calculate the coefficients $a_i^m, m = 1, \ldots, M$.

7.3.1. Transformation under D_{4h}

To analyse this case we consider again the point group C_{4v} with elements given in (7.2.11) and $R\vec{q} = \vec{q}$ for $\vec{q} \propto (0, 0, 1)$. This 3-dimensional representation decomposes into

$$A_1 \oplus E. \tag{7.3.8}$$

For the trivial representation, we find that $a_1 = a_2 = 0$. Choosing $a_3 = 1$ we find that

$$O_3(\vec{q}) \quad \text{longitudinal} \tag{7.3.9}$$

transforms according to A_1.

For the 2-dimensional representation, using for example $R = R_5$, we get the equation:

$$\begin{pmatrix} a_1 O_2(\vec{q}) - a_2 O_1(\vec{q}) + a_3 O_3(\vec{q}) \\ b_1 O_2(\vec{q}) - b_2 O_1(\vec{q}) + b_3 O_3(\vec{q}) \end{pmatrix} = \begin{pmatrix} 0 & 1 \\ -1 & 0 \end{pmatrix} \begin{pmatrix} a_1 O_1(\vec{q}) + a_2 O_2(\vec{q}) + a_3 O_3(\vec{q}) \\ b_1 O_1(\vec{q}) + b_2 O_2(\vec{q}) + b_3 O_3(\vec{q}) \end{pmatrix}. \quad (7.3.10)$$

From this equations we extract $a_3 = 0$, $a_1 = b_2$ and $b_1 = -a_2$. Doing the same with R_2 leads to $a_2 = b_1 = 0$ and the operator is then

$$\begin{pmatrix} O_1(\vec{q}) \\ O_2(\vec{q}) \end{pmatrix} \quad \text{transverse.} \quad (7.3.11)$$

Note that when we use a different direction of the total momentum, e.g. $\vec{q} = (1, 0, 0)$, the operator transforming according to A_1 is then $O_1(\vec{q})$ and the operator corresponding to E is $(O_2(\vec{q}), O_3(\vec{q}))^T$, etc.

7.3.2. Transformation under D_{2h}

The procedure is the same as before: We decompose the 3-dimensional representation of C_{2v} given in (7.2.27) into

$$A_1 \oplus B_1 \oplus B_2. \quad (7.3.12)$$

For total momentum $(1, 1, 0)$ or $(-1, -1, 0)$ the operators are:

$$A_1 : \quad O_1(\vec{q}) + O_2(\vec{q}) \qquad \text{longitudinal} \quad (7.3.13)$$
$$B_2 : \quad O_1(\vec{q}) - O_2(\vec{q}) \qquad \text{transverse 1} \quad (7.3.14)$$
$$B_1 : \quad O_3(\vec{q}) \qquad \text{transverse 2} \quad (7.3.15)$$

and for total momentum $(-1, 1, 0)$ or $(1, -1, 0)$ we get

$$A_1 : \quad O_1(\vec{q}) - O_2(\vec{q}) \qquad \text{longitudinal} \quad (7.3.16)$$
$$B_2 : \quad O_1(\vec{q}) + O_2(\vec{q}) \qquad \text{transverse 1} \quad (7.3.17)$$
$$B_1 : \quad O_3(\vec{q}) \qquad \text{transverse 2} \quad (7.3.18)$$

and similarly for other $\vec{q}$'s.

7.3.3. Transformation under D_{3d}

The representation (7.2.36) of C_{3v} decomposes into a 1- and a 2-dimensional irreducible representation

$$A_1 \oplus E. \quad (7.3.19)$$

Choosing $\vec{q} \propto (1,1,1)$ or $(-1,-1,-1)$ we find that

$$O_1(\vec{q}) + O_2(\vec{q}) + O_3(\vec{q}) \tag{7.3.20}$$

transforms according to the trivial representation A_1 (longitudinal). A doublet of operators transforming according to E (transverse) can be written as

$$\begin{pmatrix} O_{\vec{a}\cdot\vec{\gamma}}(\vec{q}) \\ O_{\vec{b}\cdot\vec{\gamma}}(\vec{q}) \end{pmatrix} \tag{7.3.21}$$

where we obtain

$$\vec{a} = \frac{1}{\sqrt{6}} \begin{pmatrix} -2 \\ 1 \\ 1 \end{pmatrix}, \vec{b} = \frac{1}{\sqrt{2}} \begin{pmatrix} 0 \\ -1 \\ 1 \end{pmatrix}. \tag{7.3.22}$$

8. Energy levels from resonance scattering

Now we want to introduce the effective range model which successfully describes pion scattering phases in experimental particle physics. With this model we also want to derive the expected energies for pion scattering on the lattice.

8.1. The effective range model

According to the Particle Data Group [4] the rho meson has a mass of $m_\rho = (775.49 \pm 0.34)$ MeV and a full width of $\Gamma_\rho = (149.1 \pm 0.8)$ MeV. Almost all rho mesons decay into two pions. The scattering phase shift is a function between 0 and π and takes the value $\pi/2$ at the resonance energy. The effective range formula [31] is a parametrisation near the rho energy and used in experimental physics to describe the phase shift curve:

$$\tan(\delta_{11}^{er}(k)) = \frac{k^3}{W(a + bk^2)}. \tag{8.1.1}$$

The two parameters a and b are related to the mass and the width of the resonance by

$$a = -bk_\rho^2 = \frac{4k_\rho^5}{m_\rho^2 \Gamma_\rho} \tag{8.1.2}$$

with the momentum

$$k_\rho = \tfrac{1}{2}\sqrt{m_\rho^2 - 4m_\pi^2}. \tag{8.1.3}$$

The width can be extracted from the $\rho - \pi\pi$ interaction Lagrangian at first order. We get

$$\Gamma_\rho = \frac{g_{\rho\pi\pi}^2}{6\pi m_\rho^2} \cdot k_\rho^3 \tag{8.1.4}$$

with the coupling

$$g_{\rho\pi\pi} \approx 6.0. \tag{8.1.5}$$

In section 6 we saw that for given total momentum $\frac{2\pi}{L}\vec{d}$ and polarisation the tangent of the scattering phase shift is given by some function $f(q)$ with $q = \frac{L}{2\pi}k_{CM}$. Using the effective range model we can compute solutions k_{CM} of

$$\tan(\delta_{11}^{er}(k_{CM})) = f(q) \tag{8.1.6}$$

varying $m_\pi L$. From k_{CM} we then obtain the energy levels in the laboratory frame via

$$W_L = \sqrt{\left(\tfrac{2\pi}{L}\vec{d}\right)^2 + 4(k_{CM}^2 + m_\pi^2)}. \tag{8.1.7}$$

The energy for two non-interacting pions is

$$W_L = \sqrt{\vec{p}_1^{\,2} + m_\pi^2} + \sqrt{\vec{p}_2^{\,2} + m_\pi^2} \tag{8.1.8}$$

with momenta

$$\vec{p}_1 = \frac{2\pi\vec{n}}{L} + \frac{2\pi\vec{d}}{L}, \quad \vec{p}_2 = -\frac{2\pi\vec{n}}{L} \tag{8.1.9}$$

where $\vec{d} \in \mathbb{Z}^3$ is fixed and $\vec{n} \in \mathbb{Z}^3$ is arbitrary. For the rho meson we have

$$W_L^\rho = \sqrt{\vec{p}^{\,2} + m_\rho^2} \quad \text{with} \quad \vec{p} = \frac{2\pi\vec{d}}{L}. \tag{8.1.10}$$

8.2. The 2-pion operators

When we calculate the free energy levels according to (8.1.8) we get all of them mixed together. To disentangle the different polarisations we calculate the energies for a small interaction and compare them with the energies from the non-interacting theory. This procedure allows us to identify the various group representations. We work with a 2-pion operator of isospin $I = 1$ and $I_z = 0$ given by [7]

$$\pi\pi(\vec{p}_1, \vec{p}_2) = \frac{1}{\sqrt{2}}\Big(\pi^-(\vec{p}_1)\pi^+(\vec{p}_2) - \pi^+(\vec{p}_1)\pi^-(\vec{p}_2)\Big). \tag{8.2.1}$$

Interchanging $\vec{p}_1$ and $\vec{p}_2$ gives

$$\pi\pi(\vec{p}_2, \vec{p}_1) = -\pi\pi(\vec{p}_1, \vec{p}_2). \tag{8.2.2}$$

With (8.2.2) and the results from the last chapter we can now write down 2-pion operators for the different polarisations and point groups. The corresponding rho operators can be read off directly from chapter 7. It is important that the rho and 2-pion operators have the identical transformation behaviour. In the following discussion we omit the factor $\frac{2\pi}{L}$ in the momenta for simplicity.

8.2.1. Group D_{4h}

We assume that the two pions have the momenta $\vec{p}_1 = \vec{d} + \vec{n}$ and $\vec{p}_2 = -\vec{n}$ where $\vec{d} = (0, 0, 1)$. The vectors $\vec{n}$ which determine the energy levels for the longitudinal polarisation, are

$$\vec{n} = (0, 0, 0), (0, 1, 0), (0, 0, 1), \ldots \tag{8.2.3}$$

and for the transverse polarisation

$$\vec{n} = (0,1,0), (1,1,0), \ldots . \tag{8.2.4}$$

The lowest energy level corresponds to the longitudinal polarisation with $\vec{n} = (0,0,0)$. In this case we have $R \cdot \vec{n} = \vec{n}$ for all group elements R, therefore the representation is 1-dimensional and trivial and the 2-pion operator is

$$\pi\pi(\vec{d}, \vec{0}) \tag{8.2.5}$$

which is the same as in [7].

The next higher level corresponds to $\vec{n} = (0,1,0)$, which appears for the longitudinal and for the transverse polarisation. According to (7.2.13) the group elements $R \in C_{4v}$ generate from $\vec{n}$ the set

$$\mathcal{P} = \left\{ \vec{n}_1 = \begin{pmatrix} 1 \\ 0 \\ 0 \end{pmatrix}, \vec{n}_2 = \begin{pmatrix} 0 \\ 1 \\ 0 \end{pmatrix}, \vec{n}_3 = \begin{pmatrix} -1 \\ 0 \\ 0 \end{pmatrix}, \vec{n}_4 = \begin{pmatrix} 0 \\ -1 \\ 0 \end{pmatrix} \right\}. \tag{8.2.6}$$

For the trivial representation A_1 we get the operator

$$\pi\pi(\left(\begin{smallmatrix} 1 \\ 0 \\ 1 \end{smallmatrix}\right), \left(\begin{smallmatrix} -1 \\ 0 \\ 0 \end{smallmatrix}\right)) + \pi\pi(\left(\begin{smallmatrix} 0 \\ 1 \\ 1 \end{smallmatrix}\right), \left(\begin{smallmatrix} 0 \\ -1 \\ 0 \end{smallmatrix}\right)) + \pi\pi(\left(\begin{smallmatrix} -1 \\ 0 \\ 1 \end{smallmatrix}\right), \left(\begin{smallmatrix} 1 \\ 0 \\ 0 \end{smallmatrix}\right)) + \pi\pi(\left(\begin{smallmatrix} 0 \\ -1 \\ 1 \end{smallmatrix}\right), \left(\begin{smallmatrix} 0 \\ 1 \\ 0 \end{smallmatrix}\right)) \tag{8.2.7}$$

which corresponds to the first excited longitudinal level. Representation B_1 gives

$$\pi\pi(\left(\begin{smallmatrix} 1 \\ 0 \\ 1 \end{smallmatrix}\right), \left(\begin{smallmatrix} -1 \\ 0 \\ 0 \end{smallmatrix}\right)) - \pi\pi(\left(\begin{smallmatrix} 0 \\ 1 \\ 1 \end{smallmatrix}\right), \left(\begin{smallmatrix} 0 \\ -1 \\ 0 \end{smallmatrix}\right)) + \pi\pi(\left(\begin{smallmatrix} -1 \\ 0 \\ 1 \end{smallmatrix}\right), \left(\begin{smallmatrix} 1 \\ 0 \\ 0 \end{smallmatrix}\right)) - \pi\pi(\left(\begin{smallmatrix} 0 \\ -1 \\ 1 \end{smallmatrix}\right), \left(\begin{smallmatrix} 0 \\ 1 \\ 0 \end{smallmatrix}\right)) \tag{8.2.8}$$

but this representation does not appear in the rho case as we have seen in section 7.3.1. For the 2-dimensional representation E we have

$$\begin{pmatrix} \pi\pi(\left(\begin{smallmatrix} 1 \\ 0 \\ 1 \end{smallmatrix}\right), \left(\begin{smallmatrix} -1 \\ 0 \\ 0 \end{smallmatrix}\right)) - \pi\pi(\left(\begin{smallmatrix} -1 \\ 0 \\ 1 \end{smallmatrix}\right), \left(\begin{smallmatrix} 1 \\ 0 \\ 0 \end{smallmatrix}\right)) \\ \pi\pi(\left(\begin{smallmatrix} 0 \\ 1 \\ 1 \end{smallmatrix}\right), \left(\begin{smallmatrix} 0 \\ -1 \\ 0 \end{smallmatrix}\right)) - \pi\pi(\left(\begin{smallmatrix} 0 \\ -1 \\ 1 \end{smallmatrix}\right), \left(\begin{smallmatrix} 0 \\ 1 \\ 0 \end{smallmatrix}\right)) \end{pmatrix} \tag{8.2.9}$$

corresponding to the lowest level for transverse polarisation.

8.2.2. Group D_{2h}

Here we have $\vec{d} = (1,1,0)$. In the case of the longitudinal polarisation (representation A_1 of C_{2v}) we have the vectors

$$\vec{n} = (0,0,0), (0,0,1), (1,0,0), \ldots, \tag{8.2.10}$$

in the case of transverse 2 (representation B_1)

$$\vec{n} = (0,0,1), (-1,0,-1), \ldots \tag{8.2.11}$$

and for transverse 1 (representation B_2)

$$\vec{n} = (-1,0,0), (-1,0,-1), (1,0,0), \ldots. \tag{8.2.12}$$

The lowest level is again longitudinal with $\vec{n} = (0,0,0)$ and result is the same as for D_{4h}:

$$\pi\pi(\vec{d}, \vec{0}). \tag{8.2.13}$$

The next higher energy level is $\vec{n} = (-1,0,0)$ contained in the transverse 1 polarisation. Here we get the set (see (7.2.33))

$$\mathcal{P} = \left\{ \vec{n}_1 = \begin{pmatrix} -1 \\ 0 \\ 0 \end{pmatrix}, \vec{n}_2 = \begin{pmatrix} 0 \\ -1 \\ 0 \end{pmatrix} \right\}. \tag{8.2.14}$$

The 2-dimensional space is a direct sum of A_1 and B_2. For the trivial representation A_1 the operator is (7.2.31)

$$\pi\pi(\left(\begin{smallmatrix} 0 \\ 1 \\ 0 \end{smallmatrix}\right), \left(\begin{smallmatrix} 1 \\ 0 \\ 0 \end{smallmatrix}\right)) + \pi\pi(\left(\begin{smallmatrix} 1 \\ 0 \\ 0 \end{smallmatrix}\right), \left(\begin{smallmatrix} 0 \\ 1 \\ 0 \end{smallmatrix}\right)) = 0. \tag{8.2.15}$$

The operator vanishes because of the symmetry (8.2.2). For the representation B_2 we can also make use of this symmetry property and (7.2.32) simplifies to

$$2\pi\pi(\left(\begin{smallmatrix} 0 \\ 1 \\ 0 \end{smallmatrix}\right), \left(\begin{smallmatrix} 1 \\ 0 \\ 0 \end{smallmatrix}\right)). \tag{8.2.16}$$

This operator belongs to the lowest energy of transverse 1.

The lowest energy state for transverse 2 is $\vec{n} = (0,0,1)$, which is also the first excited level of the longitudinal polarisation. For the set of vectors $\vec{n}_i$ we get (see (7.2.28))

$$\mathcal{P} = \left\{ \vec{n}_1 = \begin{pmatrix} 0 \\ 0 \\ 1 \end{pmatrix}, \vec{n}_2 = \begin{pmatrix} 0 \\ 0 \\ -1 \end{pmatrix} \right\}. \tag{8.2.17}$$

The space decomposes into A_1 and B_1. Now both operators are non-zero and the one transforming like A_1 is

$$\pi\pi(\left(\begin{smallmatrix} 1 \\ 1 \\ 1 \end{smallmatrix}\right), \left(\begin{smallmatrix} 0 \\ 0 \\ -1 \end{smallmatrix}\right)) + \pi\pi(\left(\begin{smallmatrix} 1 \\ 1 \\ -1 \end{smallmatrix}\right), \left(\begin{smallmatrix} 0 \\ 0 \\ 1 \end{smallmatrix}\right)) \tag{8.2.18}$$

which belongs to the longitudinal polarisation. The operator for the transverse 2 state is then

$$\pi\pi(\left(\begin{smallmatrix} 1 \\ 1 \\ 1 \end{smallmatrix}\right), \left(\begin{smallmatrix} 0 \\ 0 \\ -1 \end{smallmatrix}\right)) - \pi\pi(\left(\begin{smallmatrix} 1 \\ 1 \\ -1 \end{smallmatrix}\right), \left(\begin{smallmatrix} 0 \\ 0 \\ 1 \end{smallmatrix}\right)). \tag{8.2.19}$$

8.2.3. Group D_{3d}

For this point group we choose $\vec{d} = (1,1,1)$. The $\vec{n}$'s which give the energy levels for the longitudinal case (representation A_1 of C_{3v}) are

$$\vec{n} = (0,0,0), (-1,0,0), (1,0,0), \ldots \tag{8.2.20}$$

and for the transverse case (representation E)

$$\vec{n} = (-1,0,0), (1,0,0), \ldots . \tag{8.2.21}$$

The longitudinal polarisation with $\vec{n} = (0,0,0)$ gives the operator

$$\pi\pi(\vec{d}, \vec{0}) \tag{8.2.22}$$

as for the previous groups. The vector $\vec{n} = (-1,0,0)$ provides the lowest level for transverse polarisation and also the first excited level for longitudinal polarisation. The set corresponding to (7.2.37) and defining a 3-dimensional representation is

$$\mathcal{P} = \left\{ \vec{p}_1 = \begin{pmatrix} 0 \\ 0 \\ -1 \end{pmatrix}, \vec{p}_2 = \begin{pmatrix} 0 \\ -1 \\ 0 \end{pmatrix}, \vec{p}_3 = \begin{pmatrix} -1 \\ 0 \\ 0 \end{pmatrix} \right\}. \tag{8.2.23}$$

The trivial representation gives the operator for the longitudinal level

$$\pi\pi(\left(\begin{smallmatrix} 1 \\ 1 \\ 0 \end{smallmatrix}\right), \left(\begin{smallmatrix} 0 \\ 0 \\ 1 \end{smallmatrix}\right)) + \pi\pi(\left(\begin{smallmatrix} 1 \\ 0 \\ 1 \end{smallmatrix}\right), \left(\begin{smallmatrix} 0 \\ 1 \\ 0 \end{smallmatrix}\right)) + \pi\pi(\left(\begin{smallmatrix} 0 \\ 1 \\ 1 \end{smallmatrix}\right), \left(\begin{smallmatrix} 1 \\ 0 \\ 0 \end{smallmatrix}\right)) \tag{8.2.24}$$

and the result for the 2-dimensional representation E belonging to transverse polarisation is (see (7.2.42))

$$\begin{pmatrix} \pi\pi(\left(\begin{smallmatrix} 1 \\ 1 \\ 0 \end{smallmatrix}\right), \left(\begin{smallmatrix} 0 \\ 0 \\ 1 \end{smallmatrix}\right)) + \pi\pi(\left(\begin{smallmatrix} 1 \\ 0 \\ 1 \end{smallmatrix}\right), \left(\begin{smallmatrix} 0 \\ 1 \\ 0 \end{smallmatrix}\right)) - 2\pi\pi(\left(\begin{smallmatrix} 0 \\ 1 \\ 1 \end{smallmatrix}\right), \left(\begin{smallmatrix} 1 \\ 0 \\ 0 \end{smallmatrix}\right)) \\ \sqrt{3}\pi\pi(\left(\begin{smallmatrix} 1 \\ 1 \\ 0 \end{smallmatrix}\right), \left(\begin{smallmatrix} 0 \\ 0 \\ 1 \end{smallmatrix}\right)) - \sqrt{3}\pi\pi(\left(\begin{smallmatrix} 1 \\ 0 \\ 1 \end{smallmatrix}\right), \left(\begin{smallmatrix} 0 \\ 1 \\ 0 \end{smallmatrix}\right)) \end{pmatrix}. \tag{8.2.25}$$

8.3. Energy level plots

The following pictures show the energy levels for the two interacting pions (solid black lines), the non-interacting pions (blue dashed lines) and the rho (dashed red line). In the upper part we show also the corresponding scattering phases from the effective range model. The assumed rho to pion mass ratio is $m_\rho/m_\pi = 0.29$ and $g_{\rho\pi\pi} = 6.0$. The two dotted vertical lines refer to the $m_\pi L$ values of the $32^3 \times 64$ and $40^3 \times 64$ lattices used in our numerical work (see chapter 10).

Where the non-interacting 2-pion energy levels cross the rho energy, we can nicely see the so-called *avoided level crossing* for the interacting particles.

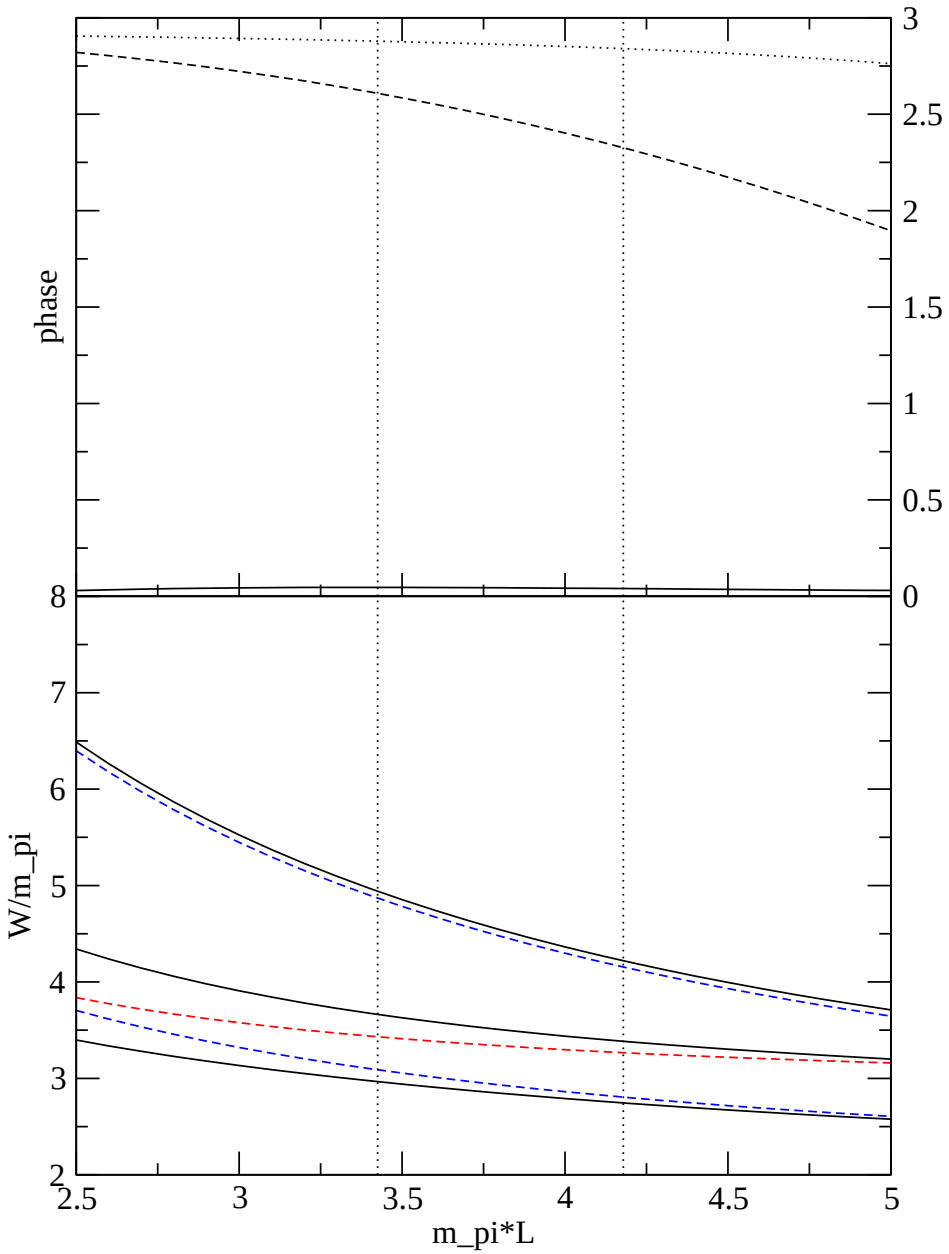

Figure 8.3.1.: Scattering phase shift and energy levels from the effective range model for total momentum $(0, 0, 1)$ and longitudinal polarisation.

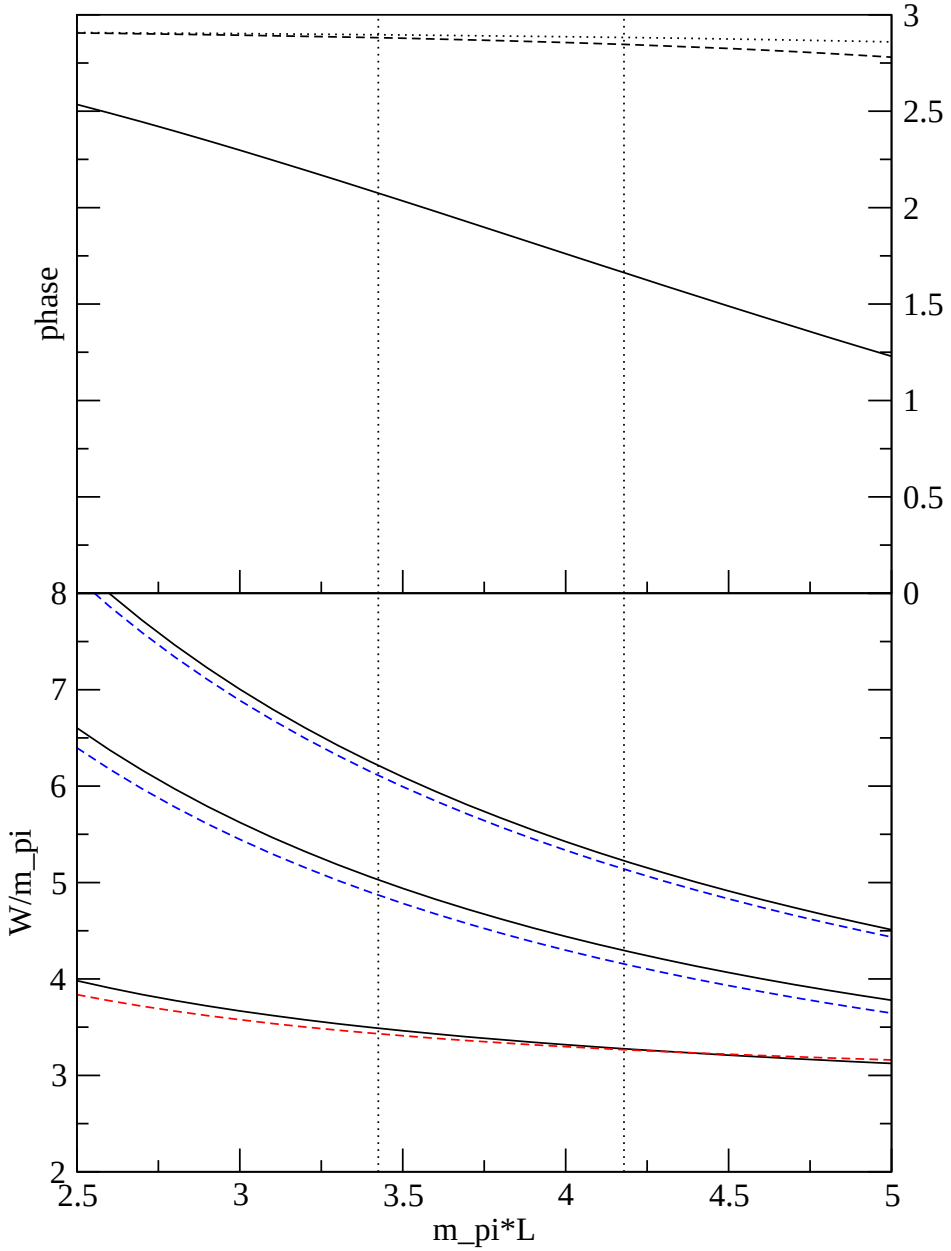

Figure 8.3.2.: Scattering phase shift and energy levels from the effective range model for total momentum $(0, 0, 1)$ and transverse polarisation.

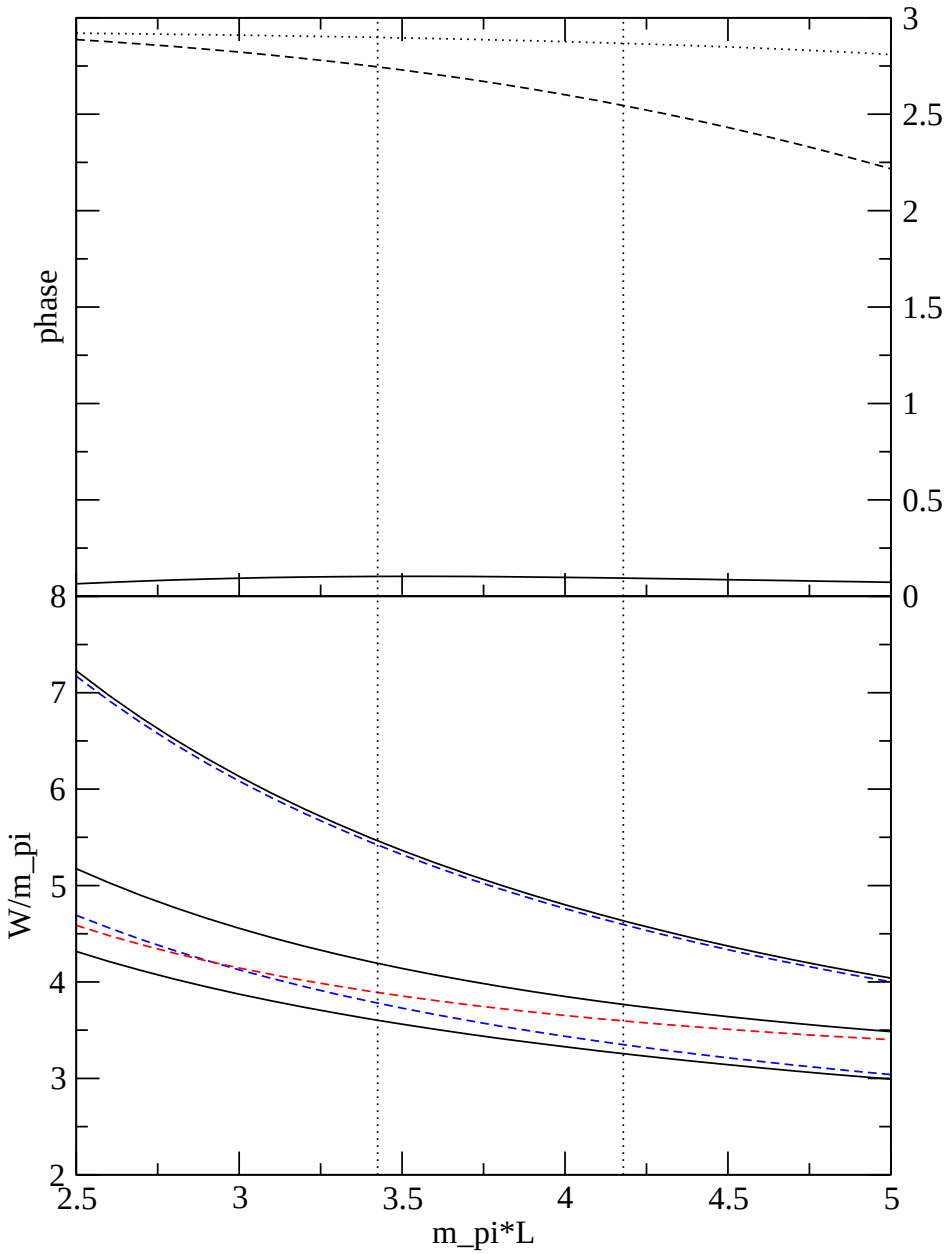

Figure 8.3.3.: Scattering phase shift and energy levels from the effective range model for total momentum $(1, 1, 0)$ and longitudinal polarisation.

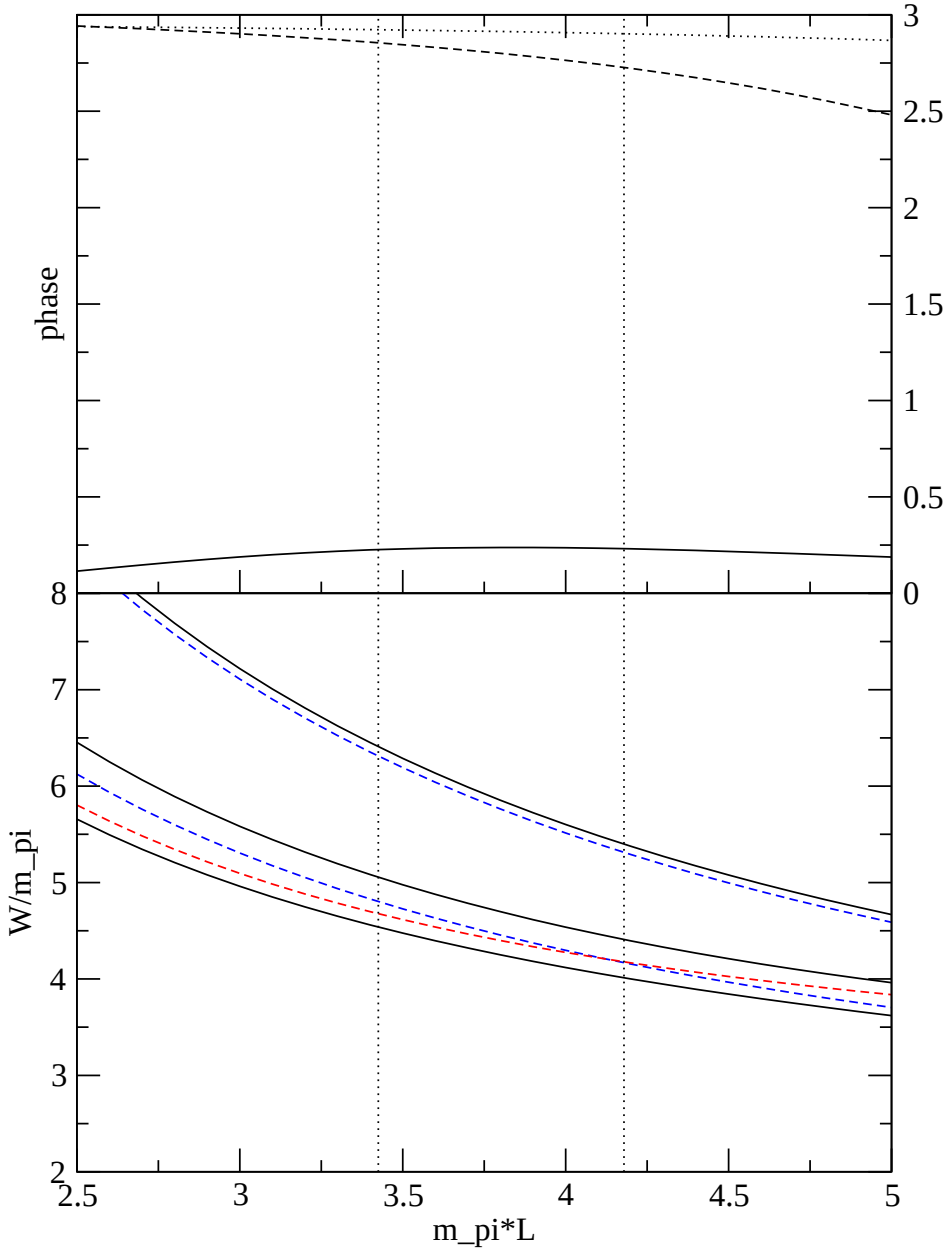

Figure 8.3.4.: Scattering phase shift and energy levels from the effective range model for total momentum $(0, 0, 2)$ and longitudinal polarisation.

9. The correlation functions

To extract energies from the meson correlation functions we make use of the variational method which we introduced in chapter 4. The correlation matrix will be constructed from the basis operators $\pi\pi^{ab}(t)$ and $\rho^a(t)$ defined in chapter 7 as

$$\rho^a(\vec{p},t) = \sum_{\vec{x}} \mathrm{e}^{i\vec{p}\vec{x}}\rho^a(\vec{x},t) \tag{9.0.1}$$

$$\begin{aligned}\pi\pi^{ab}(\vec{p}_1,\vec{p}_2,t) &= \pi^a(\vec{p}_1,t)\pi^b(\vec{p}_2,t)\\ &= \sum_{\vec{x},\vec{y}} \mathrm{e}^{i\vec{p}_1\vec{x}}\mathrm{e}^{i\vec{p}_2\vec{y}}\pi^a(\vec{x},t)\pi^b(\vec{y},t)\end{aligned} \tag{9.0.2}$$

and

$$\overline{\rho}^a(\vec{p},t) = -\sum_{\vec{x}} \mathrm{e}^{-i\vec{p}\vec{x}}\rho^a(\vec{x},t) \tag{9.0.3}$$

$$\overline{\pi\pi}^{ab}(\vec{p}_1,\vec{p}_2,t) = \sum_{\vec{x},\vec{y}} \mathrm{e}^{-i\vec{p}_1\vec{x}}\mathrm{e}^{-i\vec{p}_2\vec{y}}\pi^a(\vec{x},t)\pi^b(\vec{y},t). \tag{9.0.4}$$

9.1. The 2-pion correlation function

For the 2-pion correlation function we have to calculate the expectation values

$$Q^I_{a'b',ab}\Big(\langle\overline{\pi\pi}^{a'b'}(t)\pi\pi^{ab}(0)\rangle - \langle\overline{\pi\pi}^{a'b'}(t)\rangle\langle\pi\pi^{ab}(0)\rangle\Big) \tag{9.1.1}$$

with the isospin projectors

$$Q^0_{a'b',ab} = \tfrac{1}{3}\delta_{a'b'}\delta_{ab} \tag{9.1.2}$$

$$Q^1_{a'b',ab} = \tfrac{1}{2}(\delta_{a'a}\delta_{b'b} - \delta_{a'b}\delta_{b'a}) \tag{9.1.3}$$

$$Q^2_{a'b',ab} = \tfrac{1}{2}(\delta_{a'a}\delta_{b'b} + \delta_{a'b}\delta_{b'a}) - \tfrac{1}{3}\delta_{a'b'}\delta_{ab}. \tag{9.1.4}$$

The brackets $\langle\cdots\rangle$ denote the integration over the fields. Let us assume that the total momentum of the initial 2-pion operator $\pi\pi^{ab}(\vec{p}_1,\vec{p}_2,0)$ is $\vec{q}=\vec{p}_1+\vec{p}_2$ and we set $\vec{p}_1=\vec{q}+\vec{p}$ and $\vec{p}_2=-\vec{p}$ where $\vec{p}$ is arbitrary. Then the 2-pion operator is

$$\pi\pi^{ab}(\vec{q}+\vec{p},-\vec{p},0) = \sum_{\vec{x}_3,\vec{x}_4} \mathrm{e}^{i(\vec{q}+\vec{p})\vec{x}_3}\mathrm{e}^{-i\vec{p}\vec{x}_4}\pi^a(\vec{x}_3,0)\pi^b(\vec{x}_4,0) \tag{9.1.5}$$

Similarly

$$\overline{\pi\pi}^{a'b'}(\vec{q}'+\vec{p}',-\vec{p}',t)=\sum_{\vec{x}_1,\vec{x}_2}\mathrm{e}^{-i(\vec{q}'+\vec{p}')\vec{x}_1}\mathrm{e}^{i\vec{p}'\vec{x}_2}\pi^{a'}(\vec{x}_1,t)\pi^{b'}(\vec{x}_2,t). \tag{9.1.6}$$

With these definitions the connected part of the correlator is

$$\begin{aligned}Q^I_{a'b',ab}\langle\overline{\pi\pi}^{a'b'}(t)\pi\pi^{ab}(0)\rangle = Q^I_{a'b',ab}\sum_{\vec{x}_1,\vec{x}_2,\vec{x}_3,\vec{x}_4}&\mathrm{e}^{-i(\vec{q}'+\vec{p}')\vec{x}_1}\mathrm{e}^{i\vec{p}'\vec{x}_2}\mathrm{e}^{i(\vec{q}+\vec{p})\vec{x}_3}\mathrm{e}^{-i\vec{p}\vec{x}_4}\\ &\times\langle\pi^{a'}(\vec{x}_1,t)\pi^{b'}(\vec{x}_2,t)\pi^{a}(\vec{x}_3,0)\pi^{b}(\vec{x}_4,0)\rangle\end{aligned} \tag{9.1.7}$$

The definition of a pion interpolator is $\pi^a(\vec{x},t)=\bar{\psi}(\vec{x},t)\gamma_5F^a\psi(\vec{x},t)$ and F^a can be one of the three Pauli matrices $a=1,2,3$. Doing all possible contractions in (9.1.7) and using $\mathrm{tr}(F^a)=0$ we can express $\langle\overline{\pi\pi}^{a'b'}(t)\pi\pi^{ab}(0)\rangle$ in terms of all-to-all quark propagators $G(\vec{x},t_2|\vec{y},t_1)$:

$$\begin{aligned}
&\langle\pi^{a'}(\vec{x}_1,t)\pi^{b'}(\vec{x}_2,t)\pi^{a}(\vec{x}_3,0)\pi^{b}(\vec{x}_4,0)\rangle\\
&\quad=\langle\mathrm{tr}_{DC}(G(\vec{x}_4,0|\vec{x}_1,t)\gamma_5G(\vec{x}_1,t|\vec{x}_4,0)\gamma_5)\mathrm{tr}_{DC}(G(\vec{x}_3,0|\vec{x}_2,t)\gamma_5G(\vec{x}_2,t|\vec{x}_3,0)\gamma_5)\\
&\qquad\qquad\times\mathrm{tr}(F^{a'}F^b)\mathrm{tr}(F^{b'}F^a)\\
&\qquad-\mathrm{tr}_{DC}(G(\vec{x}_4,0|\vec{x}_1,t)\gamma_5G(\vec{x}_1,t|\vec{x}_3,0)\gamma_5G(\vec{x}_3,0|\vec{x}_2,t)\gamma_5G(\vec{x}_2,t|\vec{x}_4,0)\gamma_5)\\
&\qquad\qquad\times\mathrm{tr}(F^{a'}F^aF^{b'}F^b)\\
&\qquad-\mathrm{tr}_{DC}(G(\vec{x}_4,0|\vec{x}_1,t)\gamma_5G(\vec{x}_1,t|\vec{x}_2,t)\gamma_5G(\vec{x}_2,t|\vec{x}_3,0)\gamma_5G(\vec{x}_3,0|\vec{x}_4,0)\gamma_5)\\
&\qquad\qquad\times\mathrm{tr}(F^{a'}F^{b'}F^aF^b)\\
&\qquad-\mathrm{tr}_{DC}(G(\vec{x}_4,0|\vec{x}_2,t)\gamma_5G(\vec{x}_2,t|\vec{x}_3,0)\gamma_5G(\vec{x}_3,0|\vec{x}_1,t)\gamma_5G(\vec{x}_1,t|\vec{x}_4,0)\gamma_5)\\
&\qquad\qquad\times\mathrm{tr}(F^{b'}F^aF^{a'}F^b)\\
&\quad+\mathrm{tr}_{DC}(G(\vec{x}_4,0|\vec{x}_2,t)\gamma_5G(\vec{x}_2,t|\vec{x}_4,0)\gamma_5)\mathrm{tr}_{DC}(G(\vec{x}_3,0|\vec{x}_1,t)\gamma_5G(\vec{x}_1,t|\vec{x}_3,0)\gamma_5)\\
&\qquad\qquad\times\mathrm{tr}(F^{b'}F^b)\mathrm{tr}(F^{a'}F^a)\\
&\qquad-\mathrm{tr}_{DC}(G(\vec{x}_4,0|\vec{x}_2,t)\gamma_5G(\vec{x}_2,t|\vec{x}_1,t)\gamma_5G(\vec{x}_1,t|\vec{x}_3,0)\gamma_5G(\vec{x}_3,0|\vec{x}_4,0)\gamma_5)\\
&\qquad\qquad\times\mathrm{tr}(F^{b'}F^{a'}F^aF^b)\\
&\qquad-\mathrm{tr}_{DC}(G(\vec{x}_4,0|\vec{x}_3,0)\gamma_5G(\vec{x}_3,0|\vec{x}_1,t)\gamma_5G(\vec{x}_1,t|\vec{x}_2,t)\gamma_5G(\vec{x}_2,t|\vec{x}_4,0)\gamma_5)\\
&\qquad\qquad\times\mathrm{tr}(F^aF^{a'}F^{b'}F^b)\\
&\qquad-\mathrm{tr}_{DC}(G(\vec{x}_4,0|\vec{x}_3,0)\gamma_5G(\vec{x}_3,0|\vec{x}_2,t)\gamma_5G(\vec{x}_2,t|\vec{x}_1,t)\gamma_5G(\vec{x}_1,t|\vec{x}_4,0)\gamma_5)\\
&\qquad\qquad\times\mathrm{tr}(F^aF^{b'}F^{a'}F^b)\\
&\quad+\mathrm{tr}_{DC}(G(\vec{x}_4,0|\vec{x}_3,0)\gamma_5G(\vec{x}_3,0|\vec{x}_4,0)\gamma_5)\mathrm{tr}_{DC}(G(\vec{x}_2,t|\vec{x}_1,t)\gamma_5G(\vec{x}_1,t|\vec{x}_2,t)\gamma_5)\\
&\qquad\qquad\times\mathrm{tr}(F^aF^b)\mathrm{tr}(F^{a'}F^{b'})\rangle_g.
\end{aligned} \tag{9.1.8}$$

Here $\mathrm{tr}_{DC}(\cdots)$ is the trace over spin and colour. For isospin $I = 1$ the disconnected part is zero and the connected one is then

$$
\begin{aligned}
&Q^1_{a'b',ab}\langle\pi^{a'}(\vec{x}_1,t)\pi^{b'}(\vec{x}_2,t)\pi^{a}(\vec{x}_3,0)\pi^{b}(\vec{x}_4,0)\rangle \\
&\quad = -12\langle \mathrm{tr}_{DC}(G(\vec{x}_4,0|\vec{x}_1,t)\gamma_5 G(\vec{x}_1,t|\vec{x}_4,0)\gamma_5)\mathrm{tr}_{DC}(G(\vec{x}_3,0|\vec{x}_2,t)\gamma_5 G(\vec{x}_2,t|\vec{x}_3,0)\gamma_5) \\
&\qquad - \mathrm{tr}_{DC}(G(\vec{x}_4,0|\vec{x}_2,t)\gamma_5 G(\vec{x}_2,t|\vec{x}_4,0)\gamma_5)\mathrm{tr}_{DC}(G(\vec{x}_3,0|\vec{x}_1,t)\gamma_5 G(\vec{x}_1,t|\vec{x}_3,0)\gamma_5) \\
&\qquad\quad - \mathrm{tr}_{DC}(G(\vec{x}_4,0|\vec{x}_3,0)\gamma_5 G(\vec{x}_3,0|\vec{x}_2,t)\gamma_5 G(\vec{x}_2,t|\vec{x}_1,t)\gamma_5 G(\vec{x}_1,t|\vec{x}_4,0)\gamma_5) \\
&\qquad\quad - \mathrm{tr}_{DC}(G(\vec{x}_4,0|\vec{x}_1,t)\gamma_5 G(\vec{x}_1,t|\vec{x}_2,t)\gamma_5 G(\vec{x}_2,t|\vec{x}_3,0)\gamma_5 G(\vec{x}_3,0|\vec{x}_4,0)\gamma_5) \\
&\qquad\quad + \mathrm{tr}_{DC}(G(\vec{x}_4,0|\vec{x}_3,0)\gamma_5 G(\vec{x}_3,0|\vec{x}_1,t)\gamma_5 G(\vec{x}_1,t|\vec{x}_2,t)\gamma_5 G(\vec{x}_2,t|\vec{x}_4,0)\gamma_5) \\
&\qquad + \mathrm{tr}_{DC}(G(\vec{x}_4,0|\vec{x}_2,t)\gamma_5 G(\vec{x}_2,t|\vec{x}_1,t)\gamma_5 G(\vec{x}_1,t|\vec{x}_3,0)\gamma_5 G(\vec{x}_3,0|\vec{x}_4,0)\gamma_5)\rangle_g. \quad (9.1.9)
\end{aligned}
$$

Figure 9.1.1 shows the diagrams corresponding to (9.1.9).

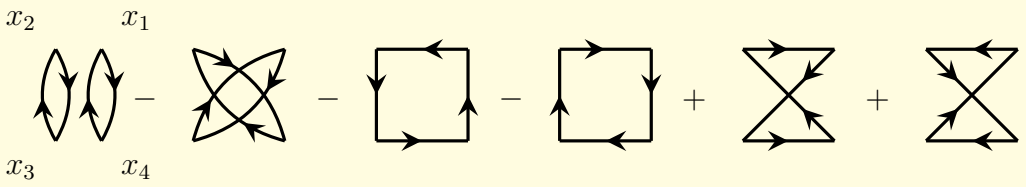

Figure 9.1.1.: Diagrams for the correlator (9.1.9). The time runs upward.

For isospin $I = 2$ the disconnected part also vanishes and what remains from (9.1.8) is

$$
\begin{aligned}
&Q^2_{a'b',ab}\langle\pi^{a'}(\vec{x}_1,t)\pi^{b'}(\vec{x}_2,t)\pi^{a}(\vec{x}_3,0)\pi^{b}(\vec{x}_4,0)\rangle \\
&\quad = 20\langle \mathrm{tr}_{DC}(G(\vec{x}_4,0|\vec{x}_1,t)\gamma_5 G(\vec{x}_1,t|\vec{x}_4,0)\gamma_5)\mathrm{tr}_{DC}(G(\vec{x}_3,0|\vec{x}_2,t)\gamma_5 G(\vec{x}_2,t|\vec{x}_3,0)\gamma_5) \\
&\qquad + \mathrm{tr}_{DC}(G(\vec{x}_4,0|\vec{x}_2,t)\gamma_5 G(\vec{x}_2,t|\vec{x}_4,0)\gamma_5)\mathrm{tr}_{DC}(G(\vec{x}_3,0|\vec{x}_1,t)\gamma_5 G(\vec{x}_1,t|\vec{x}_3,0)\gamma_5) \\
&\qquad\quad - \mathrm{tr}_{DC}(G(\vec{x}_4,0|\vec{x}_1,t)\gamma_5 G(\vec{x}_1,t|\vec{x}_3,0)\gamma_5 G(\vec{x}_3,0|\vec{x}_2,t)\gamma_5 G(\vec{x}_2,t|\vec{x}_4,0)\gamma_5) \\
&\qquad - \mathrm{tr}_{DC}(G(\vec{x}_4,0|\vec{x}_2,t)\gamma_5 G(\vec{x}_2,t|\vec{x}_3,0)\gamma_5 G(\vec{x}_3,0|\vec{x}_1,t)\gamma_5 G(\vec{x}_1,t|\vec{x}_4,0)\gamma_5)\rangle_g. \quad (9.1.10)
\end{aligned}
$$

Finally for $I = 0$ we have

$$\begin{aligned}
&Q^0_{a'b',ab}\langle\pi^{a'}(\vec{x}_1,t)\pi^{b'}(\vec{x}_2,t)\pi^a(\vec{x}_3,0)\pi^b(\vec{x}_4,0)\rangle \\
&\quad= \langle 4\mathrm{tr}_{DC}(G(\vec{x}_4,0|\vec{x}_1,t)\gamma_5 G(\vec{x}_1,t|\vec{x}_4,0)\gamma_5)\mathrm{tr}_{DC}(G(\vec{x}_3,0|\vec{x}_2,t)\gamma_5 G(\vec{x}_2,t|\vec{x}_3,0)\gamma_5) \\
&\qquad+ 2\mathrm{tr}_{DC}(G(\vec{x}_4,0|\vec{x}_1,t)\gamma_5 G(\vec{x}_1,t|\vec{x}_3,0)\gamma_5 G(\vec{x}_3,0|\vec{x}_2,t)\gamma_5 G(\vec{x}_2,t|\vec{x}_4,0)\gamma_5) \\
&\qquad- 6\mathrm{tr}_{DC}(G(\vec{x}_4,0|\vec{x}_1,t)\gamma_5 G(\vec{x}_1,t|\vec{x}_2,t)\gamma_5 G(\vec{x}_2,t|\vec{x}_3,0)\gamma_5 G(\vec{x}_3,0|\vec{x}_4,0)\gamma_5) \\
&\qquad+ 2\mathrm{tr}_{DC}(G(\vec{x}_4,0|\vec{x}_2,t)\gamma_5 G(\vec{x}_2,t|\vec{x}_3,0)\gamma_5 G(\vec{x}_3,0|\vec{x}_1,t)\gamma_5 G(\vec{x}_1,t|\vec{x}_4,0)\gamma_5) \\
&\quad+ 4\mathrm{tr}_{DC}(G(\vec{x}_4,0|\vec{x}_2,t)\gamma_5 G(\vec{x}_2,t|\vec{x}_4,0)\gamma_5)\mathrm{tr}_{DC}(G(\vec{x}_3,0|\vec{x}_1,t)\gamma_5 G(\vec{x}_1,t|\vec{x}_3,0)\gamma_5) \\
&\qquad- 6\mathrm{tr}_{DC}(G(\vec{x}_4,0|\vec{x}_2,t)\gamma_5 G(\vec{x}_2,t|\vec{x}_1,t)\gamma_5 G(\vec{x}_1,t|\vec{x}_3,0)\gamma_5 G(\vec{x}_3,0|\vec{x}_4,0)\gamma_5) \\
&\qquad- 6\mathrm{tr}_{DC}(G(\vec{x}_4,0|\vec{x}_3,0)\gamma_5 G(\vec{x}_3,0|\vec{x}_1,t)\gamma_5 G(\vec{x}_1,t|\vec{x}_2,t)\gamma_5 G(\vec{x}_2,t|\vec{x}_4,0)\gamma_5) \\
&\qquad- 6\mathrm{tr}_{DC}(G(\vec{x}_4,0|\vec{x}_3,0)\gamma_5 G(\vec{x}_3,0|\vec{x}_2,t)\gamma_5 G(\vec{x}_2,t|\vec{x}_1,t)\gamma_5 G(\vec{x}_1,t|\vec{x}_4,0)\gamma_5) \\
&\qquad\qquad+ 12\mathrm{tr}_{DC}(G(\vec{x}_4,0|\vec{x}_3,0)\gamma_5 G(\vec{x}_3,0|\vec{x}_4,0)\gamma_5) \\
&\qquad\qquad\qquad \mathrm{tr}_{DC}(G(\vec{x}_2,t|\vec{x}_1,t)\gamma_5 G(\vec{x}_1,t|\vec{x}_2,t)\gamma_5)\rangle_g
\end{aligned} \tag{9.1.11}$$

and the disconnected part is

$$\begin{aligned}
&Q^0_{a'b',ab}\langle\pi^{a'}(\vec{x}_1,t)\pi^{b'}(\vec{x}_2,t)\rangle\langle\pi^a(\vec{x}_3,0)\pi^b(\vec{x}_4,0)\rangle \\
&\qquad= 12\langle\mathrm{tr}_{DC}(G(\vec{x}_1,t|\vec{x}_2,t)\gamma_5 G(\vec{x}_2,t|\vec{x}_1,t)\gamma_5)\rangle \\
&\qquad\qquad \langle\mathrm{tr}_{DC}(G(\vec{x}_3,0|\vec{x}_4,0)\gamma_5 G(\vec{x}_4,0|\vec{x}_3,0)\gamma_5)\rangle_g
\end{aligned} \tag{9.1.12}$$

Now we come back to the case $I = 1$ and rewrite the result in the form used by Aoki et al. [7]. For calculating contributions to (9.1.9) like the first and second diagram in figure 9.1.1 we have to introduce stochastic noise vectors $\xi_j(\vec{x})$ satisfying

$$\tfrac{1}{N}\sum_{j=1}^{N}\xi_j^*(\vec{x})\xi_j(\vec{y}) = \delta_{\vec{x},\vec{y}} \quad \text{for} \quad N\to\infty. \tag{9.1.13}$$

For the numerical evaluation we choose complex $Z(2)$ noise [17].

We define the quark propagator Q with momentum $\vec{p}$ as

$$Q_{AB}(\vec{x},t|\vec{p},t_{src},\xi_j) = \sum_{\vec{y}} G_{AB}(\vec{x},t|\vec{y},t_{src})[\mathrm{e}^{i\vec{p}\vec{y}}\xi_j(\vec{y})] \tag{9.1.14}$$

where A, B are multiindices for spin and colour and the expression in square brackets is our source term placed at $t = t_{src}$. For the box diagrams we introduce sequential propagators W

$$\begin{aligned}
&W_{AB}(\vec{x},t|\vec{q},t_1|\vec{p},t_{src},\xi_j) \\
&\qquad= \sum_{\vec{y},\vec{z},C} G_{AC}(\vec{x},t|\vec{z},t_1)[\mathrm{e}^{i\vec{q}\vec{z}}\gamma_5 G(\vec{z},t_1|\vec{y},t_{src})\xi_j(\vec{y})\mathrm{e}^{i\vec{p}\vec{y}}]_{CB} \\
&\qquad= \sum_{\vec{z},C} G_{AC}(\vec{x},t|\vec{z},t_1)[\mathrm{e}^{i\vec{q}\vec{z}}\gamma_5 Q(\vec{z},t_1|\vec{p},t_{src},\xi_j)]_{CB}.
\end{aligned} \tag{9.1.15}$$

The name sequential propagator comes from the fact that we use the quark propagator Q together with some phase factor and γ_5 as a new source for the propagator W.

Furthermore we can simplify the phase factor in (9.1.7) using momentum conservation and therefore set $\vec{q}' = \vec{q}$. To recover Aoki's results we replace the momentum $\vec{p}'$ by $\vec{p}' - \vec{q}$ and get the new phase factor

$$\text{phase} = \mathrm{e}^{-i\vec{p}'\vec{x}_1}\mathrm{e}^{i(\vec{p}'-\vec{q})\vec{x}_2}\mathrm{e}^{i(\vec{p}+\vec{q})\vec{x}_3}\mathrm{e}^{-i\vec{p}\vec{x}_4}. \tag{9.1.16}$$

With the help of the γ_5-hermiticity relation (4.2.5) we can write the contribution of the first term in (9.1.9) as

$$\sum_{\substack{\vec{x}_1,\vec{x}_2,\vec{x}_3,\vec{x}_4,\\ \vec{y}_1,\vec{y}_2}} \text{phase} \cdot \delta_{\vec{x}_4,\vec{y}_1}\delta_{\vec{x}_3,\vec{y}_2}\mathrm{tr}_{DC}(G^\dagger(\vec{x}_1,t|\vec{x}_4,0)G(\vec{x}_1,t|\vec{y}_1,0)) \times\mathrm{tr}_{DC}(G^\dagger(\vec{x}_2,t|\vec{x}_3,0)G(\vec{x}_2,t|\vec{y}_2,0))$$

$$= \frac{1}{N^2}\sum_{\substack{\vec{x}_1,\vec{x}_2,\vec{x}_3,\vec{x}_4,\\ \vec{y}_1,\vec{y}_2,j,k}} \text{phase} \cdot \mathrm{tr}_{DC}(\xi_j^*(\vec{x}_4)G^\dagger(\vec{x}_1,t|\vec{x}_4,0)G(\vec{x}_1,t|\vec{y}_1,0)\xi_j(\vec{y}_1)) \times\mathrm{tr}_{DC}(\eta_k^*(\vec{x}_3)G^\dagger(\vec{x}_2,t|\vec{x}_3,0)G(\vec{x}_2,t|\vec{y}_2,0)\eta_k(\vec{y}_2))$$

$$= \frac{1}{N^2}\sum_{\vec{x}_1,\vec{x}_2}\sum_{j,k}\mathrm{e}^{-i\vec{p}'\vec{x}_1}\mathrm{e}^{i(\vec{p}'-\vec{q})\vec{x}_2}\mathrm{tr}_{DC}(Q^\dagger(\vec{x}_1,t|\vec{p},0,\xi_j)Q(\vec{x}_1,t|\vec{0},0,\xi_j)) \times\mathrm{tr}_{DC}(Q^\dagger(\vec{x}_2,t|\vec{0},0,\eta_k)Q(\vec{x}_2,t|\vec{p}+\vec{q},0,\eta_k)) \tag{9.1.17}$$

For the second term we get

$$-\frac{1}{N^2}\sum_{\vec{x}_1,\vec{x}_2,}\sum_{j,k}\mathrm{e}^{-i\vec{p}'\vec{x}_1}\mathrm{e}^{i(\vec{p}'-\vec{q})\vec{x}_2}\mathrm{tr}_{DC}(Q^\dagger(\vec{x}_2,t|\vec{p},0,\xi_j)Q(\vec{x}_2,t|\vec{0},0,\xi_j)) \times \mathrm{tr}_{DC}(Q^\dagger(\vec{x}_1,t|\vec{0},0,\eta_k)Q(\vec{x}_1,t|\vec{p}+\vec{q},0,\eta_k)) \tag{9.1.18}$$

Also for the third term we insert sources and rearrange the trace

$$-\frac{1}{N}\sum_{\substack{\vec{x}_1,\vec{x}_2,\vec{x}_3,\vec{x}_4,\\ \vec{y},j}} \text{phase} \cdot \mathrm{tr}_{DC}([\xi_j^*(\vec{y})\gamma_5 G(\vec{y},0|\vec{x}_3,0)]\gamma_5 G(\vec{x}_3,0|\vec{x}_2,t)\gamma_5 \times G(\vec{x}_2,t|\vec{x}_1,t)[\gamma_5 G(\vec{x}_1,t|\vec{x}_4,0)\xi_j(\vec{x}_4)])$$

$$= -\frac{1}{N}\sum_{\vec{x}}\sum_{j}\mathrm{e}^{i(\vec{p}'-\vec{q})\vec{x}}\mathrm{tr}_{DC}(W^\dagger(\vec{x},t|-(\vec{p}+\vec{q}),0|\vec{p},0,\xi_j)W(\vec{x},t|-\vec{p}',t|\vec{0},0,\xi_j)) \tag{9.1.19}$$

The 4th term is

$$-\frac{1}{N}\sum_{\vec{x}}\sum_{j}\mathrm{e}^{i(\vec{p}'-\vec{q})\vec{x}}\mathrm{tr}_{DC}(W^\dagger(\vec{x},t|\vec{p}',t|\vec{0},0,\xi_j)W(\vec{x},t|\vec{p}+\vec{q},0|-\vec{p},0,\xi_j)), \tag{9.1.20}$$

the 5th term

$$\frac{1}{N}\sum_{\vec{x}}\sum_{j}\mathrm{e}^{i(\vec{p}\,'-\vec{q})\vec{x}}\mathrm{tr}_{DC}(W^{\dagger}(\vec{x},t|\vec{p}\,',t|\vec{0},0,\xi_j)W(\vec{x},t|-\vec{p},0|\vec{p}+\vec{q},0,\xi_j)) \tag{9.1.21}$$

and the 6th term reads

$$\frac{1}{N}\sum_{\vec{x}}\sum_{j}\mathrm{e}^{i(\vec{p}\,'-\vec{q})\vec{x}}\mathrm{tr}_{DC}(W^{\dagger}(\vec{x},t|\vec{p},0|-(\vec{p}+\vec{q}),0,\xi_j)W(\vec{x},t|-\vec{p}\,',t|\vec{0},0,\xi_j)). \tag{9.1.22}$$

When we use longitudinal polarisations in our applications the momenta $\vec{p}$ and $\vec{p}\,'$ are equal to zero. Therefore the final form of the correlator (9.1.7) is

$$\begin{aligned}
&-12\Big\langle\frac{1}{N^2}\sum_{\vec{x}_1,\vec{x}_2}\sum_{j,k}\mathrm{e}^{-i\vec{q}\vec{x}_2}\mathrm{tr}_{DC}(Q^{\dagger}(\vec{x}_1,t|\vec{0},0,\xi_j)Q(\vec{x}_1,t|\vec{0},0,\xi_j))\\
&\qquad\qquad\times\mathrm{tr}_{DC}(Q^{\dagger}(\vec{x}_2,t|\vec{0},0,\eta_k)Q(\vec{x}_2,t|\vec{q},0,\eta_k))\\
&-\frac{1}{N^2}\sum_{\vec{x}_1,\vec{x}_2}\sum_{j,k}\mathrm{e}^{-i\vec{q}\vec{x}_2}\mathrm{tr}_{DC}(Q^{\dagger}(\vec{x}_2,t|\vec{0},0,\xi_j)Q(\vec{x}_2,t|\vec{0},0,\xi_j))\\
&\qquad\qquad\times\mathrm{tr}_{DC}(Q^{\dagger}(\vec{x}_1,t|\vec{0},0,\eta_k)Q(\vec{x}_1,t|\vec{q},0,\eta_k))\\
&-\frac{1}{N}\sum_{\vec{x}}\sum_{j}\mathrm{e}^{-i\vec{q}\vec{x}}\mathrm{tr}_{DC}(W^{\dagger}(\vec{x},t|-\vec{q},0|\vec{0},0,\xi_j)W(\vec{x},t|\vec{0},t|\vec{0},0,\xi_j))\\
&-\frac{1}{N}\sum_{\vec{x}}\sum_{j}\mathrm{e}^{-i\vec{q}\vec{x}}\mathrm{tr}_{DC}(W^{\dagger}(\vec{x},t|\vec{0},t|\vec{0},0,\xi_j)W(\vec{x},t|\vec{q},0|\vec{0},0,\xi_j))\\
&+\frac{1}{N}\sum_{\vec{x}}\sum_{j}\mathrm{e}^{-i\vec{q}\vec{x}}\mathrm{tr}_{DC}(W^{\dagger}(\vec{x},t|\vec{0},t|\vec{0},0,\xi_j)W(\vec{x},t|\vec{0},0|\vec{q},0,\xi_j))\\
&+\frac{1}{N}\sum_{\vec{x}}\sum_{j}\mathrm{e}^{-i\vec{q}\vec{x}}\mathrm{tr}_{DC}(W^{\dagger}(\vec{x},t|\vec{0},0|-\vec{q},0,\xi_j)W(\vec{x},t|\vec{0},t|\vec{0},0,\xi_j))\Big\rangle_g.
\end{aligned} \tag{9.1.23}$$

This coincides with the result from [7]. The calculation of the remaining correlators contains the same steps as in this section. Therefore we will not consider all the details in the following.

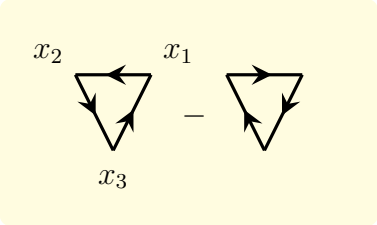

Figure 9.2.1.: Diagrams for the correlator (9.2.4). The time runs upward.

9.2. The $\pi\pi \to \rho$, $\rho \to \pi\pi$ and $\rho \to \rho$ correlation functions

For the $\rho \to \pi\pi$ correlation function we have to calculate

$$Q_{abc}\langle\overline{\pi\pi}^{ab}(t)\rho^c(0)\rangle \tag{9.2.1}$$

where the projection operator

$$Q_{abc} = -\epsilon_{abc} \tag{9.2.2}$$

is the Levi-Civita tensor. Using momentum conservation expression (9.2.1) becomes

$$\begin{aligned} &Q_{abc}\langle\overline{\pi\pi}^{ab}(t)\rho^c(0)\rangle \\ &\qquad = Q_{abc}\sum_{\vec{x}_1,\vec{x}_2,\vec{x}_3} \mathrm{e}^{-i\vec{p}'\vec{x}_1}\mathrm{e}^{i(\vec{p}'-\vec{q})\vec{x}_2}\mathrm{e}^{i\vec{q}\vec{x}_3}\cdot\langle\pi^a(\vec{x}_1,t)\pi^b(\vec{x}_2,t)\rho^c(\vec{x}_3,0)\rangle. \end{aligned} \tag{9.2.3}$$

The correlator is

$$\begin{aligned} &Q_{abc}\langle\pi^a(\vec{x}_1,t)\pi^b(\vec{x}_2,t)\rho^c(\vec{x}_3,0)\rangle \\ &\qquad = \langle 12i\big(\mathrm{tr}_{DC}(G(\vec{x}_3,0|\vec{x}_1,t)\gamma_5 G(\vec{x}_1,t|\vec{x}_2,t)\gamma_5 G(\vec{x}_2,t|\vec{x}_3,0)\gamma_i) \\ &\qquad\qquad - \mathrm{tr}_{DC}(G(\vec{x}_3,0|\vec{x}_2,t)\gamma_5 G(\vec{x}_2,t|\vec{x}_1,t)\gamma_5 G(\vec{x}_1,t|\vec{x}_3,0)\gamma_i)\big)\rangle_g \end{aligned} \tag{9.2.4}$$

and the corresponding diagrams are given in figure 9.2.1. Finally we express (9.2.3) in terms of Q and W propagators using $\vec{p}' = \vec{0}$:

$$\begin{aligned} &Q_{abc}\langle\overline{\pi\pi}^{ab}(t)\rho^c(0)\rangle \\ &\qquad = 12i\Big\langle\frac{1}{N}\sum_{\vec{x}}\sum_j \mathrm{e}^{-i\vec{q}\vec{x}}\mathrm{tr}_{DC}(Q^\dagger(\vec{x},t|-\vec{q},0,\xi_j)W(\vec{x},t|\vec{0},t|\vec{0},0,\xi_j)\gamma_i\gamma_5) \\ &\qquad\qquad - \sum_{\vec{x}}\sum_j \mathrm{e}^{-i\vec{q}\vec{x}}\mathrm{tr}_{DC}(W^\dagger(\vec{x},t|\vec{0},t|\vec{0},0,\xi_j)Q(\vec{x},t|\vec{q},0,\xi_j)\gamma_i\gamma_5)\Big\rangle_g \end{aligned} \tag{9.2.5}$$

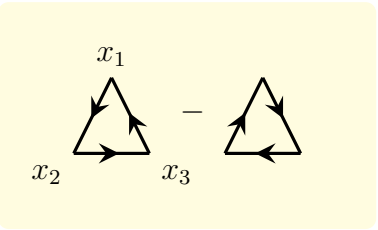

Figure 9.2.2.: Diagrams for the correlator (9.2.7). The time runs upward.

For $\pi\pi \to \rho$ we have

$$Q_{abc}\langle\overline{\rho}^c(t)\pi\pi^{ab}(0)\rangle = -Q_{abc}\sum_{\vec{x}_1,\vec{x}_2,\vec{x}_3} \mathrm{e}^{-i\vec{q}\vec{x}_1}\mathrm{e}^{i(\vec{q}+\vec{p})\vec{x}_2}\mathrm{e}^{-i\vec{p}\vec{x}_3}\cdot\langle\rho^c(\vec{x}_1,t)\pi^a(\vec{x}_2,0)\pi^b(\vec{x}_3,0)\rangle \quad (9.2.6)$$

and the correlator is

$$\begin{aligned} &Q_{abc}\langle\rho^c(\vec{x}_1,t)\pi^a(\vec{x}_2,0)\pi^b(\vec{x}_3,0)\rangle \\ &\quad = \langle 12i\big(\mathrm{tr}_{DC}(G(\vec{x}_1,t|\vec{x}_2,0)\gamma_5 G(\vec{x}_2,0|\vec{x}_3,0)\gamma_5 G(\vec{x}_3,0|\vec{x}_1,t)\gamma_{i'}) \\ &\qquad - \mathrm{tr}_{DC}(G(\vec{x}_1,t|\vec{x}_3,0)\gamma_5 G(\vec{x}_3,0|\vec{x}_2,0)\gamma_5 G(\vec{x}_2,0|\vec{x}_1,t)\gamma_{i'})\big)\rangle_g. \end{aligned} \quad (9.2.7)$$

The two diagrams are shown in figure 9.2.2 For $\vec{p} = 0$ the final result with Q and W propagators is

$$\begin{aligned} &Q_{abc}\langle\overline{\rho}^c(t)\pi\pi^{ab}(0)\rangle = \\ &\quad = -12i\Big\langle\frac{1}{N}\sum_{\vec{x}}\sum_j \mathrm{e}^{-i\vec{q}\vec{x}}\mathrm{tr}_{DC}(W(\vec{x},t|\vec{q},0|\vec{0},0,\xi_j)Q^\dagger(\vec{x},t|\vec{0},0,\xi_j)\gamma_5\gamma_{i'}) \\ &\qquad - \sum_{\vec{x}}\sum_j \mathrm{e}^{-i\vec{q}\vec{x}}\mathrm{tr}_{DC}(Q(\vec{x},t|\vec{0},0,\xi_j)W^\dagger(\vec{x},t|-\vec{q},0|\vec{0},0,\xi_j)\gamma_5\gamma_{i'})\Big\rangle_g. \end{aligned} \quad (9.2.8)$$

For the rho 2-point function we have

$$\sum_a\langle\overline{\rho}^a(t)\rho^a(0)\rangle = -\sum_a\sum_{\vec{x}_1,\vec{x}_2}\mathrm{e}^{-i\vec{q}\vec{x}_1}\mathrm{e}^{i\vec{q}\vec{x}_2}\cdot\langle\rho^a(\vec{x}_1,t)\rho^a(\vec{x}_2,0)\rangle \quad (9.2.9)$$

and the correlator

$$\begin{aligned} &\sum_a\langle\rho^a(\vec{x}_1,t)\rho^a(\vec{x}_2,0)\rangle = \\ &\quad = -\sum_a\langle\mathrm{tr}_{DC}(G(\vec{x}_2,0|\vec{x}_1,t)\gamma_{i'}G(\vec{x}_1,t|\vec{x}_2,0)\gamma_i)\mathrm{tr}(F^aF^a)\rangle \\ &\quad = \langle -6\big(\mathrm{tr}_{DC}(G(\vec{x}_2,0|\vec{x}_1,t)\gamma_{i'}G(\vec{x}_1,t|\vec{x}_2,0)\gamma_i)\big)\rangle_g. \end{aligned} \quad (9.2.10)$$

In terms of Q-propagators the rho 2-point function is

$$\sum_a \langle \overline{\rho}^a(t)\rho^a(0)\rangle$$
$$= 6\frac{1}{N}\sum_{\vec{x}}\sum_j \mathrm{e}^{-i\vec{q}\vec{x}}\Big\langle \mathrm{tr}_{DC}(Q^\dagger(\vec{x},t|\vec{0},0,\xi_j)\gamma_5\gamma_{i'}Q(\vec{x},t|\vec{q},0,\xi_j)\gamma_i\gamma_5)\Big\rangle_g . \quad (9.2.11)$$

Finally, it turns out to be preferable to work with operators of definite isospin I and I_z instead of using the isospin projectors. For $I=1$ we choose a 2-pion operator of the form (8.2.1) and fix $a=3$ in the rho operators (9.0.1) and (9.0.3). From the correlation functions

$$\begin{aligned} G_{\pi\pi\to\pi\pi}(t) &= \tfrac{-1}{12}Q^1_{a'b',ab}\langle\overline{\pi\pi}^{a'b'}(t)\pi\pi^{ab}(0)\rangle \\ G_{\pi\pi\to\rho}(t) &= \tfrac{-i}{12}Q_{abc}\langle\overline{\rho}^c(t)\pi\pi^{ab}(0)\rangle \\ G_{\rho\to\pi\pi}(t) &= \tfrac{i}{12}Q_{abc}\langle\overline{\pi\pi}^{ab}(t)\rho^c(0)\rangle \\ G_{\rho\to\rho}(t) &= \tfrac{1}{6}\langle\overline{\rho}^a(t)\rho^a(0)\rangle \end{aligned} \quad (9.2.12)$$

we construct the matrix of correlators

$$C(t) = \begin{pmatrix} G_{\pi\pi\to\pi\pi}(t) & G_{\rho\to\pi\pi}(t) \\ G_{\pi\pi\to\rho}(t) & G_{\rho\to\rho}(t) \end{pmatrix}. \quad (9.2.13)$$

This matrix will be used for the determination of the two lowest energies by means of the generalised eigenvalue problem (4.3.7).

At the end we see that we have to calculate propagators of the form

$$\begin{gathered} Q(\vec{x}_1,t|\vec{0},0,\xi_j) \\ Q(\vec{x}_1,t|\pm\vec{q},0,\xi_j) \\ W(\vec{x}_1,t|\pm\vec{q},0|\vec{0},0,\xi_j) \\ W(\vec{x}_1,t|\vec{0},0|\pm\vec{q},0,\xi_j) \\ W(\vec{x}_1,t|\vec{0},t|\vec{0},0,\xi_j). \end{gathered} \quad (9.2.14)$$

Thus we need $12\cdot N\cdot(7+N_T)$ inversions where N is the number of noise vectors and N_T the number of timeslices. The factor 12 results from the fact that an inversion is required for every value of the spin and colour indices. The last propagator is most expensive to calculate because we need one for every timeslice. To save computing time we restricted t to a smaller set.

10. Results

10.1. Results and discussion for the $32^3 \times 64$ and $40^3 \times 64$ lattices

For collecting the data we chose two ensembles of gauge field configurations on a $32^3 \times 64$ and a $40^3 \times 64$ lattice generated with $N_f = 2$ flavours of clover improved Wilson fermions and the plaquette gauge action for $\beta = 5.29$ and $\kappa = 0.13632$. The clover coefficient was taken to be 1.9192 according to the non-perturbatively determined interpolation formula given in [28]. This choice of parameters corresponds to a lattice spacing $a = 0.072$ fm, a pion mass of about 290 MeV and spatial lattice sizes $L \approx 2.3$ fm for the smaller and $L \approx 2.9$ fm for the larger lattice (see e.g., [14]). The correlation functions were computed at the "Norddeutscher Verbund für Hoch- und Höchstleistungsrechnen (HLRN)" using the CHROMA software package [18, 5] for ensembles of 95 $(32^3 \times 64)$/92 $(40^3 \times 64)$ configurations and $N = 2$ complex $Z(2)$ noise vectors. For sources and sinks we used 100 steps of Wuppertal smearing [26] with a smearing parameter of 0.25, where the links were smeared by 25 steps of APE smearing [6] with smearing parameter 2.5. The total momentum was chosen as $(1,1,0)\frac{2\pi}{L}$ for $32^3 \times 64$ and $(0,0,1)\frac{2\pi}{L}, (1,1,0)\frac{2\pi}{L}, (0,0,2)\frac{2\pi}{L}$ for $40^3 \times 64$. For all momenta we restricted ourselves to the longitudinal polarisation whose computational cost is much smaller than for transverse polarisation. We can see this from chapter 8 where the transverse polarisations require two-pion operators with different momentum combinations. Table 10.1.1 gives an overview of the most important parameters. We used the jackknife method (see Appendix B) to compute the statistical errors. The correlation between different timeslices was taken into account in the fits by calculating the full correlation matrix. Figure 10.1.1 shows the $\pi\pi \to \pi\pi$, $\pi\pi \to \rho$ and $\rho \to \rho$ correlation functions on the $32^3 \times 64$ lattice with statistical errors. For the larger lattice the pictures are very similar and therefore not shown here. In section 9 we mentioned that sequential propagators of the form $W(\vec{x}, t|\vec{0}, t|\vec{0}, 0, \xi_j)$ are the most expensive to calculate because we need one of them for every time t. Therefore we restricted the number of considered timeslices to the interval $[4, 23]$. The first timeslices can be ignored because for small t the correlation functions contain also higher energy eigenstates and are therefore omitted in 2-parameter fits anyway. For large t the errors of the correlators become large and the results are useless. On the $40^3 \times 64$ lattice we exploited the fact that the propagator $W(\vec{x}, t|\vec{0}, t|\vec{0}, 0, \xi_j)$, which must be computed for all $t \in [4, 23]$, appears in the correlators for all values of the total momentum. This allowed us to calculate the correlation functions for all total momenta considered in one

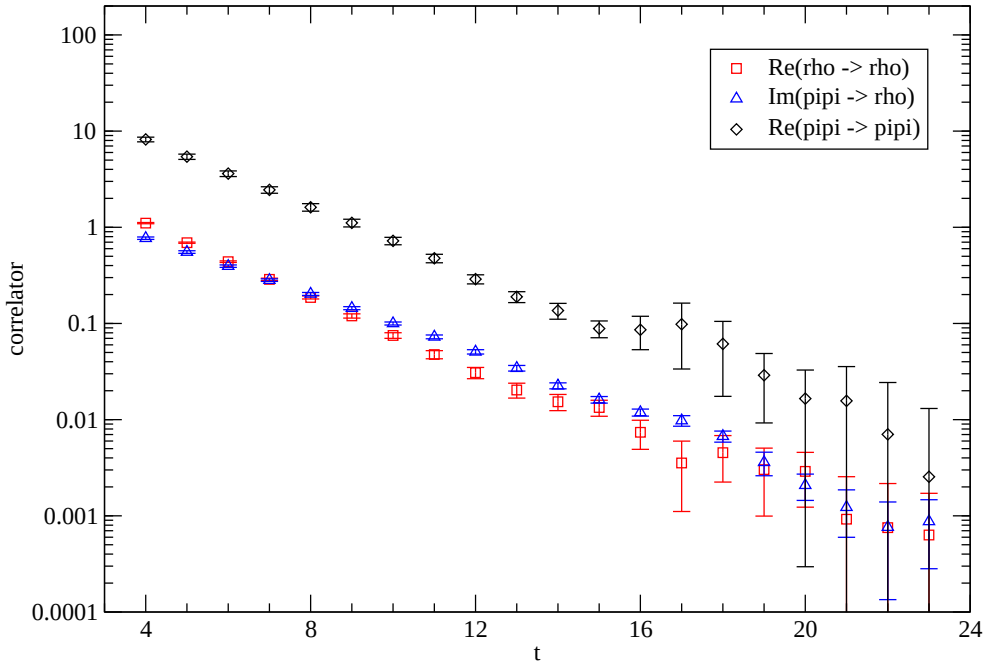

Figure 10.1.1.: Correlation functions on the $32^3 \times 64$ lattice.

run without the need to evaluate the above mentioned propagator anew for each total momentum. This procedure saves quite some computing time.

Due to the discrete symmetries of the lattice action the correlation functions for $\pi\pi \to \rho$ and $\rho \to \pi\pi$ are purely imaginary and must coincide up to a minus sign. In figure 10.1.2 we can see that the two correlators agree very well within errors. Because the errors of $G_{\rho\to\pi\pi}$ are much larger especially for large times we replace $G_{\rho\to\pi\pi}$ by $G^*_{\pi\pi\to\rho}$ in the analysis of the data.

We solve the generalised eigenvalue problem (GEVP) for the two choices $t_0 = 4$ and $t_0 = 5$ and extract the effective energies. Figure 10.1.3 shows them for the ground and first excited state on the $32^3 \times 64$ lattice. The GEVP method seems to work well and both energy levels show the expected plateau. Furthermore both levels are well separated for t not too large. The same holds also for the energy levels on the $40^3 \times 64$ lattice.

Next we analyse the normalised spectral amplitudes. We get them from the eigenvectors $\vec{v}^{\,(k)}$ of the GEVP (4.3.7) where k labels the k-th eigenvector. Following [23] we

Lattice	momenta	$t_{beg} - t_{end}$	N_{conf}
$32^3 \times 64$	(1,1,0)	$4 - 23$	95
$40^3 \times 64$	(0,0,1), (1,1,0),(0,0,2)	$4 - 23$	92
β	κ	m_π	L
5.29	0.13632	290 MeV	2.3 fm
5.29	0.13632	290 MeV	2.9 fm

Table 10.1.1.: Parameters for the analysis.

solve

$$\sum_i w_i^{(k)} v_i^{(l)} = \delta^{kl} \mathrm{e}^{E_k t_0/2} \tag{10.1.1}$$

for the spectral amplitudes $\vec{w}^{(k)}$. The index i denotes the vector component and E_k is the energy belonging to the k-th eigenvalue. The normalised spectral amplitudes $\vec{c}^{(k)}$ are then

$$c_i^{(k)} = \frac{w_i^{(k)}}{\sqrt{\sum_{k'} |w_i^{(k')}|^2}}. \tag{10.1.2}$$

The components of $\vec{c}^{(k)}$ should be independent of the time t. This is satisfied within the statistical errors as is shown in figures 10.2.1-10.2.4, where we plotted $|c_i^{(k)}|^2$ against the time. In most of the cases it is the ground state which predominantly couples to the two-pion operator while the excited state couples more strongly to the rho operator than to the two-pion operator. This observation is consistent with the ordering of the energy levels in figures 8.3.1 and 8.3.3. An exception is the total momentum $(0, 0, 2)$ on the $40^3 \times 64$ lattice, where $m_\pi L$ is close to the crossing point of the free rho and two-pion energies. Therefore we expect that the two free states will strongly mix in this case, which is indeed seen in figure 10.2.4. The extracted energies are listed in tables C.0.1-C.0.8 for different fit intervals and values of t_0. We see that the ground state energy does not depend on the fit interval or t_0 within errors. The figures C.0.1 and C.0.2 illustrate this fact showing the values for $t_0 = 4$. Moreover we can see some dependence of the energy of the excited state on the fit interval especially for the $40^3 \times 64$ lattice in figure C.0.3.

For the scattering phase shift we compared the values for the continuum dispersion relation from chapter 5

$$\begin{aligned} W_{CM} &= \sqrt{W_L^2 - \vec{P}^2}, \\ W_{CM} &= 2\sqrt{\vec{k}_{CM}^2 + m_\pi^2} \end{aligned} \tag{10.1.3}$$

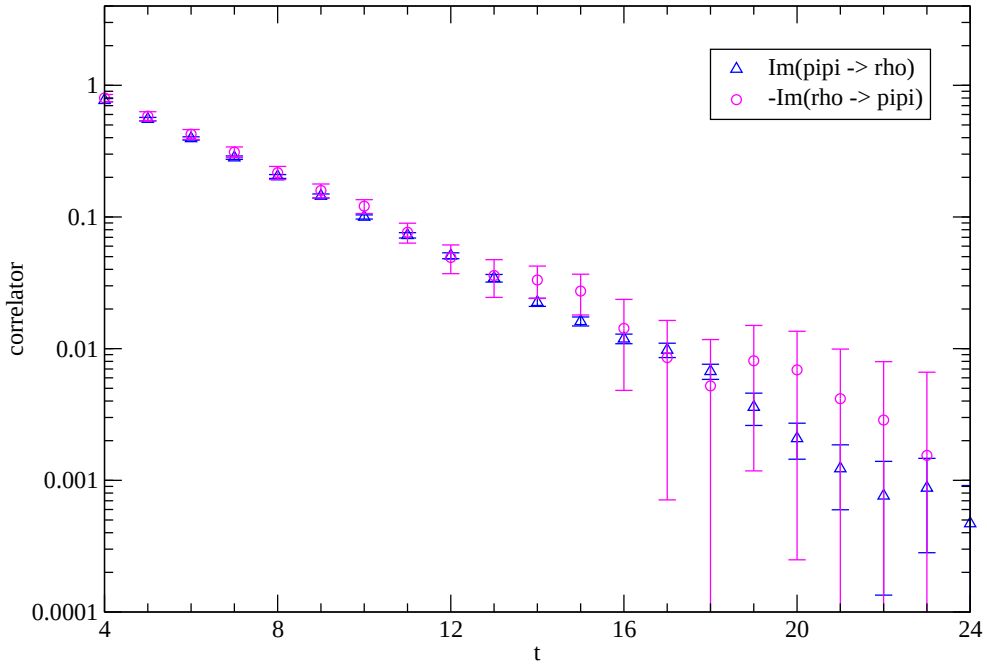

Figure 10.1.2.: Correlation functions for $G_{\pi\pi\to\rho}$ and $G_{\rho\to\pi\pi}$ on the $32^3 \times 64$ lattice.

with those determined by means of the lattice dispersion relation [7]

$$\begin{aligned} \cosh(W_{CM}) &= \cosh(W_L) - 2\sin^2(|\vec{P}|/2) \\ 2\sin^2(|\vec{k}_{CM}|/2) &= \cosh(W_{CM}/2) - \cosh(m_\pi). \end{aligned} \tag{10.1.4}$$

Tables C.0.9-C.0.16 show the scattering phase shifts for $t_0 = 4$ and different fit intervals. The values for the continuum and the lattice dispersion relation coincide within the statistical errors, which suggests that our data are not too strongly affected by the finite lattice spacing.

The final plot for the scattering phase shifts for the $32^3 \times 64$ and $40^3 \times 64$ lattices using the continuum dispersion relation is shown in figure 10.1.4. The points correspond to the energies marked with a * in tables C.0.1-C.0.8 and the error bars display the statistical error. The solid and dotted black curves correspond to the phase shifts from the effective range model for the coupling $g_{\rho\pi\pi} = 6.0$ and different m_ρ/m_π. The pion and rho meson masses on both lattices determined from standard meson 2-point functions are given in table 10.1.2. Unfortunately, the relatively large errors of the data make definite conclusions difficult. Figure 10.1.4 suggests nevertheless that m_ρ/m_π for the

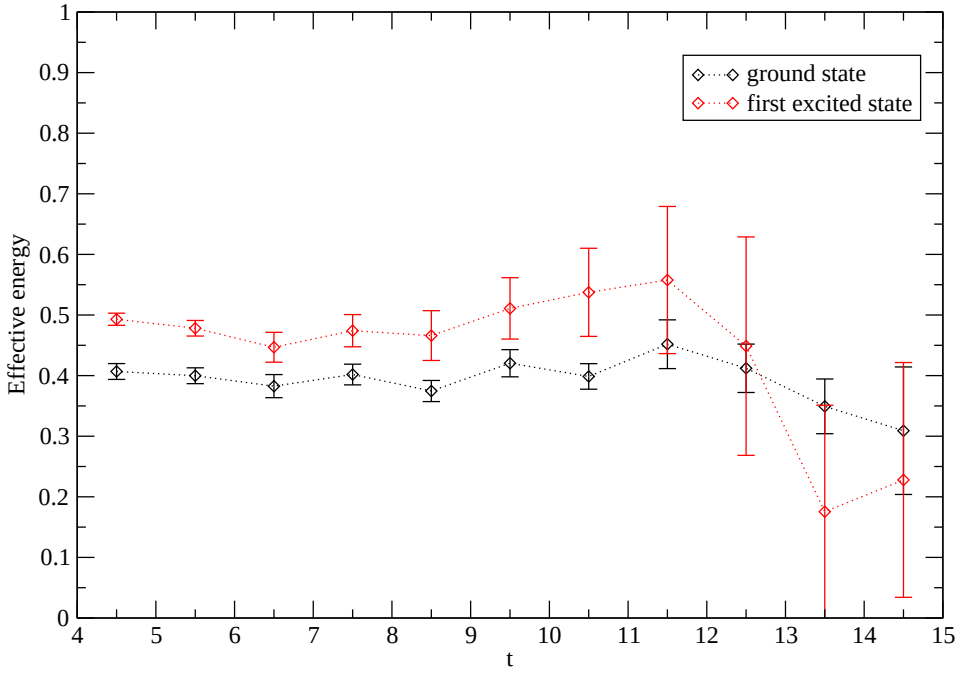

Figure 10.1.3.: Effective energies on the $32^3 \times 64$ lattice for $t_0 = 4$.

$32^3 \times 64$ and $40^3 \times 64$ lattice is around 3.3 and 2.9, respectively. While the ratio on the $40^3 \times 64$ lattice is compatible with the expectations based on table 10.1.2, the value on the smaller lattice is somewhat too large. A possible explanation is the small value of $m_\pi L$ which is around 3.43. For the $40^3 \times 64$ lattice we have $m_\pi L \approx 4.18$, which seems to be large enough to suppress effects of the finite volume. Note that m_π also shows some volume dependence when the lattice size is increased from $32^3 \times 64$ to $40^3 \times 64$.

One source of systematic uncertainties is the dependence of the fitted energies on the fit interval. As figures C.0.1-C.0.3 and tables C.0.1-C.0.8 show, the size of this effect does not exceed the statistical errors. However, a careful analysis must be left for the future.

Lattice size	m_π	m_ρ
$32^3 \times 64$	0.10704(49)	0.3072(52)
$40^3 \times 64$	0.10444(43)	0.3062(31)

Table 10.1.2.: Pion and rho masses from standard meson 2-point functions [39].

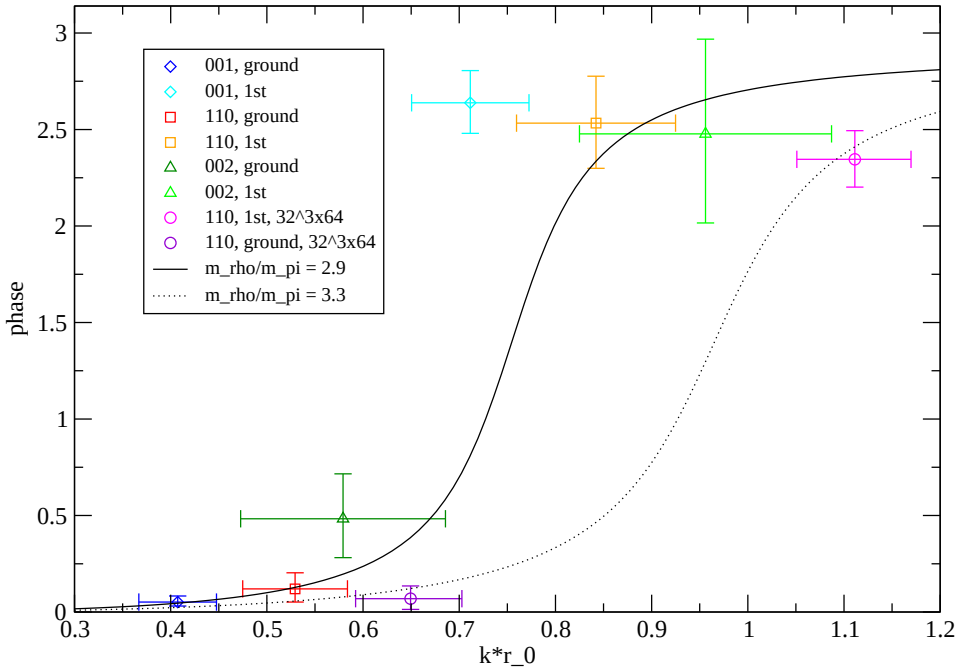

Figure 10.1.4.: Scattering phase shifts (points) for the $40^3 \times 64$ lattice compared with the effective range model (lines) using the continuum dispersion relation.

10.2. Summary and outlook

Using lattice QCD we have calculated the $\pi\pi \to \pi\pi$ scattering phase shift in the isospin $I = 1$ channel for two different lattice volumes with a pion mass around 290 MeV and a lattice spacing of about 0.072 fm. The rho interacts with the 2-pion state via a 3-point interaction, whose strength is characterised by the coupling constant $g_{\rho\pi\pi}$. The rho mass should satisfy the constraint $2m_\pi < m_\rho < 4m_\pi$. The first inequality has to be fulfilled so that the rho can decay. The second one takes into account the fact that we want to stay in the elastic scattering region. On the $32^3 \times 64$ lattice we chose the total momentum as $(1, 1, 0) \times 2\pi/32$ and on the $40^3 \times 64$ lattice we considered three different total momenta, $(0, 0, 1), (1, 1, 0)$ and $(0, 0, 2)$ in units of $2\pi/40$. In all cases the polarisation was longitudinal. For these momenta we expected the lowest energy levels to be well separated. In the computation of the scattering phases from these energies we used the continuum as well as a lattice motivated dispersion relation. Both yield consistent results which indicates that the lattice spacing is small enough to avoid significant effects.

On the other hand, on the $32^3 \times 64$ lattice the value $m_\pi L = 3.43$ is quite small compared with other simulations [7, 19, 20, 8]. This may be the reason why the data can be described by the effective range model only for a mass ratio $m_\rho/m_\pi \approx 3.3$ which is considerably larger than the value $m_\rho/m_\pi \approx 2.9$ expected from the analysis of standard rho two-point functions. On the $40^3 \times 64$ lattice we have $m_\pi L = 4.18$ and the extracted phase shifts are compatible with the expectations (see figure 10.1.4). Therefore it seems to be important to work on a sufficiently large lattice because otherwise the results could be affected by finite size effects. The requirements of small m_π (so that the rho can decay) and large L increase the required computing time and memory noticeably.

We have restricted ourselves to longitudinal polarisation because in this case only two momenta, the total momentum $\vec{q}$ and momentum $\vec{0}$, are needed in the two-pion operator. Furthermore, propagators for momentum $\vec{0}$ have to be calculated just once for different total momenta. From the predictions of the effective range model in figures 8.3.1, 8.3.3 and 8.3.4 and also from our results in figure 10.1.4 we see that the ground state scattering phase shift is nearly zero while the phase shift for the first excited state is around 2.5. It would be preferable if we had also data points close to the resonance energy, where the phase shift is $\pi/2$. This could be achieved by considering transverse polarisation, e.g. for total momentum $(0, 0, 1) \times 2\pi/L$, where the ground state scattering phase shift is expected to be around 1.5 for $m_\pi L \approx 4.0$ (see figure 8.3.2). Our results show (not unexpectedly) that very accurate energies are required in order to determine the width and the mass of rho resonance with reasonable precision. Unfortunately, our present data is not quite sufficient for that purpose. Higher statistics and optimised sources should however allow for some improvement.

To collect more data points one could think about using even higher momenta, but we think that this idea is not really recommended because already momentum $(0, 0, 2)$ has quite large errors. Another possibility is to include more energy eigenstates and enlarging the correlation matrix, either by using propagators with a different number of smearing steps or including meson interpolators with different Dirac structure, for example $\gamma_0\gamma_5$ and $\gamma_0\gamma_i$ for the pion and rho interpolator, respectively. This method has been tested successfully in [11, 12]. But also this approach would lead to an increase of computing time and one has to analyse carefully if including transverse polarisations or enlarging the correlation matrix is more promising.

Moreover, energy levels higher than the first excited one will not necessarily lead to phase shifts in the interesting resonance region, as exemplified by the figures in chapter 8. But working with a larger basis of operators is expected to increase the reliability of the lower energies, in particular. In this connection the recently proposed distillation method should be very useful [29].

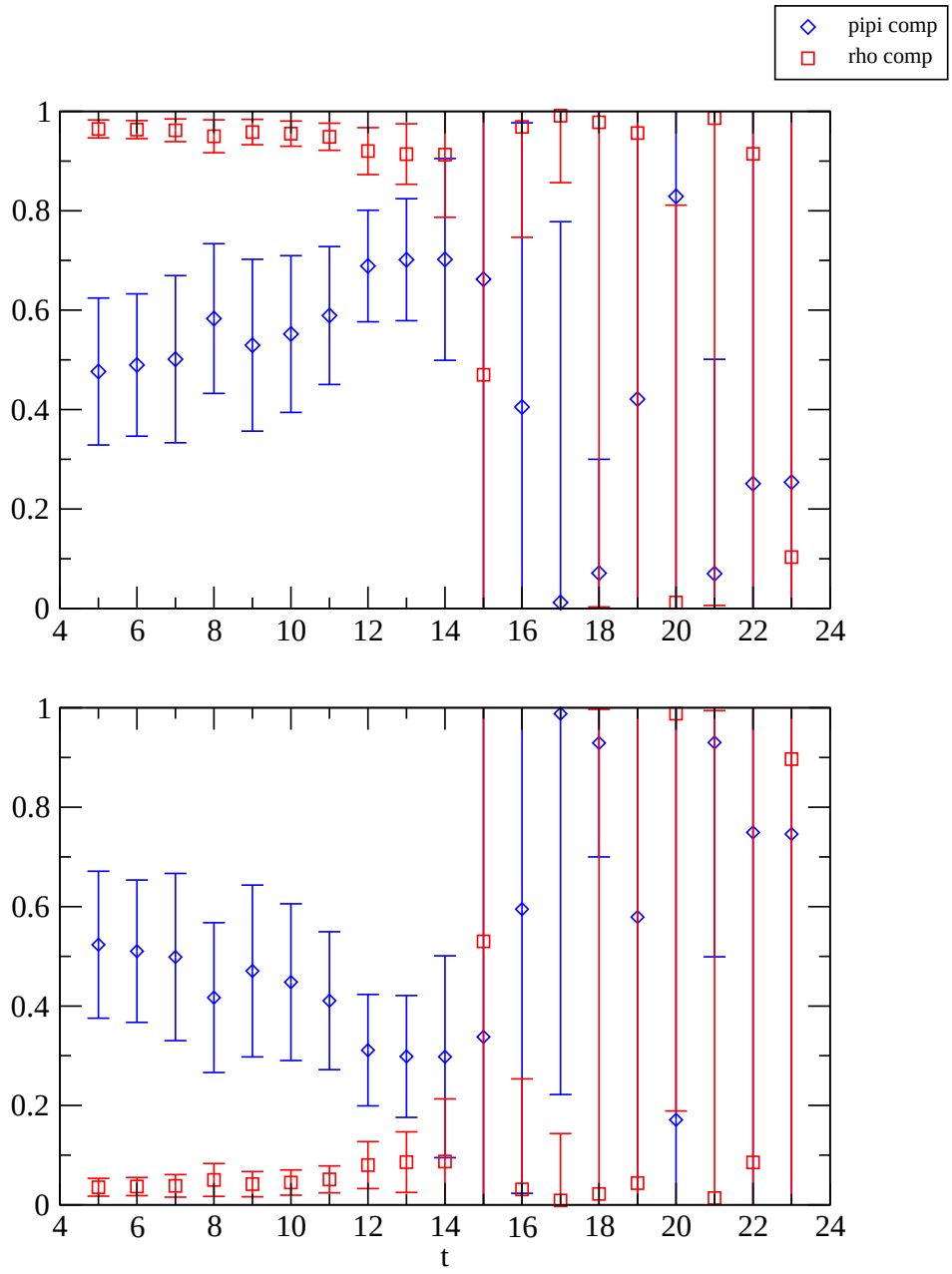

Figure 10.2.1.: Absolute square of normalised spectral amplitudes for the $32^3 \times 64$ lattice, momentum $(1, 1, 0)$. Lower panel: ground state, upper panel: first excited state.

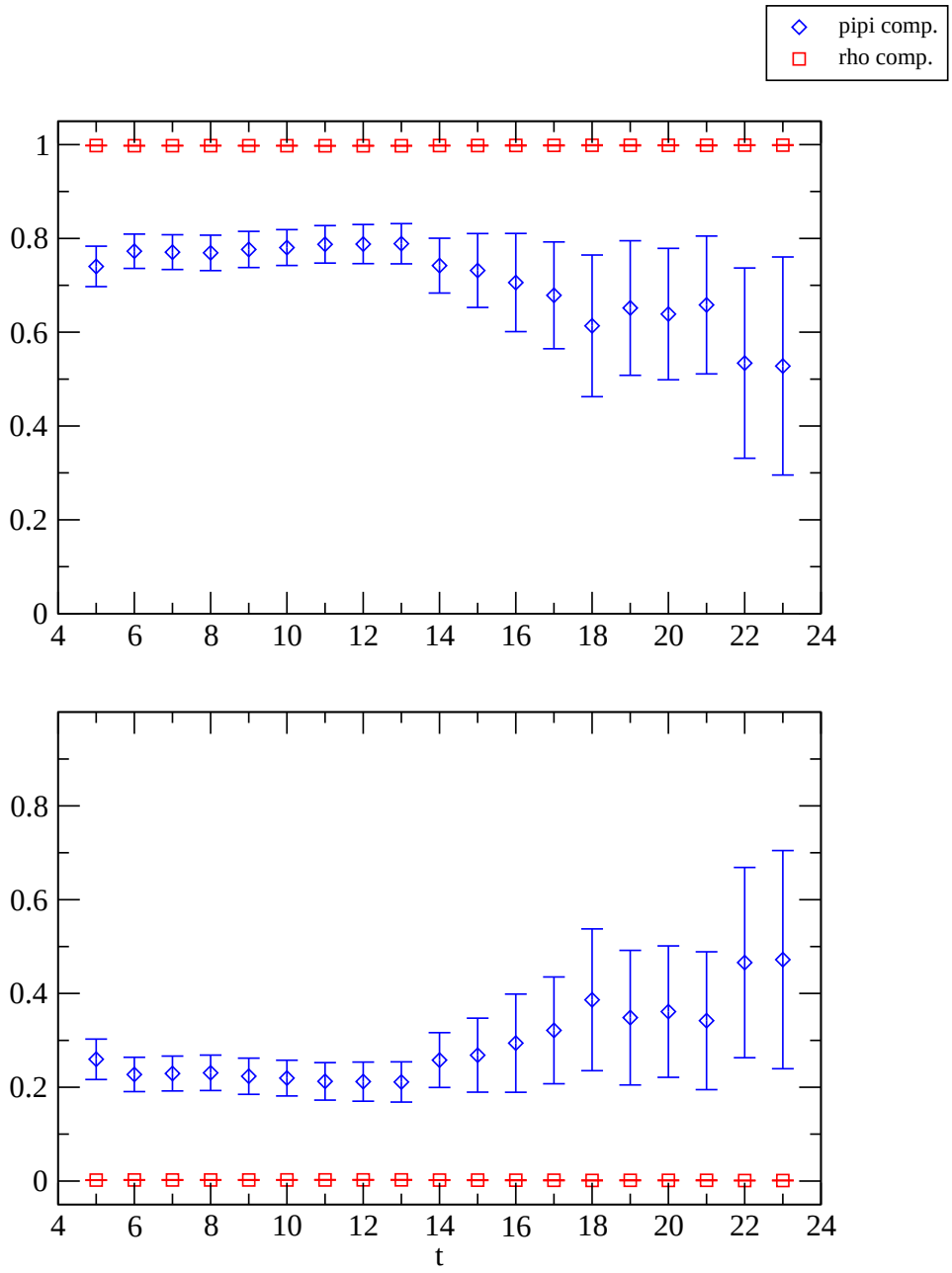

Figure 10.2.2.: Absolute square of normalised spectral amplitudes for the $40^3 \times 64$ lattice, momentum $(0, 0, 1)$. Lower panel: ground state, upper panel: first excited state.

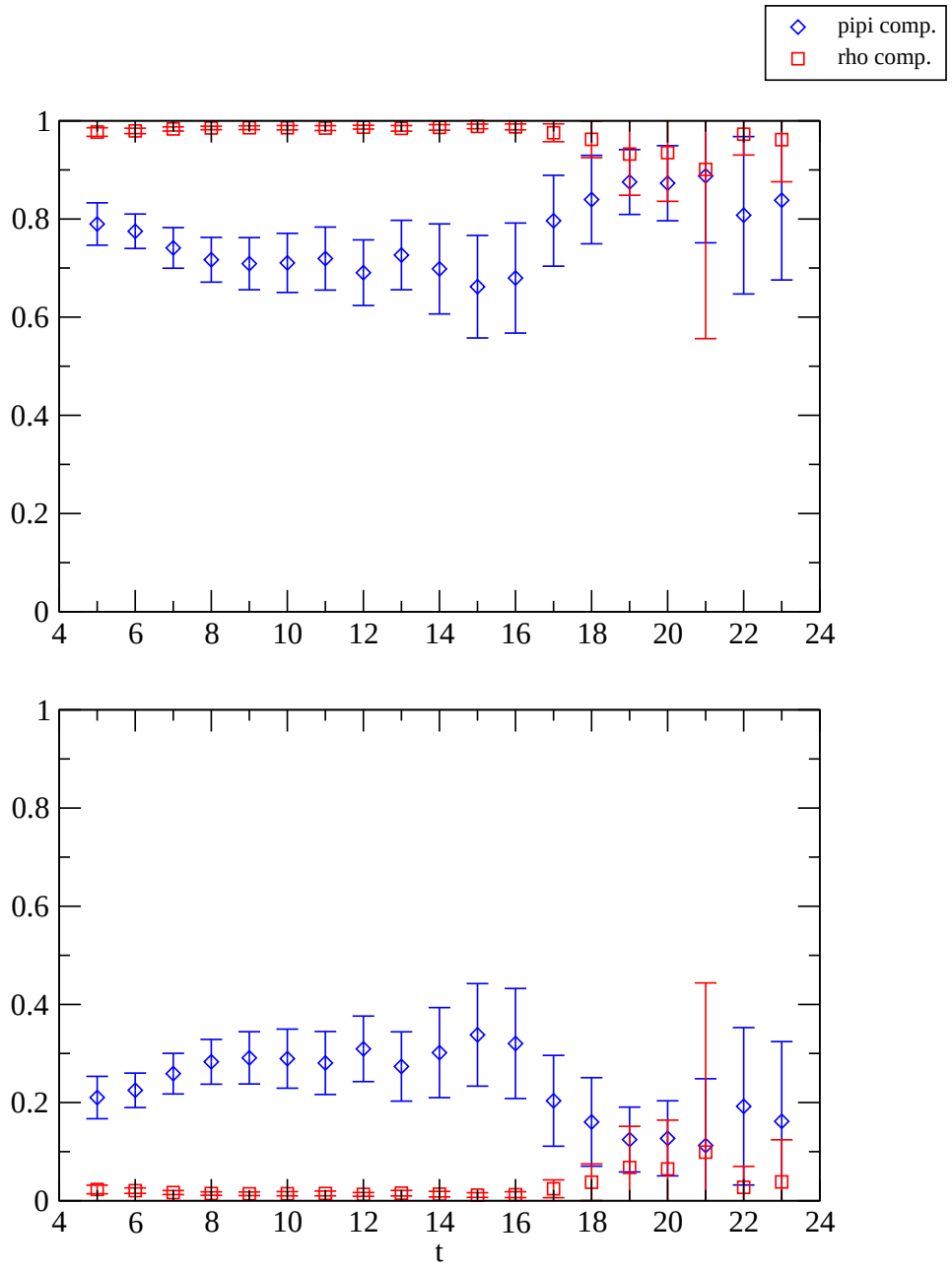

Figure 10.2.3.: Absolute square of normalised spectral amplitudes for the $40^3 \times 64$ lattice, momentum $(1, 1, 0)$. Lower panel: ground state, upper panel: first excited state.

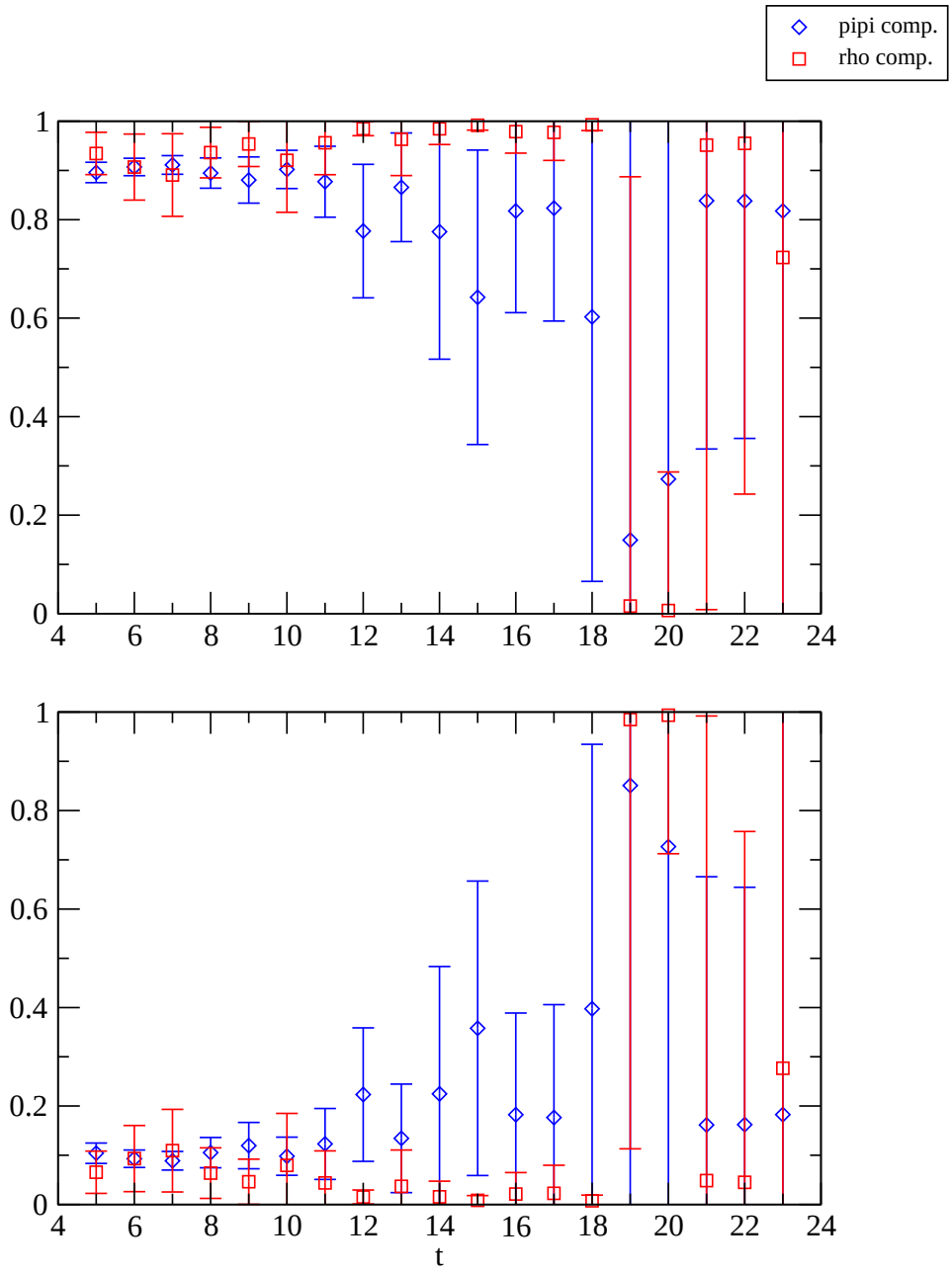

Figure 10.2.4.: Absolute square of normalised spectral amplitudes for the $40^3 \times 64$ lattice, momentum $(0, 0, 2)$. Lower panel: ground state, Upper panel: first excited state.

A. Calculation of the generalised zeta function

In Chapter 5 we defined the generalised zeta function $Z_{lm}^{\vec{d}}$ as

$$Z_{lm}^{\vec{d}}(s;q^2) = \sum_{\vec{r}\in P_{\vec{d}}} \frac{r^l Y_{lm}(\theta,\phi)}{(\vec{r}^{\,2}-q^2)^s} \tag{A.0.1}$$

with the set

$$P_{\vec{d}} = \{\vec{r}\in\mathbb{R}^3 |\, \vec{r} = \hat{\gamma}^{-1}(\vec{n}+\tfrac{1}{2}\vec{d})\}, \quad \vec{n},\vec{d}\in\mathbb{Z}^3. \tag{A.0.2}$$

Here $\vec{d}$ is fixed in the direction of the total momentum $\vec{P} = \frac{2\pi}{L}\vec{d}$ and we can decompose $\vec{n}$ in a component parallel to $\vec{d}$, $\vec{n}_\parallel = \frac{(\vec{n}\cdot\vec{d})\vec{d}}{d^2}$, and a component perpendicular to $\vec{d}$, $\vec{n}_\perp = \vec{n}-\vec{n}_\parallel$. The operator $\hat{\gamma}^{-1}$ then applies an inverse Lorentz transfrom. This means that

$$\hat{\gamma}^{-1}\vec{n} = \tfrac{1}{\gamma}\vec{n}_\parallel + \vec{n}_\perp. \tag{A.0.3}$$

The sum in (A.0.1) converges if $\mathfrak{Re}(2s) > l+3$ and can be analytically continued to the complex s-plane. In the following we describe a method for evaluating $Z_{lm}^{\vec{d}}(s;q^2)$ at $s=1$ excluding the singular case where $q^2 = \vec{r}^{\,2}$ for some $\vec{r}\in P_{\vec{d}}$.

A.1. General formalism

Following Yamazaki et al. [47] we divide the sum in (A.0.1) into two parts

$$\sum_{\vec{r}\neq q^2} \frac{Q(\vec{r})}{(\vec{r}^{\,2}-q^2)^s} = \sum_{\vec{r}^{\,2}<q^2} \frac{Q(\vec{r})}{(\vec{r}^{\,2}-q^2)^s} + \sum_{\vec{r}^{\,2}>q^2} \frac{Q(\vec{r})}{(\vec{r}^{\,2}-q^2)^s}, \tag{A.1.1}$$

where we replaced the harmonic polynomial by $Q(\vec{r})$. The different gamma functions are defined as

$$\Gamma(s) = \int_0^\infty \mathrm{d}t\; t^{s-1}\mathrm{e}^{-t}, \tag{A.1.2}$$

$$\Gamma(s,c) = \int_c^\infty \mathrm{d}t\; t^{s-1}\mathrm{e}^{-t}, \tag{A.1.3}$$

$$\gamma(s,c) = \int_0^c \mathrm{d}t\; t^{s-1}\mathrm{e}^{-t}. \tag{A.1.4}$$

The functions $\Gamma(s,c)$ and $\gamma(s,c)$ are called incomplete gamma functions. With the help of (A.1.2) we can write

$$\frac{1}{c^s} = \frac{1}{\Gamma(s)} \int_0^\infty \mathrm{d}t\, t^{s-1} \mathrm{e}^{-ct} \tag{A.1.5}$$

for $c > 0$ and $\mathfrak{Re}(s) > 0$ and replace $(\vec{r}^{\,2} - q^2)^{-s}$ in the second term of (A.1.1) to get

$$\sum_{\vec{r}^{\,2}>q^2} \frac{Q(\vec{r})}{(\vec{r}^{\,2} - q^2)^s} = \frac{1}{\Gamma(s)} \sum_{\vec{r}^{\,2}>q^2} Q(\vec{r}) \Big\{ \int_0^1 \mathrm{d}t\, t^{s-1} \mathrm{e}^{-t(\vec{r}^{\,2}-q^2)} + \int_1^\infty \mathrm{d}t\, t^{s-1} \mathrm{e}^{-t(\vec{r}^{\,2}-q^2)} \Big\}. \tag{A.1.6}$$

In the first integral we can use $\sum_{\vec{r}^{\,2}>q^2} \cdots = \sum_{\vec{r}} \cdots - \sum_{\vec{r}^{\,2}<q^2} \ldots$ and write

$$\begin{aligned} \sum_{\vec{r}^{\,2}>q^2} \frac{Q(\vec{r})}{(\vec{r}^{\,2} - q^2)^s} &= \frac{1}{\Gamma(s)} \int_0^1 \mathrm{d}t\, t^{s-1} \mathrm{e}^{tq^2} \sum_{\vec{r}} Q(\vec{r}) \mathrm{e}^{-t\vec{r}^{\,2}} \\ &\quad - \frac{1}{\Gamma(s)} \sum_{\vec{r}^{\,2}<q^2} Q(\vec{r}) \int_0^1 \mathrm{d}t\, t^{s-1} \mathrm{e}^{-t(\vec{r}^{\,2}-q^2)} \\ &\quad + \frac{1}{\Gamma(s)} \sum_{\vec{r}^{\,2}>q^2} Q(\vec{r}) \int_1^\infty \mathrm{d}t\, t^{s-1} \mathrm{e}^{-t(\vec{r}^{\,2}-q^2)}. \end{aligned} \tag{A.1.7}$$

From the incomplete gamma functions we get $\int_1^\infty \mathrm{d}t t^{s-1} \mathrm{e}^{-ct} = c^{-s}\Gamma(s,c)$ and $\int_0^1 \mathrm{d}t t^{s-1} \mathrm{e}^{-ct}$ $= c^{-s}\gamma(s,c)$ and we can write down the general expression

$$\begin{aligned} \sum_{\vec{r}^{\,2}>q^2} \frac{Q(\vec{r})}{(\vec{r}^{\,2} - q^2)^s} &= -\frac{1}{\Gamma(s)} \sum_{\vec{r}^{\,2}<q^2} \frac{Q(\vec{r})}{(\vec{r}^{\,2} - q^2)^s} \\ &\quad + \frac{1}{\Gamma(s)} \int_0^1 \mathrm{d}t\, t^{s-1} \mathrm{e}^{tq^2} \sum_{\vec{r}} Q(\vec{r}) \mathrm{e}^{-t\vec{r}^{\,2}} \\ &\quad + \frac{1}{\Gamma(s)} \sum_{\vec{r}^{\,2}<q^2} \frac{Q(\vec{r})}{(\vec{r}^{\,2} - q^2)^s} (1 - \gamma(s, \vec{r}^{\,2} - q^2)) \\ &\quad + \frac{1}{\Gamma(s)} \sum_{\vec{r}^{\,2}>q^2} \frac{Q(\vec{r})}{(\vec{r}^{\,2} - q^2)^s} \Gamma(s, \vec{r}^{\,2} - q^2). \end{aligned} \tag{A.1.8}$$

Let us now look at the sum $\sum_{\vec{r}} Q(\vec{r}) \mathrm{e}^{-t\vec{r}^{\,2}}$ in the second term. With the definition of $\vec{r}$ in (A.0.2) we can write

$$\sum_{\vec{r}} Q(\vec{r}) \mathrm{e}^{-t\vec{r}^{\,2}} = \sum_{\vec{n}\in\mathbb{Z}^3} Q(\hat{\gamma}^{-1}(\vec{n} + \tfrac{1}{2}\vec{d})) \mathrm{e}^{-t(\hat{\gamma}^{-1}(\vec{n}+\frac{1}{2}\vec{d}))^2}. \tag{A.1.9}$$

We utilise the Poisson summation formula

$$\sum_{\vec{n}\in\mathbb{Z}^3} f(\vec{n}) = \sum_{\vec{n}\in\mathbb{Z}^3} \int \mathrm{d}^3x\, f(\vec{x})\mathrm{e}^{2\pi i\vec{n}\vec{x}} \tag{A.1.10}$$

where we set

$$f(\vec{x}) = Q(\hat{\gamma}^{-1}(\vec{x}+\tfrac{1}{2}\vec{d}))\mathrm{e}^{-t(\hat{\gamma}^{-1}(\vec{x}+\frac{1}{2}\vec{d}))^2} \tag{A.1.11}$$

and use also a variable transformation $\hat{\gamma}^{-1}\vec{x} = \vec{y}$ to get

$$\begin{aligned}\sum_{\vec{r}} Q(\vec{r})\mathrm{e}^{-t\vec{r}^{\,2}} = \gamma \int \mathrm{d}^3y\, Q(\vec{y})\mathrm{e}^{-t\vec{y}^2} \\ + \gamma \sum_{\vec{n}\in\mathbb{Z}^3\setminus\{0\}} (-1)^{\vec{n}\vec{d}}\mathrm{e}^{-\pi^2(\hat{\gamma}\vec{n})^2/t} \int \mathrm{d}^3y\, Q(\vec{y}+\tfrac{\pi i}{t}\hat{\gamma}\vec{n})\mathrm{e}^{-t\vec{y}^2}.\end{aligned} \tag{A.1.12}$$

Now we can set $s = 1$. The gamma functions are then $\Gamma(1) = 1$, $\gamma(1,c) = 1-\mathrm{e}^{-c}$ and $\Gamma(1,c) = \mathrm{e}^{-c}$. We can bring the first term in (A.1.8) to the left hand side and get

$$\boxed{\begin{aligned}\sum_{\vec{r}} \frac{Q(\vec{r})}{(\vec{r}^{\,2}-q^2)^s}\Big|_{s=1} &= \sum_{\vec{r}} \frac{Q(\vec{r})}{(\vec{r}^{\,2}-q^2)}\mathrm{e}^{-(\vec{r}^{\,2}-q^2)} \\ &+ \gamma \int_0^1 \mathrm{d}t\, \mathrm{e}^{tq^2} \sum_{\vec{n}\in\mathbb{Z}^3\setminus\{0\}} (-1)^{\vec{n}\vec{d}}\mathrm{e}^{-\pi^2(\hat{\gamma}\vec{n})^2/t} \\ &\qquad \times \int \mathrm{d}^3y\, Q(\vec{y}+\tfrac{\pi i}{t}\hat{\gamma}\vec{n})\mathrm{e}^{-t\vec{y}^2} \\ &+ \lim_{s\to 1}\gamma \int_0^1 \mathrm{d}t\, t^{s-1}\mathrm{e}^{tq^2} \int \mathrm{d}^3y\, Q(\vec{y})\mathrm{e}^{-t\vec{y}^2}.\end{aligned}} \tag{A.1.13}$$

We will use this formula to calculate the zeta functions for the different momenta.

A.2. Derivation for D_{4h}, D_{2h} and D_{3d}

For the total momentum $(0,0,1)$ and longitudinal polarisation we need (see (6.2.12))

$$\frac{1}{\gamma q\pi^{3/2}}(Z_{00}^{\vec{d}}(1;q^2) + \tfrac{2}{\sqrt{5}q^2}Z_{20}^{\vec{d}}(1;q^2)) = \frac{1}{2\gamma q\pi^2}\sum_{\vec{r}}(1+\tfrac{3r_3^2-\vec{r}^{\,2}}{q^2})(\vec{r}^{\,2}-q^2)^{-s}\Big|_{s=1}. \tag{A.2.1}$$

First we want to calculate

$$\int \mathrm{d}^3y\, Q(\vec{y})\mathrm{e}^{-t\vec{y}^2} = \int \mathrm{d}^3y\, \left(\mathrm{e}^{-t\vec{y}^2} + \tfrac{3y_3^2}{q^2}\mathrm{e}^{-t\vec{y}^2} - \tfrac{\vec{y}^2}{q^2}\mathrm{e}^{-t\vec{y}^2}\right) \tag{A.2.2}$$

where $Q(\vec{r}) = 1 + \frac{3r_3^2 - \vec{r}^2}{q^2}$. The second and third term cancel, and we find

$$\int \mathrm{d}^3y\, Q(\vec{y})\mathrm{e}^{-t\vec{y}^2} = \left(\frac{\pi}{t}\right)^{3/2}. \tag{A.2.3}$$

What remains of the last term in (A.1.13) is an integral of the form

$$\gamma\pi^{3/2}\int_0^1 \mathrm{d}t\, t^{(s-\frac{3}{2})-1}\mathrm{e}^{-t(-q^2)}. \tag{A.2.4}$$

Expanding the exponential in a power series, integrating the terms and taking the limit $s \to 1$ we get

$$\lim_{s\to 1}\gamma\int_0^1 \mathrm{d}t\, t^{s-1}\mathrm{e}^{tq^2}(\tfrac{\pi}{t})^{3/2} = \gamma\pi^{3/2}\sum_{l=0}^{\infty}\frac{(q^2)^l}{l!(l-\frac{1}{2})}. \tag{A.2.5}$$

Finally we have to calculate

$$\begin{aligned}\int \mathrm{d}^3y\, Q(\vec{y} + \tfrac{\pi i}{t}\hat{\gamma}\vec{n})\mathrm{e}^{-t\vec{y}^2} \\ = \int \mathrm{d}^3y\left[1 + \frac{3(y_3 + \frac{\pi i}{t}(\hat{\gamma}\vec{n})_3)^2}{q^2} - \frac{(\vec{y} + \frac{\pi i}{t}\hat{\gamma}\vec{n})^2}{q^2}\right]\mathrm{e}^{-t\vec{y}^2}.\end{aligned} \tag{A.2.6}$$

One finds

$$\int \mathrm{d}^3y\, Q(\vec{y} + \tfrac{\pi i}{t}\hat{\gamma}\vec{n})\mathrm{e}^{-t\vec{y}^2} = \left(\frac{\pi}{t}\right)^{3/2}\left(1 + \frac{\pi^2}{q^2t^2}\left[(\hat{\gamma}\vec{n})^2 - 3(\hat{\gamma}\vec{n})_3^2\right]\right). \tag{A.2.7}$$

Gathering all terms we can write the final result as

$$\boxed{\begin{aligned}\sum_{\vec{r}}\frac{(1+\frac{3r_3^2-\vec{r}^2}{q^2})}{(\vec{r}^2-q^2)^s}\Big|_{s=1} &= \sum_{\vec{r}}\frac{(1+\frac{3r_3^2-\vec{r}^2}{q^2})}{(\vec{r}^2-q^2)}\mathrm{e}^{-(\vec{r}^2-q^2)} \\ &\quad +\gamma\int_0^1 \mathrm{d}t\,\mathrm{e}^{tq^2}\sum_{\vec{n}\in\mathbb{Z}^3\setminus\{0\}}(-1)^{\vec{n}\vec{d}}\mathrm{e}^{-\pi^2(\hat{\gamma}\vec{n})^2/t} \\ &\quad \times\left(\frac{\pi}{t}\right)^{3/2}\left(1+\frac{\pi^2}{q^2t^2}\left[(\hat{\gamma}\vec{n})^2 - 3(\hat{\gamma}\vec{n})_3^2\right]\right) \\ &\quad +\gamma\pi^{3/2}\sum_{l=0}^{\infty}\frac{(q^2)^l}{l!(l-\frac{1}{2})}.\end{aligned}} \tag{A.2.8}$$

The integral in (A.2.8) is calculated by Chebycheff integration.

For the transverse polarisation we have to calculate (see (6.2.13))

$$\frac{1}{\gamma q\pi^{3/2}}(Z_{00}^{\vec{d}}(1;q^2) - \tfrac{1}{\sqrt{5}q^2}Z_{20}^{\vec{d}}(1;q^2)) = \frac{1}{2\gamma q\pi^2}\sum_{\vec{r}}(1 - \tfrac{3r_3^2-\vec{r}^2}{2q^2})(\vec{r}^2-q^2)^{-s}\Big|_{s=1} \tag{A.2.9}$$

with $Q(\vec{r}) = 1 - \frac{3r_3^2-\vec{r}^2}{2q^2}$ and get

$$\begin{aligned}\sum_{\vec{r}} \frac{Q(\vec{r})}{(\vec{r}^2-q^2)^s}\Big|_{s=1} =& \sum_{\vec{r}} \frac{(1-\frac{3r_3^2-\vec{r}^2}{2q^2})}{(\vec{r}^2-q^2)} \mathrm{e}^{-(\vec{r}^2-q^2)} \\ &+\gamma \int_0^1 \mathrm{d}t\, \mathrm{e}^{tq^2} \sum_{\vec{n}\in\mathbb{Z}^3\setminus\{0\}} (-1)^{\vec{n}\vec{d}} \mathrm{e}^{-\pi^2(\hat{\gamma}\vec{n})^2/t} \\ &\quad \times \left(\frac{\pi}{t}\right)^{3/2} \left(1 - \frac{\pi^2}{2q^2t^2}\left[(\hat{\gamma}\vec{n})^2 - 3(\hat{\gamma}\vec{n})_3^2\right]\right) \\ &+\gamma\pi^{3/2} \sum_{l=0}^{\infty} \frac{(q^2)^l}{l!(l-\frac{1}{2})}.\end{aligned} \tag{A.2.10}$$

For total momentum $(1,1,0)$ and longitudinal polarisation we have (see (6.2.17))

$$\begin{aligned}&\frac{1}{\gamma q\pi^{3/2}}((Z_{00}^{\vec{d}}(1;q^2))^* - \tfrac{1}{\sqrt{5}q^2}(Z_{20}^{\vec{d}}(1;q^2))^* + \tfrac{i\sqrt{6}}{\sqrt{5}q^2}(Z_{22}^{\vec{d}}(1;q^2))^*) \\ &\qquad = \frac{1}{2\gamma q\pi^2} \sum_{\vec{r}} (1 - \tfrac{3r_3^2-\vec{r}^2}{2q^2} + \tfrac{3i(r_1-ir_2)^2}{2q^2})(\vec{r}^2-q^2)^{-s}\Big|_{s=1}\end{aligned} \tag{A.2.11}$$

with $Q(\vec{r}) = 1 - \frac{3r_3^2-\vec{r}^2}{2q^2} + \frac{3i(r_1-ir_2)^2}{2q^2}$ and the final result is

$$\begin{aligned}\sum_{\vec{r}} \frac{Q(\vec{r})}{(\vec{r}^2-q^2)^s}\Big|_{s=1} =& \sum_{\vec{r}} \frac{(1-\frac{3r_3^2-\vec{r}^2}{q^2}) + \frac{3r_1r_2}{q^2}}{(\vec{r}^2-q^2)} \mathrm{e}^{-(\vec{r}^2-q^2)} \\ &+\gamma \int_0^1 \mathrm{d}t\, \mathrm{e}^{tq^2} \sum_{\vec{n}\in\mathbb{Z}^3\setminus\{0\}} (-1)^{\vec{n}\vec{d}} \mathrm{e}^{-\pi^2(\hat{\gamma}\vec{n})^2/t} \\ &\quad \times \left(\frac{\pi}{t}\right)^{3/2} \left(1 - \frac{\pi^2}{2q^2t^2}\left[(\hat{\gamma}\vec{n})^2 - 3(\hat{\gamma}\vec{n})_3^2 + 6(\hat{\gamma}\vec{n})_1(\hat{\gamma}\vec{n})_2\right]\right) \\ &+\gamma\pi^{3/2} \sum_{l=0}^{\infty} \frac{(q^2)^l}{l!(l-\frac{1}{2})}.\end{aligned} \tag{A.2.12}$$

For transverse 1 polarisation we have (see (6.2.19))

$$\begin{aligned}&\frac{1}{\gamma q\pi^{3/2}}((Z_{00}^{\vec{d}}(1;q^2))^* - \tfrac{1}{\sqrt{5}q^2}(Z_{20}^{\vec{d}}(1;q^2))^* - \tfrac{i\sqrt{6}}{\sqrt{5}q^2}(Z_{22}^{\vec{d}}(1;q^2))^*) \\ &\qquad = \frac{1}{2\gamma q\pi^2} \sum_{\vec{r}} (1 - \tfrac{3r_3^2-\vec{r}^2}{2q^2} - \tfrac{3i(r_1-ir_2)^2}{2q^2})(\vec{r}^2-q^2)^{-s}\Big|_{s=1}\end{aligned} \tag{A.2.13}$$

with $Q(\vec{r}) = 1 - \frac{3r_3^2-\vec{r}^2}{2q^2} - \frac{3i(r_1-ir_2)^2}{2q^2}$ and we get

$$\begin{aligned}\sum_{\vec{r}} \frac{Q(\vec{r})}{(\vec{r}^2-q^2)^s}\Big|_{s=1} =& \sum_{\vec{r}} \frac{(1-\frac{3r_3^2-\vec{r}^2}{q^2}) - \frac{3r_1r_2}{q^2}}{(\vec{r}^2-q^2)} \mathrm{e}^{-(\vec{r}^2-q^2)} \\ &+\gamma \int_0^1 \mathrm{d}t\, \mathrm{e}^{tq^2} \sum_{\vec{n}\in\mathbb{Z}^3\setminus\{0\}} (-1)^{\vec{n}\vec{d}} \mathrm{e}^{-\pi^2(\hat{\gamma}\vec{n})^2/t} \\ &\quad \times \left(\frac{\pi}{t}\right)^{3/2} \left(1 - \frac{\pi^2}{2q^2t^2}\Big[(\hat{\gamma}\vec{n})^2 - 3(\hat{\gamma}\vec{n})_3^2 - 6(\hat{\gamma}\vec{n})_1(\hat{\gamma}\vec{n})_2\Big]\right) \\ &+\gamma\pi^{3/2} \sum_{l=0}^{\infty} \frac{(q^2)^l}{l!(l-\frac{1}{2})}.\end{aligned} \tag{A.2.14}$$

In the case of transverse 2 polarisation we get the same result as in (A.2.8).

Finally, for total momentum $(1,1,1)$ and longitudinal polarisation we need (see (6.2.23))

$$\begin{aligned}&\frac{1}{\gamma q\pi^{3/2}}((Z_{00}^{\vec{d}}(1;q^2))^* + \tfrac{2i\sqrt{6}}{\sqrt{5}q^2}(Z_{22}^{\vec{d}}(1;q^2))^*) \\ &\qquad = \frac{1}{2\gamma q\pi^2} \sum_{\vec{r}} (1 + \tfrac{6r_1r_2}{q^2} + \tfrac{3i(r_1^2-r_2^2)}{q^2})(\vec{r}^2-q^2)^{-s}\Big|_{s=1}\end{aligned} \tag{A.2.15}$$

with $Q(\vec{r}) = 1 + \frac{6r_1r_2}{q^2} + \frac{3i(r_1^2-r_2^2)}{q^2}$ and get

$$\begin{aligned}\sum_{\vec{r}} \frac{Q(\vec{r})}{(\vec{r}^2-q^2)^s}\Big|_{s=1} =& \sum_{\vec{r}} \frac{(1+\frac{6r_1r_2}{q^2})}{(\vec{r}^2-q^2)} \mathrm{e}^{-(\vec{r}^2-q^2)} \\ &+\gamma \int_0^1 \mathrm{d}t\, \mathrm{e}^{tq^2} \sum_{\vec{n}\in\mathbb{Z}^3\setminus\{0\}} (-1)^{\vec{n}\vec{d}} \mathrm{e}^{-\pi^2(\hat{\gamma}\vec{n})^2/t} \\ &\quad \times \left(\frac{\pi}{t}\right)^{3/2} \left(1 - \frac{6\pi^2}{q^2t^2}\Big[(\hat{\gamma}\vec{n})_1(\hat{\gamma}\vec{n})_2\Big]\right) \\ &+\gamma\pi^{3/2} \sum_{l=0}^{\infty} \frac{(q^2)^l}{l!(l-\frac{1}{2})}.\end{aligned} \tag{A.2.16}$$

For the transverse polarisation we have (see (6.2.24))

$$\begin{aligned}&\frac{1}{\gamma q\pi^{3/2}}((Z_{00}^{\vec{d}}(1;q^2))^* - \tfrac{i\sqrt{6}}{\sqrt{5}q^2}(Z_{22}^{\vec{d}}(1;q^2))^*) \\ &\qquad = \frac{1}{2\gamma q\pi^2} \sum_{\vec{r}} (1 - \tfrac{3r_1r_2}{q^2} - \tfrac{3i(r_1^2-r_2^2)}{2q^2})(\vec{r}^2-q^2)^{-s}\Big|_{s=1}\end{aligned} \tag{A.2.17}$$

with $Q(\vec{r}) = 1 - \frac{3r_1r_2}{q^2} - \frac{3i(r_1^2-r_2^2)}{2q^2}$ and the final result is

$$\begin{aligned}\sum_{\vec{r}} \frac{Q(\vec{r})}{(\vec{r}^{\,2}-q^2)^s}\Big|_{s=1} =& \sum_{\vec{r}} \frac{(1-\frac{3r_1r_2}{q^2})}{(\vec{r}^{\,2}-q^2)} \mathrm{e}^{-(\vec{r}^{\,2}-q^2)} \\ &+\gamma \int_0^1 \mathrm{d}t\, \mathrm{e}^{tq^2} \sum_{\vec{n}\in\mathbb{Z}^3\setminus\{0\}} (-1)^{\vec{n}\vec{d}} \mathrm{e}^{-\pi^2(\hat{\gamma}\vec{n})^2/t} \\ &\times \left(\frac{\pi}{t}\right)^{3/2} \left(1 + \frac{3\pi^2}{q^2t^2}\Big[(\hat{\gamma}\vec{n})_1(\hat{\gamma}\vec{n})_2\Big]\right) \\ &+\gamma\pi^{3/2} \sum_{l=0}^{\infty} \frac{(q^2)^l}{l!(l-\frac{1}{2})}.\end{aligned} \tag{A.2.18}$$

B. The jackknife method

When we want to extract for example meson masses from correlation functions we collect the data for a set of N different gauge configurations. In the example we would get correlators

$$C_i(0), C_i(1), \ldots, C_i(N_T - 1) \quad i = 1, \ldots, N \tag{B.0.1}$$

on every timeslice $t = 0, \ldots, N_T - 1$ and determine the mass from a fit of the time dependence of the averaged correlator. Because direct calculation of the error propagation is mostly too complicated or the data set is too small to get a reliable estimate of the variance, one uses the so-called jackknife method. For uncorrelated data sets the method works as follows: Assume that we want to extract an observable f from N data sets. From the data set we remove the first value and do the analysis for the $N-1$ remaining sets which gives us a value f_1. Then we remove the second value from the complete data set and get a value f_2 from the analysis and so on up to the Nth value. This gives us a set of N values f_i, $i = 1, \ldots N$ from which we get the statistical error

$$\sigma_{\hat{f}}^2 = \frac{N-1}{N} \sum_{n=1}^{N} (f_n - \hat{f})^2 \tag{B.0.2}$$

where $\hat{f}$ is the observable evaluated on the whole set. The final result for f is then given by

$$\hat{f} \pm \sigma_{\hat{f}}. \tag{B.0.3}$$

Instead of $\hat{f}$ one can also consider

$$\tilde{f} = \frac{1}{N} \sum_{n=1}^{N} f_n \tag{B.0.4}$$

which should be of the same size as $\hat{f}$.

C. Energy and phase shift tables

In the tables C.0.1 - C.0.8 we show the energies extracted from the eigenvalues of the GEVP with a two-parameter fit. The fits were performed for different fit intervals and values of t_0; χ^2/dof is χ^2 per degree of freedom. The figures C.0.1 - C.0.3 visualise the energy tables. Here t_{beg} denotes the time where the fit interval begins.

Tables C.0.9 - C.0.16 show kr_0 with the corresponding scattering phase shift. For the Sommer parameter in lattice units we have used the value $r_0/a = 6.983(49)$ obtained in the chiral limit. We give the results computed with the help of the continuum dispersion relation (10.1.3) as well as those computed by means of the lattice dispersion relation (10.1.4)

time	$t_0 = 4$	χ^2/dof	$t_0 = 5$	χ^2/dof
5-20	0.398(7)	1.07	-	
6-20	0.396(8)	1.12	0.398(7)	1.19
7-20	0.396(8)	1.21	0.397(8)	1.29
8-20	0.391(11)	1.27	0.392(11)	1.37
5-23	0.397(7)*	0.989	-	
6-23	0.396(8)	1.04	0.396(7)	1.14
7-23	0.396(8)	1.11	0.396(8)	1.21
8-23	0.390(10)	1.11	0.389(10)	1.20
9-23	0.402(15)	1.07	0.401(15)	1.16
10-23	0.394(16)	1.03	0.393(16)	1.11

Table C.0.1.: Ground state energy in lattice units on the $32^3 \times 64$ lattice. The total momentum is $(1, 1, 0)\frac{2\pi}{L}$.

time	$t_0 = 4$	χ^2/dof	$t_0 = 5$	χ^2/dof
5-15	0.474(11)	0.89	-	
6-15	0.462(15)	0.85	0.462(15)	0.84
7-15	0.471(19)	0.85	0.471(18)	0.84
8-15	0.474(32)*	0.99	0.475(31)	0.98
9-15	-		0.507(49)	0.92
5-20	0.473(11)	0.75	-	
6-20	0.465(15)	0.75	0.466(14)	0.75
7-20	0.473(19)	0.76	0.474(18)	0.76
8-20	0.473(30)	0.83	0.474(29)	0.83
9-20	0.513(47)	0.70	0.515(46)	0.68
10-20	-		0.515(74)	0.76

Table C.0.2.: Excited state energy in lattice units on the $32^3 \times 64$ lattice. The total momentum is $(1, 1, 0)\frac{2\pi}{L}$.

time	$t_0 = 4$	χ^2/dof	$t_0 = 5$	χ^2/dof
5-15	0.302(3)	3.06	-	
6-15	0.296(4)	2.81	0.296(4)	2.79
7-15	0.288(4)	1.21	0.288(4)	1.21
8-15	0.286(4)	0.68	0.286(4)	0.67
9-15	0.284(5)	0.78	0.284(5)	0.77
10-15	0.285(6)	0.96	0.285(6)	0.94
11-15	0.286(6)	1.12	0.286(6)	1.10
5-20	0.300(3)	2.35	-	
6-20	0.295(4)	2.10	0.295(4)	2.08
7-20	0.289(4)	1.22	0.289(4)	1.22
8-20	0.286(4)*	0.74	0.286(4)	0.73
9-20	0.287(4)	0.80	0.287(4)	0.79
10-20	0.288(5)	0.87	0.288(5)	0.87
11-20	0.289(5)	0.92	0.289(5)	0.91

Table C.0.3.: Ground state energy in lattice units on the $40^3 \times 64$ lattice. The total momentum is $(0, 0, 1)\frac{2\pi}{L}$.

time	$t_0 = 4$	χ^2/dof	$t_0 = 5$	χ^2/dof
5-15	0.366(6)	3.24	-	
6-15	0.361(7)	3.49	0.361(7)	3.52
7-15	0.343(9)	2.31	0.343(9)	2.32
8-15	0.330(10)	1.90	0.329(10)	1.91
9-15	0.318(13)	1.84	0.318(13)	1.85
10-15	0.308(15)	1.97	0.308(15)	1.98
11-15	0.317(20)	2.44	0.317(20)	2.45
5-20	0.365(6)	2.30	-	
6-20	0.361(7)	2.37	0.361(7)	2.39
7-20	0.345(8)	1.69	0.345(8)	1.70
8-20	0.331(10)*	1.38	0.331(10)	1.39
9-20	0.322(12)	1.34	0.322(12)	1.35
10-20	0.314(13)	1.36	0.314(13)	1.37
11-20	0.326(17)	1.32	0.326(17)	1.33

Table C.0.4.: Excited state energy in lattice units on the $40^3 \times 64$ lattice. The total momentum is $(0, 0, 1)\frac{2\pi}{L}$.

time	$t_0 = 4$	χ^2/dof	$t_0 = 5$	χ^2/dof
5-15	0.361(4)	1.80	-	
6-15	0.357(5)	1.80	0.357(5)	3.52
7-15	0.348(6)	1.08	0.348(6)	2.32
8-15	0.339(7)	0.43	0.339(7)	1.91
9-15	0.339(8)	0.52	0.339(8)	1.85
10-15	0.336(9)	0.57	0.336(9)	1.98
11-15	0.342(11)	0.43	0.342(11)	2.45
5-20	0.361(4)	1.56	-	
6-20	0.357(5)	1.52	0.356(5)	2.39
7-20	0.350(5)	0.98	0.350(5)	1.70
8-20	0.341(6)*	0.48	0.341(6)	1.39
9-20	0.340(7)	0.51	0.340(7)	1.35
10-20	0.337(8)	0.53	0.337(8)	1.37
11-20	0.342(9)	0.47	0.342(9)	1.33

Table C.0.5.: Ground state energy in lattice units on the $40^3 \times 64$ lattice. The total momentum is $(1, 1, 0)\frac{2\pi}{L}$.

time	$t_0 = 4$	χ^2/dof	$t_0 = 5$	χ^2/dof
5-15	0.425(6)	1.33	-	
6-15	0.425(8)	1.50	0.425(8)	1.48
7-15	0.414(11)	1.36	0.414(11)	1.35
8-15	0.392(14)	0.77	0.392(14)	0.77
9-15	0.388(18)	0.88	0.387(18)	0.89
10-15	0.387(23)	1.11	0.387(23)	1.11
11-15	0.412(35)	1.09	0.412(35)	1.10
5-20	0.425(7)	1.11	-	
6-20	0.424(8)	1.19	0.424(8)	1.18
7-20	0.414(11)	1.09	0.414(11)	1.08
8-20	0.389(14)*	0.55	0.389(14)	0.55
9-20	0.384(18)	0.58	0.384(18)	0.58
10-20	0.384(23)	0.64	0.384(23)	0.64
11-20	0.405(34)	0.59	0.405(34)	0.59

Table C.0.6.: Excited state energy in lattice units on the $40^3 \times 64$ lattice. The total momentum is $(1, 1, 0)\frac{2\pi}{L}$.

time	$t_0 = 4$	χ^2/dof	$t_0 = 5$	χ^2/dof
5-15	0.432(5)	0.75	-	
6-15	0.430(7)	0.81	0.430(7)	1.48
7-15	0.424(9)	0.78	0.423(10)	1.35
8-15	0.412(11)	0.31	0.413(11)	0.77
9-15	0.409(14)	0.35	0.410(15)	0.89
10-15	0.414(19)	0.39	0.415(20)	1.11
11-15	0.404(27)	0.41	0.403(27)	1.10
5-20	0.432(5)	0.71	-	
6-20	0.429(7)	0.74	0.429(7)	1.18
7-20	0.424(9)	0.73	0.424(10)	1.08
8-20	0.412(11)*	0.46	0.413(11)	0.55
9-20	0.411(14)	0.51	0.413(14)	0.58
10-20	0.417(19)	0.54	0.419(19)	0.64
11-20	0.407(24)	0.54	0.408(24)	0.59

Table C.0.7.: Ground state energy in lattice units on the $40^3 \times 64$ lattice. The total momentum is $(0, 0, 2)\frac{2\pi}{L}$.

time	$t_0 = 4$	χ^2/dof	$t_0 = 5$	χ^2/dof
5-15	0.479(9)	1.62	-	
6-15	0.475(12)	1.78	0.476(11)	1.81
7-15	0.483(17)	1.96	0.484(16)	1.98
8-15	0.463(21)	1.95	0.464(21)	1.99
9-15	0.463(30)	2.34	0.464(30)	2.39
10-15	0.481(44)	2.83	0.484(45)	2.89
11-15	0.497(77)	3.75	0.502(78)	3.82
5-20	0.478(9)	1.22	-	
6-20	0.476(12)	1.31	0.476(11)	1.31
7-20	0.485(17)	1.36	0.485(16)	1.36
8-20	0.466(21)*	1.30	0.467(20)	1.31
9-20	0.465(29)	1.43	0.467(29)	1.44
10-20	0.492(42)	1.47	0.495(42)	1.48
11-20	0.506(70)	1.64	0.511(71)	1.66

Table C.0.8.: Excited state energy in lattice units on the $40^3 \times 64$ lattice. The total momentum is $(0, 0, 2)\frac{2\pi}{L}$.

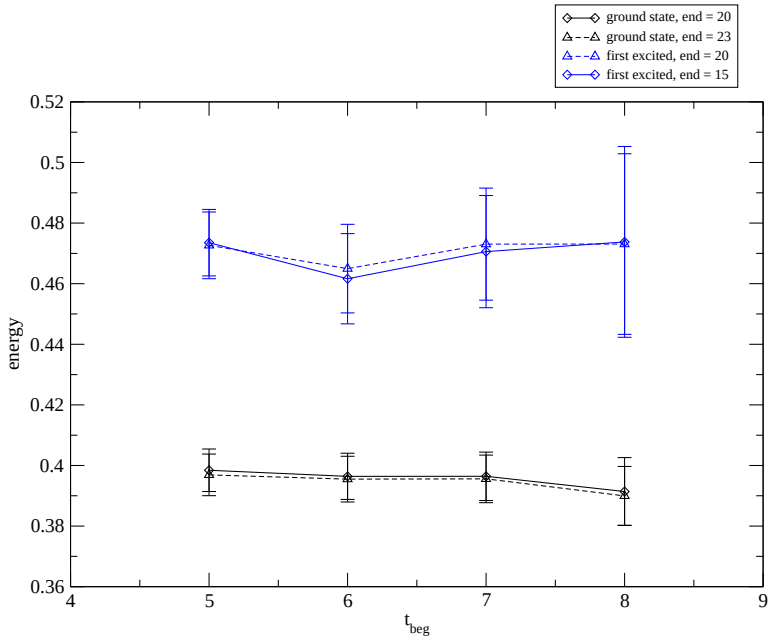

Figure C.0.1.: Dependence of the energy on the fit interval for the $32^3 \times 64$ lattice and total momentum $(1,1,0)\frac{2\pi}{L}$.

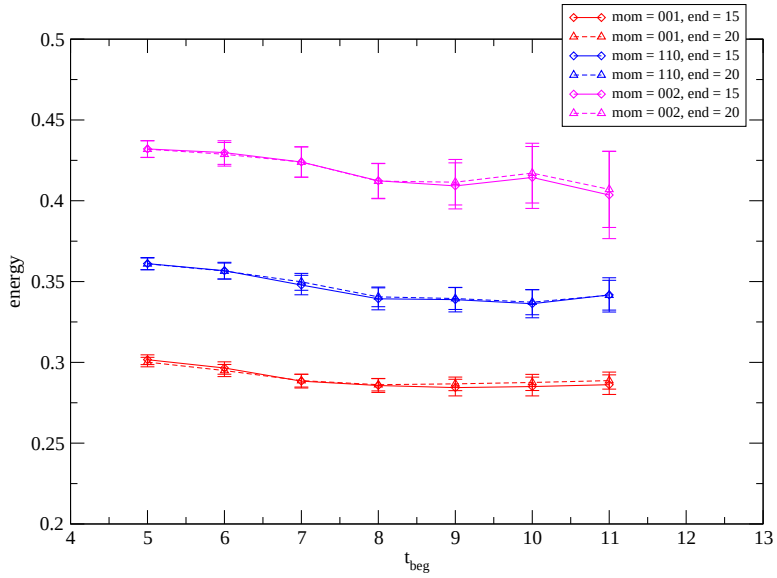

Figure C.0.2.: Dependence of the ground state energy on the fit interval for the $40^3 \times 64$ lattice and total momenta $(0,0,1)\frac{2\pi}{L}$, $(1,1,0)\frac{2\pi}{L}$ and $(0,0,2)\frac{2\pi}{L}$.

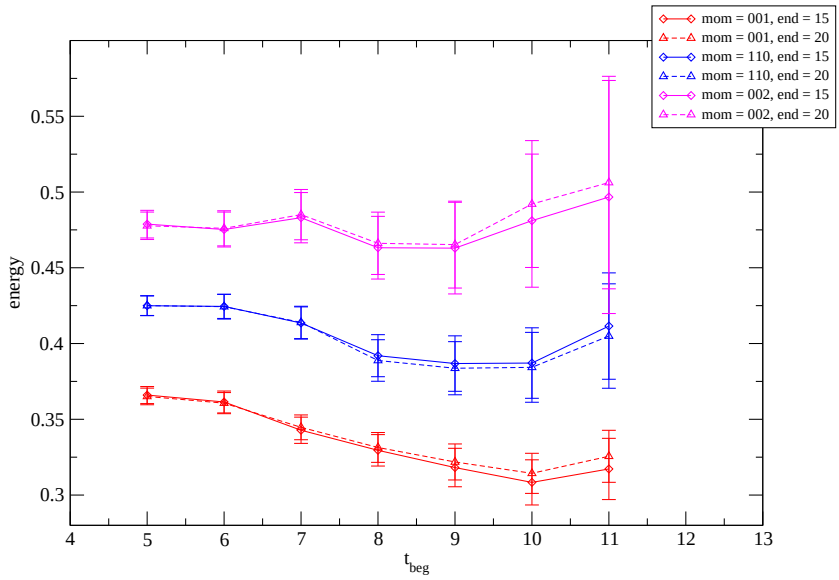

Figure C.0.3.: Dependence of the excited state energy on the fit interval for the $40^3 \times 64$ lattice and total momenta $(0,0,1)\frac{2\pi}{L}, (1,1,0)\frac{2\pi}{L}$ and $(0,0,2)\frac{2\pi}{L}$.

time	$k_{cont}r_0$	phase_{cont}	$k_{lat}r_0$	phase_{lat}
5-20	0.661(58)	$0.056\binom{70}{-61}$	0.680(57)	$0.033\binom{74}{-65}$
6-20	0.646(64)	$0.073\binom{74}{-61}$	0.666(63)	$0.051\binom{78}{-66}$
7-20	0.646(67)	$0.073\binom{77}{-63}$	0.666(66)	$0.050\binom{81}{-69}$
8-20	0.607(99)	$0.112\binom{99}{-62}$	0.628(97)	$0.092\binom{106}{-73}$
5-23	0.649(57)	$0.069\binom{67}{-57}$	0.669(56)	$0.046\binom{71}{-62}$
6-23	0.639(64)	$0.081\binom{72}{-59}$	0.659(63)	$0.059\binom{76}{-64}$
7-23	0.640(66)	$0.080\binom{75}{-61}$	0.659(65)	$0.058\binom{79}{-67}$
8-23	0.596(87)	$0.122\binom{82}{-52}$	0.617(85)	$0.103\binom{88}{-62}$
9-23	0.685(119)	$0.026\binom{156}{-120}$	0.705(118)	$0.001\binom{162}{-130}$
10-23	0.625(139)	$0.095\binom{149}{-84}$	0.645(136)	$0.074\binom{157}{-99}$

Table C.0.9.: Scattering phase shift and kr_0 computed from the ground state energy on the $32^3 \times 64$ lattice for $t_0 = 4$ and total momentum $(1, 1, 0)\frac{2\pi}{L}$.

time	$k_{cont}r_0$	phase_{cont}	$k_{lat}r_0$	phase_{lat}
5-20	1.107(61)	$2.357\binom{149}{-145}$	1.126(61)	$2.310\binom{153}{-149}$
6-20	1.066(82)	$2.454\binom{193}{-186}$	1.085(83)	$2.409\binom{198}{-191}$
7-20	1.109(102)	$2.352\binom{250}{-238}$	1.128(102)	$2.305\binom{257}{-243}$
8-20	1.109(165)	$2.351\binom{407}{-374}$	1.128(165)	$2.304\binom{420}{-382}$
9-20	1.309(237)	$1.799\binom{642}{-471}$	1.329(239)	$1.733\binom{736}{-650}$
5-15	1.111(61)	$2.346\binom{149}{-145}$	1.130(61)	$2.298\binom{153}{-149}$
6-15	1.048(85)	$2.496\binom{149}{-145}$	1.067(85)	$2.452\binom{200}{-192}$
7-15	1.096(102)	$2.383\binom{248}{-236}$	1.115(103)	$2.337\binom{255}{-242}$
8-15	1.113(174)	$2.342\binom{432}{-394}$	1.132(175)	$2.295\binom{446}{-403}$

Table C.0.10.: Scattering phase shift and kr_0 computed from the excited state energy on the $32^3 \times 64$ lattice for $t_0 = 4$ and total momentum $(1, 1, 0)\frac{2\pi}{L}$.

time	$k_{cont}r_0$	phase_{cont}	$k_{lat}r_0$	phase_{lat}
5-15	0.675(29)	$2.978\binom{67}{-65}$	0.686(29)	$2.953\binom{68}{-67}$
6-15	0.646(39)	$3.044\binom{87}{-83}$	0.657(39)	$3.020\binom{88}{-85}$
7-15	0.584(49)	$0.028\binom{93}{-84}$	0.596(49)	$0.007\binom{95}{-87}$
8-15	0.520(61)	$0.133\binom{90}{-69}$	0.531(61)	$0.117\binom{94}{-75}$
9-15	0.516(69)	$0.139\binom{100}{-72}$	0.527(68)	$0.123\binom{104}{-79}$
10-15	0.495(83)	$0.165\binom{107}{-63}$	0.507(81)	$0.150\binom{113}{-73}$
11-15	0.539(93)	$0.106\binom{149}{-106}$	0.550(92)	$0.087\binom{153}{-115}$
5-20	0.674(28)	$2.981\binom{64}{-63}$	0.685(28)	$2.955\binom{65}{-64}$
6-20	0.645(38)	$3.047\binom{83}{-80}$	0.656(38)	$3.023\binom{84}{-82}$
7-20	0.599(42)	$0.001\binom{83}{-77}$	0.610(42)	$3.121\binom{85}{-80}$
8-20	0.529(54)	$0.120\binom{84}{-68}$	0.541(54)	$0.102\binom{87}{-73}$
9-20	0.521(61)	$0.131\binom{91}{-70}$	0.533(60)	$0.115\binom{94}{-75}$
10-20	0.503(72)	$0.155\binom{98}{-65}$	0.515(71)	$0.140\binom{102}{-73}$
11-20	0.537(81)	$0.108\binom{128}{-96}$	0.549(79)	$0.090\binom{132}{-103}$

Table C.0.11.: Scattering phase shift and kr_0 computed from the ground state energy on the $40^3 \times 64$ lattice for $t_0 = 4$ and total momentum $(1, 1, 0)\frac{2\pi}{L}$.

time	$k_{cont}r_0$	phase_{cont}	$k_{lat}r_0$	phase_{lat}
5-15	1.033(36)	$1.887\binom{139}{-132}$	1.045(36)	$1.842\binom{143}{-136}$
6-15	1.031(43)	$1.896\binom{170}{-161}$	1.043(44)	$1.851\binom{176}{-165}$
7-15	0.975(59)	$2.102\binom{209}{-198}$	0.987(59)	$2.063\binom{214}{-202}$
8-15	0.860(82)	$2.480\binom{248}{-239}$	0.871(82)	$2.447\binom{252}{-242}$
9-15	0.831(112)	$2.567\binom{322}{-306}$	0.841(112)	$2.536\binom{327}{-310}$
10-15	0.833(143)	$2.562\binom{410}{-384}$	0.843(143)	$2.530\binom{417}{-389}$
11-15	0.965(197)	$2.139\binom{607}{-422}$	0.976(198)	$2.100\binom{617}{-318}$
5-20	1.034(36)	$1.886\binom{142}{-135}$	1.045(36)	$1.841\binom{146}{-139}$
6-20	1.030(44)	$1.900\binom{173}{-163}$	1.042(44)	$1.855\binom{179}{-168}$
7-20	0.977(59)	$2.095\binom{210}{-199}$	0.988(59)	$2.055\binom{216}{-203}$
8-20	0.842(83)	$2.533\binom{243}{-234}$	0.853(83)	$2.501\binom{247}{-238}$
9-20	0.813(109)	$2.618\binom{305}{-291}$	0.824(109)	$2.588\binom{310}{-295}$
10-20	0.817(144)	$2.608\binom{404}{-377}$	0.827(144)	$2.577\binom{410}{-383}$
11-20	0.930(199)	$2.257\binom{681}{-585}$	0.941(199)	$2.220\binom{618}{-594}$

Table C.0.12.: Scattering phase shift and kr_0 computed from the excited state energy on the $40^3 \times 64$ lattice for $t_0 = 4$ and total momentum $(1, 1, 0)\frac{2\pi}{L}$.

time	$k_{cont}r_0$	phase_{cont}	$k_{lat}r_0$	phase_{lat}
5-15	0.526(26)	$3.053\binom{44}{-41}$	0.531(26)	$3.044\binom{45}{-42}$
6-15	0.489(34)	$3.109\binom{48}{-42}$	0.494(34)	$3.102\binom{49}{-44}$
7-15	0.425(42)	$0.038\binom{39}{-28}$	0.431(42)	$0.033\binom{41}{-30}$
8-15	0.403(45)	$0.054\binom{33}{-20}$	0.408(44)	$0.051\binom{35}{-22}$
9-15	0.392(55)	$0.061\binom{37}{-17}$	0.397(54)	$0.058\binom{39}{-19}$
10-15	0.397(60)	$0.058\binom{44}{-20}$	0.403(60)	$0.054\binom{47}{-23}$
11-15	0.407(61)	$0.051\binom{50}{-25}$	0.413(61)	$0.048\binom{52}{-28}$
5-20	0.515(26)	$3.070\binom{41}{-38}$	0.521(26)	$3.061\binom{42}{-39}$
6-20	0.477(34)	$3.124\binom{45}{-39}$	0.482(34)	$3.117\binom{46}{-40}$
7-20	0.428(39)	$0.035\binom{38}{-27}$	0.434(39)	$0.031\binom{39}{-29}$
8-20	0.407(40)	$0.051\binom{32}{-20}$	0.413(40)	$0.048\binom{33}{-22}$
9-20	0.412(43)	$0.048\binom{35}{-23}$	0.417(43)	$0.044\binom{37}{-25}$
10-20	0.419(50)	$0.043\binom{44}{-28}$	0.424(49)	$0.039\binom{46}{-30}$
11-20	0.428(51)	$0.035\binom{50}{-33}$	0.434(51)	$0.030\binom{52}{-35}$

Table C.0.13.: Scattering phase shift and kr_0 computed from the ground state energy on the $40^3 \times 64$ lattice for $t_0 = 4$ and total momentum $(0, 0, 1)\frac{2\pi}{L}$.

time	$k_{cont}r_0$	phase_{cont}	$k_{lat}r_0$	phase_{lat}
5-15	0.895(31)	$2.045\binom{119}{-114}$	0.900(32)	$2.023\binom{121}{-116}$
6-15	0.872(40)	$2.131\binom{146}{-139}$	0.877(40)	$2.110\binom{148}{-141}$
7-15	0.774(51)	$2.456\binom{156}{-150}$	0.779(51)	$2.440\binom{158}{-151}$
8-15	0.701(65)	$2.668\binom{174}{-163}$	0.706(65)	$2.654\binom{176}{-165}$
9-15	0.633(85)	$2.837\binom{198}{-178}$	0.638(85)	$2.825\binom{201}{-181}$
10-15	0.571(110)	$2.971\binom{217}{-174}$	0.576(110)	$2.961\binom{220}{-178}$
11-15	0.628(140)	$2.850\binom{316}{-260}$	0.633(139)	$2.839\binom{320}{-265}$
5-20	0.890(31)	$2.062\binom{116}{-112}$	0.896(31)	$2.041\binom{118}{-113}$
6-20	0.868(39)	$2.145\binom{140}{-134}$	0.873(39)	$2.124\binom{143}{-136}$
7-20	0.785(48)	$2.424\binom{149}{-143}$	0.790(48)	$2.407\binom{151}{-145}$
8-20	0.711(61)	$2.638\binom{167}{-158}$	0.717(61)	$2.624\binom{169}{-160}$
9-20	0.656(78)	$2.783\binom{190}{-175}$	0.661(78)	$2.771\binom{193}{-177}$
10-20	0.610(92)	$2.891\binom{202}{-176}$	0.615(92)	$2.880\binom{204}{-179}$
11-20	0.678(110)	$2.728\binom{281}{-250}$	0.683(110)	$2.715\binom{284}{-253}$

Table C.0.14.: Scattering phase shift and kr_0 computed from the excited state energy on the $40^3 \times 64$ lattice for $t_0 = 4$ and total momentum $(0, 0, 1)\frac{2\pi}{L}$.

time	$k_{cont}r_0$	phase$_{cont}$	$k_{lat}r_0$	phase$_{lat}$
5-15	0.735(41)	$0.073\binom{122}{-122}$	0.762(41)	$0.006\binom{123}{-123}$
6-15	0.719(58)	$0.120\binom{166}{-166}$	0.746(57)	$0.042\binom{169}{-168}$
7-15	0.675(79)	$0.243\binom{209}{-205}$	0.703(77)	$0.167\binom{212}{-210}$
8-15	0.581(106)	$0.479\binom{232}{-202}$	0.610(102)	$0.410\binom{238}{-220}$
9-15	0.553(151)	$0.539\binom{299}{-201}$	0.584(144)	$0.473\binom{308}{-247}$
10-15	0.599(192)	$0.438\binom{409}{-301}$	0.628(184)	$0.368\binom{417}{-350}$
5-20	0.734(41)	$0.076\binom{121}{-121}$	0.760(40)	$0.002\binom{122}{-122}$
6-20	0.711(59)	$0.142\binom{166}{-165}$	0.738(58)	$0.065\binom{169}{-168}$
7-20	0.675(79)	$0.243\binom{209}{-206}$	0.703(77)	$0.167\binom{213}{-210}$
8-20	0.579(106)	$0.483\binom{233}{-201}$	0.609(102)	$0.415\binom{239}{-219}$
9-20	0.574(143)	$0.496\binom{299}{-232}$	0.603(137)	$0.427\binom{307}{-265}$
10-20	0.621(177)	$0.384\binom{398}{-333}$	0.649(170)	$0.312\binom{405}{-364}$
11-20	0.534(303)	$0.579\binom{488}{-153}$	0.565(277)	$0.515\binom{502}{-90}$

Table C.0.15.: Scattering phase shift and kr_0 computed from the ground state energy on the $40^3 \times 64$ lattice for $t_0 = 4$ and total momentum $(0, 0, 2)\frac{2\pi}{L}$.

time	$k_{cont}r_0$	phase_{cont}	$k_{lat}r_0$	phase_{lat}
5-15	1.029(55)	$2.187\binom{230}{-221}$	1.054(55)	$2.083\binom{238}{-229}$
6-15	1.009(70)	$2.270\binom{285}{-272}$	1.034(70)	$2.169\binom{295}{-281}$
7-15	1.053(98)	$2.086\binom{426}{-395}$	1.078(98)	$1.978\binom{408}{-391}$
8-15	0.939(134)	$2.542\binom{488}{-461}$	0.963(133)	$2.450\binom{504}{-471}$
9-15	0.937(200)	$2.548\binom{723}{-664}$	0.962(198)	$2.456\binom{749}{-678}$
10-15	1.042(274)	$2.133\binom{985}{-44}$	1.067(273)	$2.026\binom{1011}{-310}$
11-15	1.128(489)	$1.747\binom{1078}{-795}$	1.153(486)	$1.625\binom{1274}{-725}$
5-20	1.023(55)	$2.213\binom{227}{-219}$	1.048(55)	$2.109\binom{235}{-226}$
6-20	1.014(71)	$2.252\binom{287}{-275}$	1.038(70)	$2.150\binom{298}{-283}$
7-20	1.065(97)	$2.037\binom{431}{-398}$	1.089(97)	$1.927\binom{412}{-286}$
8-20	0.956(131)	$2.477\binom{491}{-461}$	0.981(130)	$2.383\binom{508}{-472}$
9-20	0.951(186)	$2.497\binom{690}{-633}$	0.976(185)	$2.403\binom{715}{-647}$
10-20	1.103(248)	$1.865\binom{974}{-587}$	1.128(248)	$1.748\binom{1005}{-874}$
11-20	1.179(418)	$1.495\binom{1494}{-810}$	1.204(417)	$1.361\binom{1280}{-483}$

Table C.0.16.: Scattering phase shift and kr_0 computed from the excited state energy on the $40^3 \times 64$ lattice for $t_0 = 4$ and total momentum $(0, 0, 2)\frac{2\pi}{L}$.

Acknowledgements

First of all special thanks go to my supervisor Meinulf Göckeler, without whose help this work would never be possible. I want to thank him for always having time and patience to answer all my questions and guiding me through the tricky parts of this thesis. I also want to thank Tommy Burch who supported me in the developement of the main program and allowed me to use his jackknife and fitting routines, which saved me a lot of work. I am grateful to "Norddeutscher Verbund für Hoch- und Höchstleistungsrechnen (HLRN)" for providing computing time, to Gerrit Schierholz and Holger Perlt for their support at HLRN and to Christian Hagen who wrote the basic structure of the main program. I also thank all the people who helped me to understand the Chroma software, especially Johannes Najjar and Sara Collins. Discussions with Andreas Schäfer are gratefully acknowledged. Special thanks go to DFG for the financial support of the whole project through SFB/TRR55 and to the QCDSF collaboration for providing the gauge configurations.

I really enjoyed my job as a system administrator and I thank my colleagues Johannes Najjar, Stefan Solbrig, Martin Hetzenegger and Alessio Burello for the interesting discussions about different computer related topics and the good collaboration. Furthermore I want to mention my roommate Narjes Javadi-Motaghi who became one of my closest friends here. I want to thank her for the great time we spent together and the delicious dishes she taught me to cook.

And last but not least I thank my parents for supporting my life here with daily Skype calls and sending me tons of food packets from Switzerland.

Bibliography

[1] http://en.wikipedia.org/wiki/Standard_Model.

[2] http://pdg.lbl.gov/2011/reviews/rpp2011-rev-quark-model.pdf.

[3] http://www.cryst.ehu.es/rep/point.html.

[4] http://pdg.lbl.gov.

[5] http://usqcd.jlab.org/usqcd-docs/chroma/.

[6] M. Albanese et al. *Phys.Lett.*, B192:163–169, 1987.

[7] S. Aoki et al. *Phys.Rev.*, D76:094506, 2007. eprint: 0708.3705.

[8] S. Aoki et al. *Phys.Rev.*, D84:094505, 2011. eprint: 1106.5365.

[9] R. Barrett et al. *Templates for the Solution of Linear Systems: Building Blocks for Iterative Methods, 2nd Edition*. SIAM, Philadelphia, PA, 1994.

[10] B. Blossier et al. *JHEP*, 0904:094, 2009. eprint: 0902.1265.

[11] T. Burch et al. *Phys.Rev.*, D70:054502, 2004. hep-lat/0405006.

[12] T. Burch et al. *Phys.Rev.*, D73:094505, 2006. hep-lat/0601026.

[13] S. Collins. Lecture notes, WS 2011/12.

[14] S. Collins et al. *Phys.Rev.*, D84:074507, 2011. eprint: 1106.3580.

[15] M. Creutz. *Phys.Rev.*, D38:1228–1238, 1988. doi: 10.1103/PhysRevD.38.1228.

[16] T. DeGrand and D. Toussaint. *From actions to answers: proceedings of the 1989 Theoretical Advanced Study Institute in Elementary Particle Physics, 5-30 June, 1989, University of Colorado, Boulder*. World Scientific, 1990.

[17] S.-J. Dong and K.-F. Liu. *Phys.Lett.*, B328:130–136, 1994. hep-lat/9308015.

[18] R. G. Edwards and B. Joo. *Nucl.Phys.Proc.Suppl.*, 140:832, 2005. hep-lat/0409003.

[19] X. Feng, K. Jansen, and D. B. Renner. *Phys.Rev.*, D83:094505, 2011. eprint: 1011.5288.

[20] J. Frison et al. *PoS*, LATTICE2010:139, 2010. eprint: 1011.3413.

[21] C. Gattringer and C. B. Lang. *Quantum Chromodynamics on the Lattice*. Springer, 2010.

[22] H. Georgi. *Lie Algebras in Particle Physics*. Westview Press, 1999.

[23] M. Göckeler et al. *Nucl.Phys.*, B425:413–448, 1994. hep-lat/9402011.

[24] M. Göckeler et al. 2012. eprint: 1206.4141.

[25] R. Gupta. pages 83–219, 1997. hep-lat/9807028.

[26] S. Güsken. *Nucl.Phys.B Proc.Suppl.*, 17:361–364, 1990. doi: 10.1016/0920-5632(90)90273-W.

[27] A. Hasenfratz and F. Knechtli. *Phys.Rev.*, D64:034504, 2001. hep-lat/0103029.

[28] K. Jansen and R. Sommer. *Nucl.Phys.*, B530:185–203, 1998. hep-lat/9803017.

[29] C. B. Lang, D. Mohler, S. Prelovsek, and M. Vidmar. *Phys.Rev.*, D84:054503, 2011. eprint: 1105.5636.

[30] M. Lüscher. *Nucl.Phys.*, B354:531–578, 1991. doi: 10.1016/0550-3213(91)90366-6.

[31] M. Lüscher. *Nucl.Phys.*, B364:237–254, 1991. doi: 10.1016/0550-3213(91)90584-K.

[32] M. Lüscher and U. Wolff. *Nucl.Phys.*, B339:222–252, 1990. doi: 10.1016/0550-3213(90)90540-T.

[33] C. Michael. *Nucl.Phys.*, B259:58, 1985. doi: 10.1016/0550-3213(85)90297-4.

[34] C. Michael. *Phys. Rev. D*, 49:2616–2619, Mar 1994. doi: 10.1103/PhysRevD.49.2616.

[35] W. Miller. *Symmetry Groups and Their Applications*. Academic Press, 1972.

[36] I. Montvay and G. Münster. *Quantum Fields on a Lattice*. Cambridge University Press, 2003.

[37] C. Morningstar and M. J. Peardon. *Phys.Rev.*, D69:054501, 2004. hep-lat/0311018.

[38] M. E. Peskin and D. V. Schroeder. *An Introduction to Quantum Field Theory*. Westview Press, 2006.

[39] QCDSF collaboration. private communication.

[40] K. Rummukainen and S. A. Gottlieb. *Nucl.Phys.*, B450:397–436, 1995. hep-lat/9503028.

[41] R. T. Scalettar, D. J. Scalapino, and R. L. Sugar. *Phys.Rev.*, B34:7911–7917, 1986. doi: 10.1103/PhysRevB.34.7911.

[42] B. Sheikholeslami and R. Wohlert. *Nucl.Phys.*, B259:572, 1985. doi: 10.1016/0550-3213(85)90002-1.

[43] R. Sommer. *Nucl.Phys.*, B411:839–854, 1994. hep-lat/9310022.

[44] H. A. van der Vorst. *SIAM Journal on Scientific and Statistical Computing*, 13(2):631–644, 1992.

[45] K. G. Wilson. *Phys.Rev.*, D10:2445–2459, 1974. doi: 10.1103/PhysRevD.10.2445.

[46] K. G. Wilson. Talk at the Abingdon Meeting on Lattice Gauge Theories. 1981.

[47] T. Yamazaki et al. *Phys.Rev.*, D70:074513, 2004. hep-lat/0402025.